

# **First Principles Design of Coreless Power Transformers**

By Angel J. Carvajal

[S.B., E.E. M.I.T., 2016]

Submitted to the  
Department of Electrical Engineering and Computer Science  
in Partial Fulfillment of the Requirements for the Degree of

Master of Engineering in Electrical Engineering and Computer Science  
at the  
Massachusetts Institute of Technology  
February 2018

© 2018 Massachusetts Institute of Technology. All rights reserved.

The author hereby grants to MIT permission to reproduce and to distribute publicly paper and electronic copies of this thesis document in whole or in part in any medium now known or hereafter created.

Author:

---

Department of Electrical Engineering and Computer Science  
February 2, 2018

Certified by:

---

Dr. Chathan M. Cooke  
Principal Research Engineer, RLE  
Thesis Supervisor  
February 2, 2018

Accepted by:

---

Christopher J. Terman  
Senior Lecturer and Undergraduate Officer, Dept. of EECS  
Chairman, Masters of Engineering Thesis Committee

# **First Principles Design of Coreless Power Transformers**

By Angel J. Carvajal

Submitted to the Department of Electrical Engineering and Computer Science

February 2, 2018

in Partial Fulfillment of the Requirements for the Degree of Master of Engineering in Electrical  
Engineering and Computer Science

## **ABSTRACT**

This thesis presents a theoretical foundation and methodology for designing novel 4-coil high frequency coreless power transformers from first principles via lumped equivalent circuit models. The procedure is applied to construct a design for 100W transformer with an  $S_{21}$  parameter value of .96. Using MATLAB and LTspice, simulation tools have been developed to produce accurate predictions of inductance, resistance, coupling coefficients, and  $S_{21}$  parameter values for an ensemble of coil models. These theoretical calculations have been employed for spiral and cylindrical coils and have been validated with numerous constructed experimental designs. The utility uses a first principles approach and derives these calculations directly from the physical parameters and relative positions of the coils. Simulation outputs greatly aid the engineering task of designing an efficient coreless power transformer.

Thesis Supervisor: Dr. Chathan M. Cooke

Title: Principle Research Engineer, RLE

*Dedicated to Mami, Maryosie, and Melanie*

## Acknowledgements

This thesis is the culmination of the effort and support of numerous individuals at MIT and beyond.

Above all, I'd like to thank my thesis advisor, Dr. Chathan Cooke. Rarely does one ever get the privilege to work one-on-one with such an esteemed member of the MIT faculty and I am tremendously grateful to have had the opportunity. Dr. Cooke never failed to provide me with abundant support and encouragement throughout the whole journey. He was always available to address my concerns via all forms of communication and never lacked interest in the project. He's equipped me with the necessary tools and a specialized environment to help me focus and complete my assignments. His rigor and diligence has influenced my professional work ethic and has helped me inside and outside of the laboratory. Dr. Cooke is an individual whose excitement over science and discovery enables one to see the importance and thrill in research endeavors. It is this contagious excitement that nudges me to further pursue academia.

I would also like to thank my project sponsors: Prolec GE. This project would not be possible without the steadfast support and encouragement that Carlos Gaytan-Cavazos and his associates provided me along the way. The bi-monthly phone reports ensured I kept to schedule, structured my efforts, and reminded me to focus on the bigger picture.

I would also like to thank Daniel Schemmel, who has greatly aided me in the writing of this communication. I have the highest hopes for him as he expands the project onward as part of his PhD undertaking.

## Table of Contents

<b>1. Introduction</b>	13
<b>2. Background and Literature Review</b>	16
2.1 The Classic Transformer.....	16
<i>2.1.1 Power and Size Scaling Relationship .....</i>	17
2.2 The Transformer's Core.....	19
<i>2.2.1 Non-Resonant Inductive Coupling.....</i>	19
<i>2.2.2 Tuned Double Resonant System.....</i>	21
2.3 High Frequency Coil Characteristic of Q .....	23
<b>3. Objectives and Motivation</b>	25
<b>4. Electrical Characteristics of High-Frequency Coils</b>	28
4.1 Inductance of Coils .....	29
<i>4.1.1 Measuring Inductance .....</i>	29
<i>4.1.2 Cylindrical Coils.....</i>	30
<i>4.1.3 Spiral Coils .....</i>	33
<i>4.1.4 Experimental Confirmation of Theoretical Calculations .....</i>	35
4.2 Resistance of Coils.....	36
<i>4.2.1 Measuring Resistance .....</i>	37
<i>4.2.2 Bulk Volume Conductivity.....</i>	39
<i>4.2.3 Skin Effect .....</i>	39
<i>4.2.4 Proximity Effect for Coil Windings.....</i>	40
<i>4.2.5 Experimental Confirmation of Theoretical Calculations .....</i>	44
4.3 Coil Quality Factor, Q.....	46
<b>5. Magnetic Coupling Between Pairs of Coils</b>	48
5.1 Measuring Magnetic Coupling .....	49
5.2 Calculating Mutual Magnetic Coupling .....	51
<i>5.2.1 Cylindrical Coils.....</i>	51
<i>5.2.2 Spiral Coils .....</i>	55

5.3 Theoretical Magnetic Coupling of Nested Coils .....	57
5.4 Experimental Confirmation of Theoretical Results .....	58
<b>6. Magnetic Coupling Dynamics in Multi-Coil systems</b>	61
6.1 4-coil Transformer .....	61
6.2 Topological Choices .....	63
6.3 Coupling Coefficients Dynamics .....	64
<i>6.3.1 Symmetric Drive and Load Coils</i> .....	64
<i>6.3.2 Asymmetric Drive and Load Coils</i> .....	66
<b>7. Coreless Transformer Design Overview</b>	68
7.1 100W Design Choices.....	68
7.2 Impact of Resonant Capacitors .....	71
7.3 Data Collection .....	71
<i>7.3.1 Power Efficiency and S-Parameter Analysis</i> .....	71
7.4 Power Amplifier Drive Circuitry .....	73
<b>8. System Design Program using MATLAB and LTSpice</b>	75
8.1 Configuration and LTspice Schematic.....	76
8.2 Structure of Program.....	77
<i>8.2.1 Directory Management</i> .....	77
<i>8.2.2 Cylindrical_Coil_Simulator</i> .....	78
<i>8.2.3 Master.m</i> .....	81
<i>8.2.4 SpiceModel.m</i> .....	82
<i>8.2.5 Evaluation.m</i> .....	83
<i>8.2.6 Plotting</i> .....	84
<i>8.2.7 An Example Run</i> .....	85
8.3 Alternative Spiral Geometries for Simulation .....	88
<b>9. Experimental Validation of Design Methodology</b>	93
9.1 Transformer Topologies Explored and Compared .....	93
<i>9.1.1 Experiment 1: Changing the Distance Between Resonant Coils</i> .....	94

<i>9.1.2 Experiment 2: Nested Coils, symmetric arrangement .....</i>	96
<i>9.1.3 Experiment 3: Nested Coils, asymmetric arrangement .....</i>	98
9.2 Output Plot comparison .....	100
<b>10. Final Design</b>	101
10.1 Determining Appropriate Coils.....	101
10.2 Coil Selection by Topology and Simulation Results .....	103
10.3 Final 4-Coil Transformer Design.....	105
<i>10.3.1 Impedance .....</i>	105
<i>10.3.2 Coupling Coefficients.....</i>	108
10.4 Measured and Theoretical Performance .....	108
10.5 Powering the Transformer .....	112
<b>11. Conclusion</b>	113
11.1 Summary of Operation.....	113
11.2 Further Work.....	114
<i>11.2.1 Reduced losses with Improved conductors .....</i>	114
<i>11.2.2 System Scaling to 1kW .....</i>	114
<i>11.2.3 Proximity Effect in Curved Windings .....</i>	114
<i>11.2.4 Alternative wire shapes and coil geometries .....</i>	115
<i>11.2.5 Nested Cylindrical and Spiral Structures/ Mixed designs .....</i>	115
<i>11.2.6 Alternative Driving Methods.....</i>	116
11.3 Final remarks .....	116
<b>12. Bibliography</b>	117
<b>A Appendix – Measurements of Inductance</b>	119
A.1 Cylindrical Coils: Coil Geometry and Inductance.....	119
A.2 Spiral Coils: Coil Geometry and Inductance .....	120
<b>B Appendix – Measurements of Resistance</b>	121
B.1 Cylindrical Coils: Coil Geometry and Resistance.....	121
B.2 Spiral Coils: Coil Geometry and Resistance .....	122

<b>C Appendix – Measurements of <math>Q</math></b>	123
C.1 Cylindrical Coils: Coil Geometry and $Q$ .....	123
C.2 Spiral Coils: Coil Geometry and $Q$ .....	124
<b>D Appendix – <math>S_{21}</math> Correction Factors</b>	125
<b>E Appendix – H-Bridge Schematic</b>	132
<b>F Appendix – Software</b>	134
F.1 Design Algorithms for Lumped Equivalent Models .....	134
F.2 Possible Coils .....	138
F.3 Simulation Programs .....	139
<i>F.3.1 First Module</i> .....	139
<i>F.3.2 Second Module</i> .....	140
<i>F.3.3 Third Module</i> .....	142

## List of Figures

Fig. 2.1	Canonical transformer structure. A primary and secondary coil with a linking magnetic core.	16
Fig. 2.2	High-level view of typical transformer with highlighted values of interest.	17
Fig. 2.3	Non-resonant inductive coupling system. The green lines represent the magnetic field generated by one coil that subsequently induces a voltage on the secondary to power the load canonical transformer structure. A primary and secondary coil.	20
Fig. 2.4	Resonant coupling system.	21
Fig. 2.5	4-coil resonant coupled system.	22
Fig. 2.6	The relationship between $k$ , $Q$ , and efficiency of resonant coil coupling.	22
Fig. 2.7	(a) Skin effect in isolated wire; (b) Skin and proximity effect for equal total currents in two adjacent round wires.	24
Fig. 4.1	Lumped equivalent model of a coil.	28
Fig. 4.2	An Bode100 measurement plot of Inductance. Note the area of zero-slope, an ideal region to determine the inductance of a coil.	30
Fig. 4.3	Single layer coil geometry for Nagaoka inductance calculation.	30
Fig. 4.4	Nagaoka coefficient, $K_n$ , values versus coil ratio: length/diameter.	31
Fig. 4.5	Nagaoka coefficient, $K_n$ , values versus coil ratio: diameter/length [18].	32
Fig. 4.6	Single layer coil geometry for Wheeler spiral inductance calculation [19].	33
Fig. 4.7	Example 3-turn spiral coil depicting parameters of interest (Yellow is copper wire, Blue is wire insulation).	34
Fig. 4.8	Error in inductance as a function of number of turns for cylindrical coils.	35
Fig. 4.9	Error in inductance as a function of number of turns for spiral coils.	36
Fig. 4.10	Configuration for $N = 4$ parallel wires, each carries equal current.	37
Fig. 4.11	(a) Bode100 resistance plot for coil of $c/a = 2.5$ . (b) Bode100 resistance plot for coil of $c/a = 1.5$ . (c) Bode100 resistance plot for coil of $c/a = 1.15$ .	38

Fig. 4.12	Current distribution in round wire due to skin effect.....	40
Fig. 4.13	Surface plot of $R_p/R_o$ as a function of $c/a$ and number of turns.....	42
Fig. 4.14	Error in resistance as a function of ‘ $c/a$ ’ for cylindrical coils.....	44
Fig. 4.15	Error in resistance as a function of ‘ $c/a$ ’ for spiral coils.....	45
Fig. 4.16	Example Bode100 $Q$ measurement plot.....	46
Fig. 5.1	An equivalent circuit representation for 2 coupled coils.....	48
Fig. 5.2	An equivalent circuit representation for 2 coupled coils using their ideal lumped equivalent models.....	49
Fig. 5.3	Experimental setup for measuring the coupling coefficient between a pair of coils. The left image is the setup for $L_1$ . The right image is the setup for $L_s$ .....	51
Fig. 5.4	Two coaxial coils of radius $r1$ and $r2$ , respectively.....	52
Fig. 5.5	Stacked ring-conductors representation of two coils.....	52
Fig. 5.6	Structure and calculation for two coaxial rings offset by ‘ $d$ ’.....	53
Fig. 5.7	Nested ring-conductors representation of two spiral coils.....	56
Fig. 5.8	Theoretical $k$ values for nested coils of varying lengths.....	57
Fig. 6.1	High-level schematic of 4-coil coreless transformer. There are four enumerated coils names that refer to the four coils of the system. The drive and load side are labeled in orange. The coupling coefficients and their linkages are shown in green.....	62
Fig. 6.2	Diagram of the 4-coil system with nested coils.....	63
Fig. 7.1	Output examples and input settings for <i>Possible_Coils.m</i> .....	70
Fig. 7.2	Bode100 circuit configuration for $S_{21}$ transmission coefficient measurement.....	72
Fig. 7.3	High-Level schematic depicting the operation of the H-bridge circuit[23].....	73
Fig. 7.4	Top view of amplifier PCB [23] .....	74
Fig. 8.1	LTspice Schematic of a 4-coil double resonant transformer. Note, all the values for parameters are in brackets. This allows them to be manipulated by the ‘.param’ line (located in the bottom of the image). MATLAB alters the parameter	

values via this line. Extraneous resistors represent air gap impedances and their presence is necessary but has no impact, thus they're large.....	77	
Fig. 8.2	Depicts the geometric quantities the program required as inputs and their relationship to the rest of the system.....	79
Fig. 9.1	Bode100 $S_{21}$ measurements and construction details for configuration #1 .....	94
Fig. 9.2	Bode100 $S_{21}$ measurements and construction details for configuration #2 .....	96
Fig. 9.3	Bode100 $S_{21}$ measurements and construction details for configuration #3.....	98
Fig. 10.1	Output pots of the <i>Possible_Coils.m</i> script used to evaluate the range of coils that are good candidates for coreless transformer design.....	102
Fig. 10.2	$S_{21}$ peak evaluation plots generated by plotting option #1. The left has a 1-turn drive coil and 4-turn load coil. The right has a 2-turn drive coil and 4-turn load coil.....	104
Fig. 10.3	Optimal $S_{21}$ peaks with a 1-turn drive coil and 4-turn load coil.....	105
Fig. 10.4	Optimal $S_{21}$ plots achieved with simulation (top) and measurement (bottom). ..	110
Fig. 10.5	Perturbations in $S_{21}$ as the drive and load coils are displaced from their optimal positions. (Top) The drive coil remains static as the load coil is shifted. (Bottom) The load coil remains static as the drive coil is shifted. ....	111
Fig. 10.6	Experimental setup to Evaluate the $S_{21}$ transmission coefficient of the system. .	112
Fig. D.1	Internal hardware setup of Bode100 during calibration .....	125
Fig. D.2	Equivalent circuit of the Bode100 calibration setup.....	125
Fig. D.3	Matched equivalent input and output impedances.....	126
Fig. D.4	Matched $R_{source} = R_{load} = 50 \Omega$ (left) and matched $R_{source} = R_{load} = 25 \Omega$ (right). The first image (starting from the top) is the correct $S_{21}$ Plot. The second is what the Bode100 will initially measure. The third plot (blue) is the voltage correction factor 'alpha'. Note for the 50/50 case, the value of alpha is 1 as expected. Finally, the last plot is the corrected Bode100 plot which is derived from the second and third waveform. ....	127
Fig. D.5	Unmatched equivalent input and output .....	128
Fig. D.6	Unmatched $R_{source} = 16$ , $R_{load} = 50$ (left). Unmatched $R_{source} = 50$ , $R_{load} = 12.5$ (right). The first (top) plot is the correct $S_{21}$ plot. The second (gray)	

represents the base Bode100 measurement. The third (green) plot is the Bode100 ‘alpha’ correction factor and the fourth (red) is Bode100 output (which includes its correction factor). Since the resistors are unmatched, an external ‘beta’ correction factor and resistive factor is needed. The light blue curve is the original bode100 plot with the beta factor and the dark blue is the resistive factor. Finally, the sixth (pink) is the final ‘corrected’ plot and matches the first (top). ..... 130

Fig. D.7	Unmatched Bode100 outputs and their adjusted plots. The adjusted plots agree with simulation results. The first (top) plot is the correct $S_{21}$ plot. The first columns display each row’s source and load resistance and the Bode100 output. The second column displays the adjusted graphs and the corresponding beta and resistor factor used to obtain it.....	131
Fig. E.1	Schematic of power amplifier circuit that splits the input drive signal, creates dead-time and allows on/off capability [23] .....	132
Fig. E.2	Schematic of 12V to 5V converter and H-bridge input filter [23].....	132
Fig. E.3	Schematic of H-bridge outputs A and B [23] .....	133

## 1. Introduction

The transformer has been a pivotal device in the large-scale transmission and delivery of electrical energy since its commercial success in the late 1800's. It's official conception dates back to May 1885, when three young engineers of the Hungarian Ganz factory, Zipernowsky and associates, demonstrated what is generally considered to be the prototype of today's lighting systems. They were able to illuminate the Industrial Exhibition of Budapest-1,067 60V incandescent lamps-via 75 toroidal, iron core transformers connected in parallel to a 1350V AC generator [1]. Shortly after, William Stanley modified the Hungarian design for ease of manufacturing and costs and founded the "Stanley Transformer", which demonstrated step-up/step-down capabilities and electrified downtown Great Barrington, MA [2]. What followed were decades of expansion in AC electric power systems through the 20<sup>th</sup> century as electricity and transformers became a critical part of the economic infrastructure of most industrialized nations. Transformers increased in size and power rating, with large units used for the power transmission grid and vastly more, smaller units used in the electric power distribution system.

The basic physical principles of transformers remain the same today as they were 130 years ago, though efficiency, costs, weight, versatility, and dimensions have drastically improved. Today's transformers can operate up to the megavolt level and handle more than a million kVA with lifetimes of 25-40 years. However, transformers present a huge expense to power companies due to their high costs and weight associated with their required steel core and copper windings. Additionally, the U.S has spent an average of \$800 million in importing large power transformers per year in the last 5 years [3]. Therefore, although the steel core has been a staple in transformer engineering for years, perhaps a radically different design could mitigate the climbing costs of these indispensable devices.

Another fascinating technology that isn't as mature as the transformer is wireless power transmission (WPT). This topic is of interest because of lessons learned about power transfer across air gaps, even though often intended for variable spacing or moving situations. The conception of wireless power began in the late 19<sup>th</sup> century when both Heinrich Hertz and Nikola Tesla theorized and demonstrated its capabilities, with Tesla reporting the powering of fluorescent lamps 25 miles from the power source without using wires [4]. In 1964, William C. Brown invented the rectifying antenna and was able to power a helicopter using microwave technology. Then in 1968, Peter Glaser theorized solar powered satellites which could receive

the sun's energy 24/7 via photovoltaic cells, convert it to RF microwave energy, and beam it to Earth [5]. Unfortunately, many of the early research forays into wireless power transfer were halted and did not lead to widespread applications, but there remained a spark of optimism.

At the end of the 20<sup>th</sup> century there was regained interest in WPT specifically in areas of powering implanted medical devices and wireless consumer electronics. One interesting attribute of most wireless power systems is the use of resonant coupling and operation at high frequencies without the need for iron or other magnetic cores. In 1990, Bo Cho used a pair of coupled circuits operating at a resonance mode to transfer 48W at an energy efficiency of 72% for transcutaneous energy transmission [6]. Even a small planar coreless transformer was built using external capacitors and resonance in 1998 for transferring power and signals [7]. In the biomedical research community, John Schuder built magnetically coupled spiral coils with litz wire, operated them at a resonance mode of 480kHz, and transferred 1kW through the skin of a dog in 1971 [8]! In 1977, medical applications lead to theoretical analysis of resonant power transfer and suggested conditions to obtain high efficiencies [9]. Even though circuit applications differ, the same underlying theory of magnetically coupled resonant circuits unifies these efforts.

This thesis will continue to bridge the engineering gap between canonical transformer design and modern wireless power transfer schemes with the construction of a coreless power transformer. A thorough evaluation of the characterization of coils is investigated to understand the impact of copper conductors, magnetic coupling, and the calculation of transformer transfer characteristics. Given the formulaic complexity of such a system, heavy emphasis is given to accurate simulation results. Simulations aid in the intuitive understanding of the system and guide the trajectory to achieve higher efficiencies.

In Chapter 2, a brief survey on the current state of the art in coreless transformer design, wireless power transmission research, and electromagnetic phenomena observed during high-frequency operation of copper coils is presented. Chapter 3 details the thesis' motivation and goals. Chapter 4 presents a study of high-frequency coil design with the objective of quantifying inductance and coil losses to achieve higher  $Q$  for isolated coils. A design algorithm for calculating the high frequency resistance is elaborated. Chapter 5 considers a pair of coils in close proximity and the mutual magnetic interaction between them. A design algorithm is presented for calculating the degree of coupling among pairs of coils. Chapter 6 extends the concepts of Chapter 5 to include systems of multiple coils and introduces a configuration for

developing a coreless 4-coil transformer. Chapter 7 provides an overview of the system built in this thesis and the measurement technique used to evaluate its performance. Chapter 8 describes the design methodology used to simulate, predict, and assess the performance of possible coreless transformer designs. Chapter 9 offers an experimental validation of the simulation software developed in Chapter 8. Chapter 10 describes the final design of this work that provides a demonstration of the feasibility of coreless transformer systems. Chapter 11 concludes the thesis proper and provides a summary of operation of the final design, topics for further work, and final remarks. Finally, the appendices provide technical documentation associated with the calculations employed in this thesis.

## 2. Background and Literature Review

This section will discuss classic transformer design, the need to develop high frequency operation, the consequences due to high frequencies, and the reasons for proposing a coreless design. Next, near-field wireless power schemes will be explored and the document will build up to the scheme implemented in this thesis. The novel transformer is then introduced and the thesis will dive into the physics of the components necessary to realize a high efficiency device. One of these components is solid copper, and its behavior under high frequencies is discussed.

### 2.1 The Classic Transformer

A transformer is a device that transfers electrical energy between two or more circuits through electromagnetic induction. A varying current in one coil of the transformer produces a varying magnetic field, which in turn induces a voltage in a second coil. Power can be transferred between the two coils through the magnetic field without a metallic connection between the two circuits, the effect described by Faraday's law of induction [10]. The classic transformer does this by strongly linking together electrical circuits using a common oscillating magnetic circuit. The material used to guide the field in the magnetic circuit is known as the 'core' and tightly links the multiple electric coil circuits together magnetically. Fig. 2.1 depicts a basic transformer structure. Considering the magnetic flux to be uniform (and lossless) around the core means that both coils experience the same main flux and thus, from a result of Faraday's Law (Eq. 2.1), Eq 2.2 can be concluded: the canonical transformer voltage relationship.

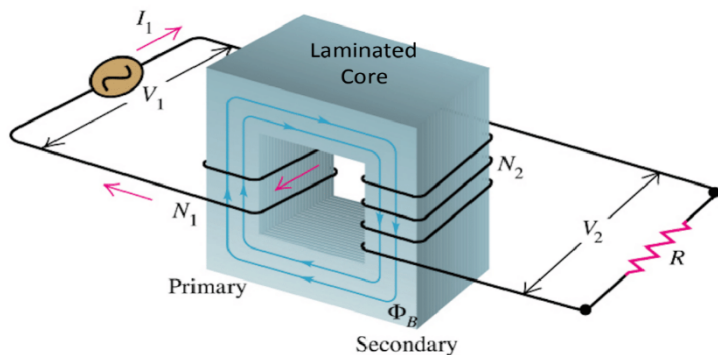


Fig. 2.1: Canonical transformer structure. A primary and secondary coil with a linking magnetic core.

$$V = N \frac{d\varphi_B}{dt} \quad (\text{volts}) \quad (\text{Eq. 2.1})$$

$$\frac{V_1}{N_1} = \frac{V_2}{N_2} \quad (\text{Eq. 2.2})$$

### 2.1.1 Power and Size Scaling Relationship

Transformers have an interesting relationship between their rated power, frequency of operation, and size. The overall power rating of a transformer can be calculated by calculating the voltage induced by its main flux on a coil winding and calculating the current in the winding. The voltage can be derived by a direct application of Faraday's law with the assumption of sinusoidal oscillations and knowing that the magnetic flux encapsulated by the magnetic core is proportional to its magnetic flux strength,  $B$ , and its cross-sectional area,  $A_c$ , Eq. 2.3. The winding current can be determined by the allowed current density of the wire,  $J_{\text{wire}}$ , and the winding window area,  $A_W$ , Eq. 2.4. Fig. 2.2 depicts a typical transformer with the areas of interest highlighted. Using Eq. 2.3 and 2.4, one can calculate the power transferred to a linked coil, Eq. 2.5. The cross-sectional area can be related to the winding area by considering a 'winding fill factor',  $K_U$ .

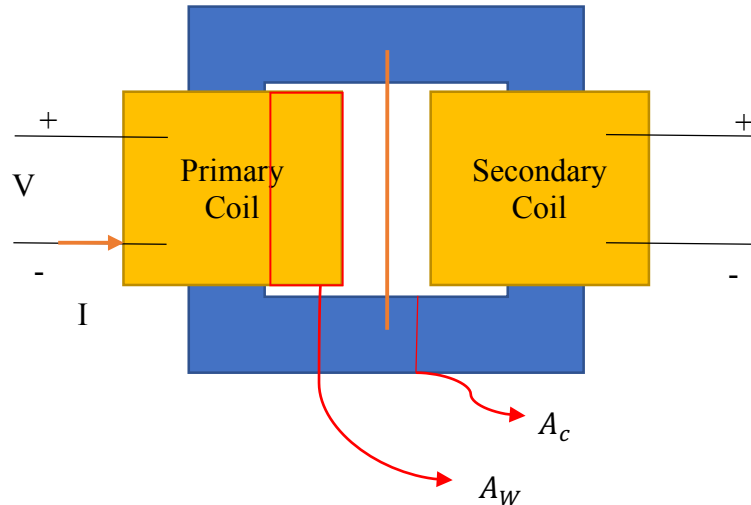


Fig. 2.2: High-level view of typical transformer with highlighted values of interest

$$V = N \frac{d\varphi_B}{dt} = \frac{1}{\sqrt{2}} \omega NBA_c = \frac{2\pi}{\sqrt{2}} NfBA_c \quad (\text{volts}) \quad (\text{Eq. 2.3})$$

$$I = J_{\text{wire}} A_W \quad (\text{amp}) \quad (\text{Eq. 2.4})$$

$$P = IV = \frac{2\pi}{\sqrt{2}} NfBA_c * J_{\text{wire}} A_W \quad (\text{watts}) \quad (\text{Eq. 2.5})$$

$$A_W = K_U A_C \quad \text{thus} \quad P \propto f A_C^2 \quad (\text{Eq. 2.6})$$

A key observation about the resulting power equation is that it's linearly proportional to frequency and quadratically proportional to area. Thus, running a transformer at the kilohertz regime as opposed to a standard frequency of 60Hz, would allow one to decrease the size of the device by an order magnitude and still process the same power! Therefore, a physically small and cheaper transformer could handle power levels that would require a massive iron core at mains frequency. A few modern-day systems take advantage of these tradeoffs. One example is aircraft electrical systems that run at 400Hz instead of 60Hz. This allows minimization of power supplies and electronics; an important benefit since it's imperative to minimize occupied space and weight of components in such environments. Any small reduction in electronic weight can be amplified 5x due to the subsequent reduction in extra structure and fuel needed to carry it around [11]. Currently in the US (and world-wide), electrical steel is specially tailored to produce desirable magnetic properties and is the most common material used. It has been estimated that on average, electrical steel accounts for nearly 25% of the total weight of large transformers, which is weight that requires specialized transportation systems to migrate [12]. Therefore, although aircraft systems are especially austere over the weight they carry due to their operating environment, large power transmission systems could also benefit from lighter transformers due to their decreased transportation costs.

However, there are a couple consequences to increasing the frequency in present transformer designs. These downsides can be attributed to winding and core losses, each of which increase with frequency. The next section will discuss the importance of the core in classic transformer design and will elaborate on its contribution to high frequency losses. Winding losses will be discussed in the last section of this literature review.

## 2.2 The Transformer's Core

The parameters that characterize transformers depend to a large extent on the properties of the core. The properties that are important in core materials are permeability, saturation, resistivity, and hysteresis loss. Magnetic permeability ( $\mu$ ) refers to the amount of magnetic flux density produced in response to a given magnetic field intensity. Saturation designates the point at which the material's flux density no-longer increases linearly with magnetic field intensity, and at full saturation does not change with increased magnetic fields. Higher resistivities minimizes energy loss due to eddy currents. Finally, hysteresis corresponds to the tendency for the magnetic core to retain its polarization during oscillations, causing losses and reducing the efficiency. To approach the ideal transformer, one desires to increase permeability, saturation, and resistivity while decreasing hysteresis losses.

For higher operating frequencies, core losses drastically increase and contribute to the majority of energy loss in transformer systems via hysteresis loss and eddy current loss. Higher operating frequencies and lower volume cause the loss density to increase drastically, resulting in higher temperature, which may deteriorate insulation and decrease the effective lifetime.

The novel design choice considered in this thesis seeks to eliminate the magnetic core and develop 'air-core', or 'coreless' highly efficient high-frequency transformers. A coreless design has a number of key benefits:

1. Allows for efficient high frequency operation that subsequently enables the use of smaller energy storage elements, thus decreasing the size and weight of the device.
2. Reduce the costs in manufacturing and transportation that would otherwise have been consumed by producing and migrating the magnetic materials.
3. A reduction in heat yields a longer lifespan and reduces costs for maintenance involving insulation and thermal care.

Wireless power transfer technology can provide intuition and act as a guide for coreless transformer design. Thus, an overview of wireless power schemes will be presented.

### 2.2.1 Non-Resonant Inductive Coupling

Inductive coupling is the simplest structure for magnetically linked circuits, with applications in cordless products used in wet environments and transcutaneous recharging of biomedical devices implanted in the body. Here, a portion of the magnetic flux from a drive-side coil couples to a

load-side coil. This is inefficient since a substantial portion of the drive flux is not linked to the load. Note that when a core is present, this non-resonant coupling is similar to the core-type transformer discussed in the prior section.

An experimental realization of the scheme involves the use of a transmitter unit consisting of an oscillator that produces an alternating current of the desired frequency in the ‘primary’ coil. Most systems generate the oscillations at higher frequency because coil size can be reduced as frequency is increased. The alternating current produces an alternating magnetic field which couples to the ‘secondary’ coil in the receiver unit and induces a voltage in it. The induced alternating current may either drive the load directly or be rectified to power the load, Fig. 2.3.

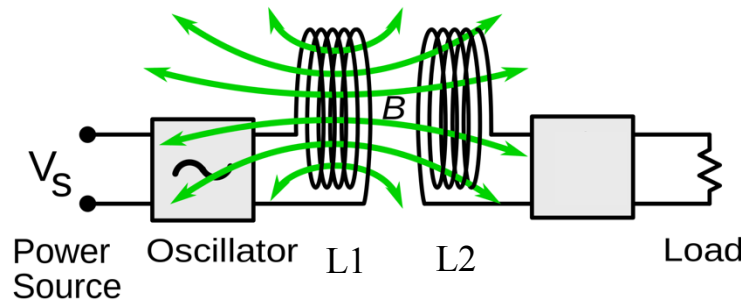


Fig. 2.3: Non-resonant inductive coupling system. The green lines represent the magnetic field generated by one coil that subsequently induces a voltage on the secondary to power the load

The power transferred is proportional to the frequency of operation and the mutual induction between the coils participating in the magnetic energy transfer. The mutual induction is a factor dependent on the coil geometry and distance between the pair of coils. The coupling coefficient,  $k$ , is a normalized value widely used to quantify the amount of coupling between two coils and is found with Eq. 2.7, where  $L_1$  and  $L_2$  represent the inductance of the two coils individually, and  $M$  is the mutual inductance.

$$k = M / \sqrt{L_1 L_2} \quad (\text{Eq. 2.7})$$

The coupling coefficient is equal to the fraction of the magnetic flux through the transmitter coil  $L_1$  that passes through the receiver coil  $L_2$  when  $L_2$  is open-circuited. If the two coils are on the same axis and ideally close enough, such that all the magnetic flux from  $L_1$  passes through  $L_2$ , then  $k=1$  and the link is 100% efficient. The greater the separation between

the coils, the more magnetic flux from the first coil fails to link to the second, and the lower the  $k$  value, and hence the link efficiency approaches zero at large separations. In order to increase efficiency, the coils must be very close together, a fraction of the coil diameters, with the coil axes aligned [13].

### 2.2.2 Tuned Double Resonant System

Now, consider adding a capacitor in parallel with each coil depicted in the previous section for non-resonant coupling, Fig. 2.4. Each resonant coil now becomes a series resonant tank circuit. A measure for the resonance property is the quality factor,  $Q$ , where:

$$Q = \frac{1}{R} \sqrt{\frac{L}{C}} \quad (\text{Eq. 2.8})$$

$R$  represents the series resistance and is composed of the resistance of the coils and the ESR of the capacitor. Thus, the  $Q$  factor represents a normalized amount of loss. For a series tank the lower the loss resistance  $R$ , the higher the  $Q$ .

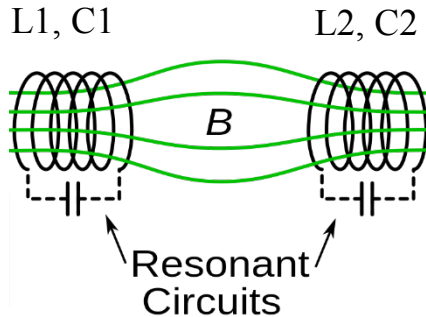


Fig. 2.4: Resonant coupling system.

Now, rename the two coils in Fig. 2.4 to  $L_2$  and  $L_3$  and consider introducing two additional coils,  $L_1$  and  $L_4$  in the manner shown in Fig. 2.5. These two added coils represent a convenient means to couple energy into and out from the resonant coil pair. Since the resonant coils are not electrically connected to the source and load, they only see the source or load impedance transformed by the ‘turns’ ratio of  $L_1$  to  $L_2$ , and  $L_4$  to  $L_3$ . These two added coils improve the isolation of the resonant circuits from the source resistance  $R_1$  and the load  $Z_L$ , so their Q factor is influenced more weakly by these external parameters. The drive and load coils are generally formed using a smaller amount of turns for minimal impedance and play a role in ensuring high efficiency under different regimes of resonant coupling.

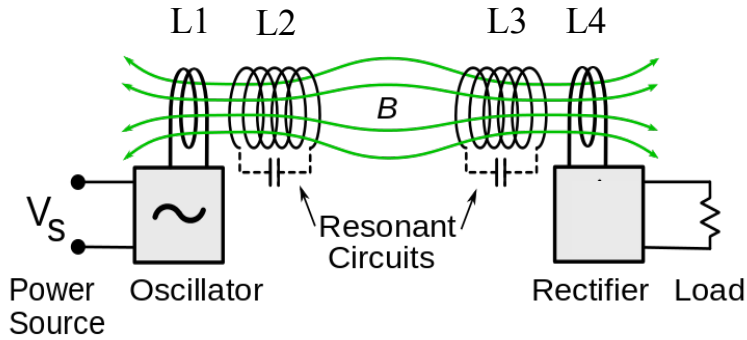


Fig. 2.5: 4-coil resonant coupled system

Calculations and simulation work [9,14] has shown that a figure of merit, *FOM*, for the performance of these coils operating as a transformer is given as Eq. 2.9. The way it relates to the overall efficiency is given by Eq. 2.10, where *Q* is defined by Eq. 2.8 and *k* by Eq. 2.7 for the two resonant coils. A graph depicting the relationship between maximum efficiency and *k* for different values of *Q* is shown in Fig. 2.6.

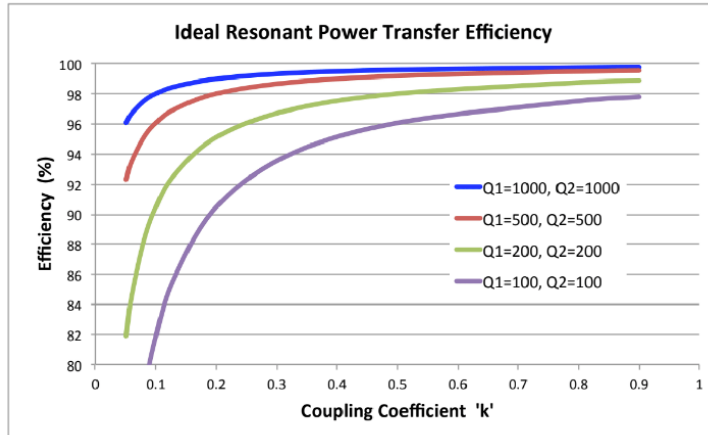


Fig. 2.6: The relationship between *k*, *Q*, and efficiency of resonant coil coupling

$$FOM = k\sqrt{Q_1 Q_2} \quad (\text{Eq. 2.9})$$

$$\eta_{max} = \frac{k^2 Q_1 Q_2}{[1 + \sqrt{1 + k^2 Q_1 Q_2}]^2} \quad (\text{Eq. 2.10})$$

Since a coreless transformer design will be lacking a magnetic core to guide the magnetic field coupling the main resonant coils, the coupling factor, *k*, typically will not be very large (<.5). Therefore, in order to reach high levels of efficiencies, the resonant coils used in the

system must be of adequate  $Q$ . The next section will discuss the difficulties in designing high- $Q$  coils and the progress made in calculating the loss parameters of coils.

### 2.3 High-Frequency Coil Characteristics for $Q$

The efficiency and range for the coreless power transfer schemes discussed are limited by the quality factor of the resonant coils that generate the electromagnetic coupling. The quality factor,  $Q$ , indicates energy stored relative to the amount of energy loss within a system; hence, a measure of energy transport efficiency. A higher- $Q$  coil results in a higher performance coil that attenuates oscillations less. In a theoretical system where the  $Q$  factor is infinite, oscillations would be maintained indefinitely.  $Q$  is calculated by Eq 2.8, where  $L$  represents the inductance of the coil in Henries,  $R$  is the resistance of the coil in Ohms, and  $C$  is the effective capacitance in Farads at the resonant coils. Therefore, to obtain high- $Q$  coils one would desire to decrease the total coil resistance while simultaneously increasing the frequency of operation (reduced  $C$ ). However, at high frequencies ‘skin’ and ‘proximity’ effect losses in the conductive material can introduce a problem in constructing high- $Q$  coils.

A coil’s high-frequency resistance includes 2 separate factors: the ‘skin’ effect and the ‘proximity’ effect. The ‘skin’ effect represents the physical process whereby the current carried in the wire conductor is confined to a thin layer near the wire surface. This conducting layer becomes thinner as frequency is increased and is caused by magnetic diffusion, which restricts the time for the penetration of the current into the interior of the wire. The result is at higher frequencies, all the current carried by a wire conductor resides near the surface, reducing the effective cross-sectional area, and increasing the effective total resistance. This skin-effect is depicted in Fig. 2.7a where the current is restricted to a skin depth of ‘ $d_s$ ’.

The ‘proximity’ effect represents the physical process whereby currents in adjacent conductors influence the radial distribution of current in a wire. For two adjacent wires with equal currents in the same direction, the current in one wire causes the current in the other to be pushed to the more distant surface region as in Fig. 2.7b. The result when wires are close together is the currents in each are restricted to flow in a more limited region of the wire cross-section. Hence, the ‘proximity’ effect acts to further increase the effective resistance of the wire.

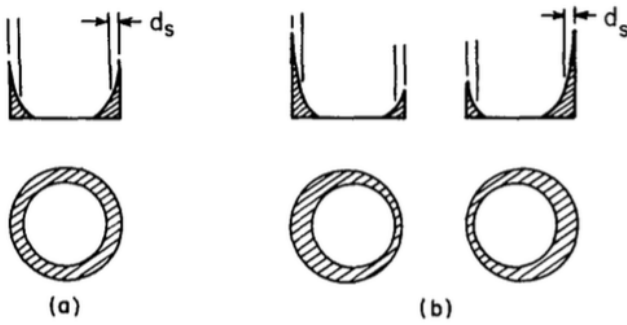


Fig. 2.7: (a) Skin effect in isolated wire; (b) Skin and proximity effect for equal total currents in two adjacent round wires [16]

Certain measures can be taken to combat these high-frequency effects. A common approach is to construct coils using litz wire. Litz wire consists of many thin wire strands, individually insulated, twisted, and woven together into a prescribed pattern. The result of these winding patterns is to equalize the proportion of the overall length over which each strand is at the outside of the conductor. Thus, it has the effect of distributing the current more equally among the wire strands, reducing the resistance. The downside to implementing coils with litz wire is that the small stranded diameters that compose the wire are more difficult to manufacture and can be too expensive for the amount of benefit they provide electrically. However, despite the adverse physics of the situation, research has been performed to quantify and mitigate the effects on high frequency coil operation.

The work presented in this section serves as foundational material that inspired the start of this thesis. Although there have been many monumental findings, there are even more open-ended curiosities left to resolve and evaluate. Now that the background information on this area of research has been reviewed, the next section will discuss the objectives and motivation for pursuing this thesis project.

### 3. Objectives and Motivation

The main goal of this thesis is to create a design methodology for building highly efficient, high frequency coreless transformers. The approach taken is to employ first principles for the underlying physics to determine all needed parameters and then calculate the performance of a full multi-coil coreless transformer. The starting point is the electrical properties and size of the wire conductor, along with the actual winding dimensions and geometry for each of the coils and their relative positions. Such a ‘material-to-performance’ calculation will enable efficient evaluation of design choices and improve understanding of optimized coreless power transformers.

Among the topics required are high frequency wire conductor losses, coil inductance and multi-coil magnetic coupling values. The resultant calculated lumped parameter circuit elements for the coupled coils can then be employed in circuit simulation to calculate the full coreless transformer performance characteristics, such as transfer efficiency. The methodology can encapsulate design algorithms that describe lumped circuit element behavior and seek to accurately predict essential values of operation such as inductance and coupling coefficients. The process can be validated with a number of example topologies. The desire is to achieve resultant power transfer behavior given basic physical attributes related to materials and geometry of design in different regimes of operation.

There have been efforts in deriving a formula for the efficiency,  $\eta$ , of a 4-coil system by relating the most influential coupling coefficients to the circuit impedance parameters [15]:

$$\sqrt{\eta} = \frac{2\omega^3 k_{12} k_{23} k_{34} L_2 L_3 \sqrt{L_1 L_4 R_S R_L}}{Z_1 Z_2 Z_3 Z_4 + k_{12}^2 L_1 L_2 Z_3 Z_4 \omega^2 + k_{23}^2 L_2 L_3 Z_1 Z_4 \omega^2 + k_{34}^2 L_3 L_4 Z_1 Z_2 \omega^2 + k_{12}^2 k_{34}^2 L_1 L_2 L_3 L_4 \omega^4}$$

Although this defines the system to some degree, intuition about the coil topology, size, and positions can't be gleaned from the formula directly and thus still poses a challenge in the design process. This formula also doesn't consider the effects of the other three coupling coefficients, ( $k_{13}, k_{24}, k_{14}$ ), which typically tend to be smaller relative to the other three, but may also have important impacts on the system performance. Nor does this simplified model deal with the reality that only certain combinations of  $k_{xy}$  values are physically realizable.

Therefore, to develop intuition and guide the engineering of these structures, simulation programs will be built using MATLAB and LTspice software. These simulations will be validated to work in a number of different cases, describing different physical scenarios, and will provide accurate predictions of efficiency given a user-defined 4-coil geometry. Physical arrangement values can be manipulated by the user in order to observe the result of changing parameters such as number of turns on specific coils, series-connected capacitance on each resonant coil, distance between coils, etc.

The efficiency plot in Fig. 2.6 reveals evidence that to achieve highly efficient design in the case of moderate valued coupling coefficients, coils must be carefully designed to maximize their  $Q$ . Since  $Q$  is inversely proportional to the resistance of the coils, there is a need for low loss coils to satisfy the high- $Q$  requirement. An adequate spacing between adjacent conductor turns of a wound coil can reduce losses, through decreased proximity effect, and enables higher  $Q$  designs. Although Smith [16] theoretically determined the proximity effect for up to 8 parallel conductors, his research lacks the effects on a system with a larger set of conductors. This means a thorough investigation and validation of the proximity effect for coils of larger turn numbers is necessary in order to accurately represent the coils in simulation.

For a 4-coil double resonant system described in section 2.2.2, there are a total of six coupling coefficients that play a role in the overall system efficiency. No modern research has taken into consideration the effect of all six parameters. Evident from the equation above that approximates the efficiency of the full system, coil inductances, impedances, and the mutual coupling among all coils play a role in power transfer. Coil coupling is defined by the configuration of the coils and the inductances of each coil individually. 4-coil systems have a flexible wide range of possible physical arrangements and thus, it is desirable to calculate  $L$  and  $k$  values to predict the efficiency of a specified coil geometry.

There are two convenient designs for transmission coils: Spiral (or Planar) and Cylindrical. Their unique trade-offs against inductance and resistance, the constituents of  $Q$ , aren't intuitive, especially considering the proximity effect. Additionally, quality of coupling with other coils of the same type hasn't been evaluated in the literature. Therefore, in order to produce optimal design, this thesis will explore their behavior and abstract their physical geometries as lumped circuit elements to be applied in simulations.

Once each coil's  $Q$  and each pair of coil's  $k$  can be precisely evaluated, simulation software, like LTSpice, will employ the lumped equivalent values of different coil arrangements. Although LTspice alone can handle multiple simulations, a joint program with MATLAB acting as the user interface can ease value manipulation for discovering trends and engineering decisions. Once validated, the result of this thesis project will greatly aid the design of coreless transformers.

Chapter 4 will dive into the preliminary work and investigation on the copper losses experienced by coils operating at high frequencies. It will experimentally show the skin and proximity effect and assess their severity over a range of designs. Design algorithms to predict the resistance and inductance for each coil geometry considered are developed and evaluated. Spiral and Cylindrical coils will be examined as well as their respective relationships with  $Q$  and  $k$ . What results is guidance on designing high- $Q$  coils.

## 4. Electrical Characteristics of High Frequency Coils

In this chapter, design relationships for inductance, resistance, and quality factor are developed for air-core cylindrical and spiral windings suitable for high frequency operation. Because of skin and proximity effect losses, high frequency windings are typically less-tightly wound than those used for classical power inductors and transformers to inhibit the exacerbation of resistance. Also, at high frequencies much less inductance is needed to achieve the same impedance levels as at low frequencies; therefore, HF windings are typically single-layered and often relatively of short length compared to their diameter. The focus of this analysis is on simple round cross-section metallic wires, typically of copper or aluminum. Other conductor shapes will require different impedance models. However, the fundamental processes and analysis procedures are well represented by the round conductor format, and hence these provide a good basis for future evaluations.

Fig. 4.1 displays a lumped equivalent model for the coils under the frequencies considered in this thesis.  $L$  is the ideal inductance of the coil, representative of the energy storage capabilities of the coil, and  $R_s$  is the equivalent series wire resistance of the coil, representative of the energy loss in the coil.

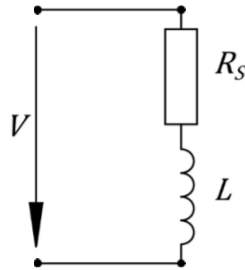


Fig. 4.1: Lumped equivalent model of a coil

This chapter will focus on the characterization of spiral and cylindrical coils by fitting them to the lumped equivalent model in Fig. 4.1. Subsection 4.1, will focus on the inductance of spiral and cylindrical coils. Subsection 4.2 focuses on the resistance of uniformly wound wire. Both of these sections introduce MATLAB design algorithms created to perform the theoretical formulas required by each coil's lumped parameters. Subsection 4.3 closes with a useful figure of merit representative of the energy transfer efficiency of the coils:  $Q$ .

## 4.1 Inductance of Coils

The inductance of a coil describes its aptitude for energy storage in the form of a magnetic field, an important property in constructing wireless power systems and transformers. Inductance is primarily a geometry driven problem with slight dependence upon the conduction properties of the winding material, typically copper or aluminum. Thus, the geometric details of the coil structures are carefully identified to enable the validity of the developed formulas.

First, an inductance measurement plot produced by the Bode100 vector network analyzer [17] is examined. Next, a method of calculating the inductance of single-layered cylindrical and spiral coils is described. MATLAB implementations of these derivations are presented as well. Finally, the developed design algorithms will be compared against measurements for over 50 manually crafted designs. While these calculations and measurements were made for solid round conductors, moderate deviations are expected if the conductor shape is changed to square or somewhat elongated forms. A high degree of accuracy means these tools could aid in the precise prediction of values important to efficiency and can lead to better transformer designs.

### 4.1.1 Measuring Inductance

Consider Fig. 4.1 as the model for a solid copper air coil. At low frequencies, the coil's series resistance,  $R_s$ , dominates the measured impedance. However, at higher frequencies, the inductance dominates the impedance and is therefore measured more precisely. Hence, to measure the inductance of a coil accurately, one must obtain the measurement in a region of high enough frequency. An example coil inductance measurement using the Bode100 is shown in Fig. 4.2, where the green-dashed line indicates a region of zero slope, an adequate frequency to obtain a measurement for this coil. Note at the highest frequencies, above 1 MHz, other parasitic effects distort the response. This region of operation is beyond the scope of this thesis.

It is desirable to find a means for calculating the inductance of the coil geometries studied in this thesis. Spiral and Cylindrical coils have different topologies and must be handled accordingly in order to obtain accurate results.

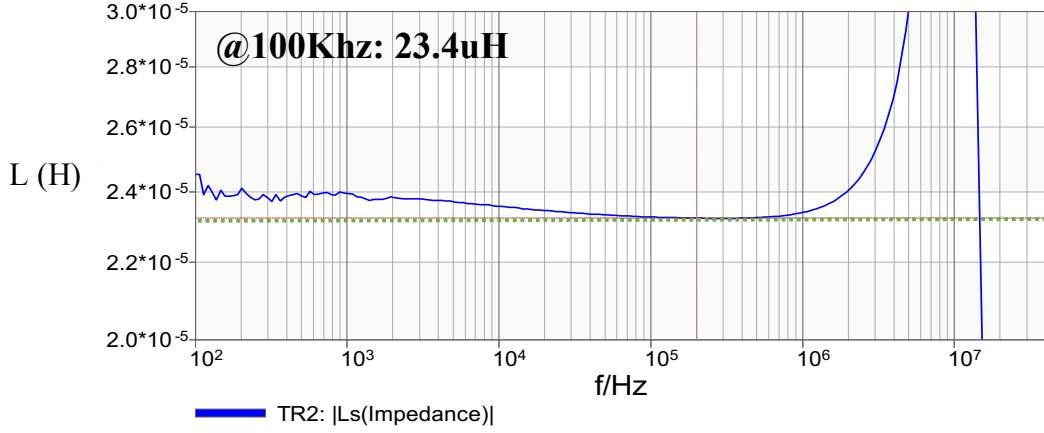


Fig. 4.2: An Bode100 measurement plot of inductance. Note the area of zero-slope, an ideal region to determine the inductance of a coil.

#### 4.1.2 Cylindrical Coils

Nagaoka calculated an ‘exact’ expression for the inductance of a single-layer solenoid, or cylindrical coil, of any length [18]. He assumed the coil was composed of thin ‘sheet-like’ conductors of  $N$  turns at a coil radius,  $r_c$ , with total coil length,  $l_c$ . The formula is that of a long solenoid multiplied by a ‘Nagaoka-factor’,  $K_n$ , which only depends upon the ratio of the coil diameter,  $d_c = 2r_c$ , to the coil length,  $l_c$ . Note, that the length of the coil for the Nagaoka formula,  $l_c$ , is defined as the *end-to-end* distance between the outer- edges of the end turns of the copper conductor. The coil radius,  $r_c$ , is the mean radius and for round wires is to the center of the wires. An example cylindrical coil is displayed in Fig. 4.3 and depicts the coil geometry quantities of interest.

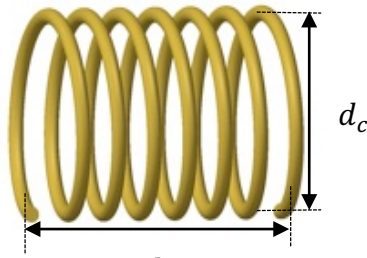


Fig. 4.3: Single layer coil geometry for Nagaoka inductance calculation

The Nagaoka general solution for the inductance,  $L_n$ , of a cylindrical coil of  $N$  turns with coil length,  $l_c$ , and coil radius  $r_c$  is:

$$L_n = 4\pi N^2 \frac{\text{Area Cross Section}}{\text{Length}} K_n \quad (\text{Eq. 4.1})$$

where  $K_n$  is the Nagaoka Coefficient:

$$K_n = \frac{4}{3\pi} \frac{1}{k'} \left\{ \frac{kr^2}{k^2} (K(k) - E(k)) + E(k) - k \right\} \quad (\text{Eq. 4.2})$$

with

$$k^2 = \frac{r_c^2}{r_c^2 + (\frac{l_c}{2})^2} \text{ and } k'^2 = \frac{(\frac{l_c}{2})^2}{r_c^2 + (\frac{l_c}{2})^2} \quad (\text{Eq. 4.3})$$

where  $K(k)$  and  $E(k)$  are the complete elliptic integrals of the first and second kind respectively over the variable  $k$ . Converting to coil diameters and relating  $k$  to  $k'$ :

$$k = \frac{1}{\sqrt{1+(\frac{l_c}{d_c})^2}}, \quad k' = \sqrt{1 - k^2} \quad (\text{Eq. 4.4})$$

Note, the Nagaoka coefficient,  $K_n$ , depends *only* on the ratio of coil (length / diameter). Hence,  $K_n$  has been calculated separately and plotted as a graph for those who cannot access the Elliptic functions to make their own calculations. Fig. 4.4 depicts  $K_n$  extending to long lengths while Fig. 4.5 depicts  $K_n$  for reciprocal ratio (diameter/ length).

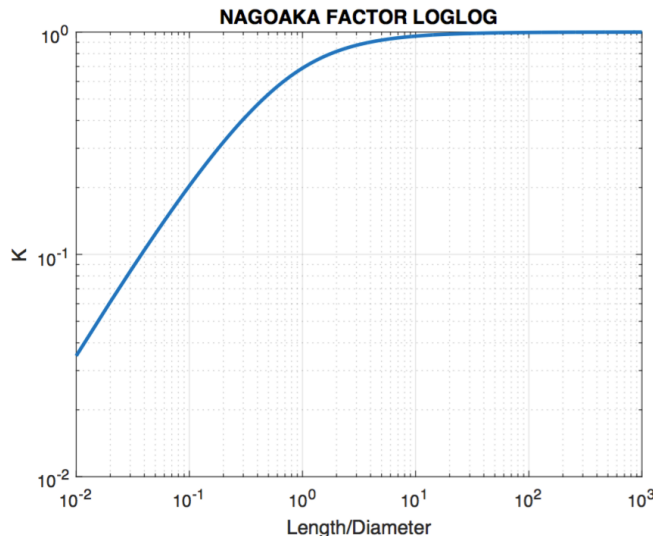


Fig. 4.4: Nagaoka coefficient,  $K_n$ , values versus coil ratio: length/diameter

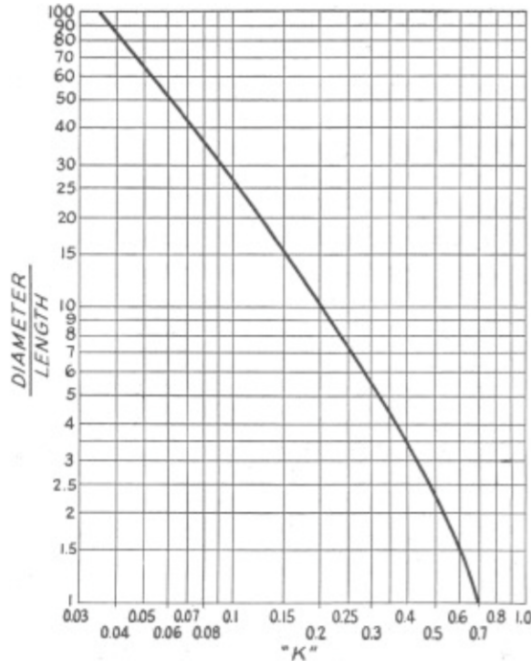


Fig. 4.5: Nagaoka coefficient,  $K_n$ , values versus coil ratio: diameter/length [15]

The Nagaoka coefficient  $K_n$  tends toward unity as the coil length becomes long compared to the coil radius, and hence the Nagaoka inductance converges to the ideal solenoid inductance. Additional forms for the Nagaoka calculated inductance in Henries, following from Eq. 4.1, are:

$$L = \mu_0 \frac{\pi r_c^2 N^2}{l_c} K_n = (4\pi * 10^{-7}) \frac{\pi r_c^2 N^2}{l_c} K_n = \frac{4\pi^2 r_c^2 N^2}{l_c} (10^{-7}) K_n \quad (H) \quad (\text{Eq. 4.5})$$

Since  $K_n$  is always  $\leq 1$ , the inductance of a short coil is always less than what the long-coil formula predicts. From Fig. 4.4, when a coil diameter is 10x the coil length, that coil inductance is about 1/5<sup>th</sup> that of the long-coil formula. Even for a coil of Length = Diameter, the inductance will be about 70% that estimated by long-coil formula.

A MATLAB function has been created to implement the equations that calculate the inductance of a cylindrical coil. The needed inputs and the resultant output are presented below.

### *Cylindrical Inductance*

#### Inputs:

- Do:** Outer diameter of the coil (inches)
- I:** end-to-end wire length of the coil,  $l_c$  (inches)
- N:** Number of turns comprising the coil

**Outputs:**

L: The Inductance of the cylindrical coil (Henries)

#### 4.1.3 Spiral Coils

Wheeler derived a formula for the inductance of a single-layer spiral coil [19]. The formula from the document is given by Eq. 4.6 and the corresponding physical geometric quantities for calculation are depicted in Fig. 4.6. The formula has been shown correct to within 5% for coils with  $c > 0.2a$ , or equivalently where the radial length of the coil that is comprised of wires is sufficiently larger than the mean radii of coil turns. Accuracy will also falter when there are too few turns or when the spacing between turns is too great.

$$L = \frac{a^2 n^2}{8a + 11c} \quad (\text{Eq. 4.6})$$

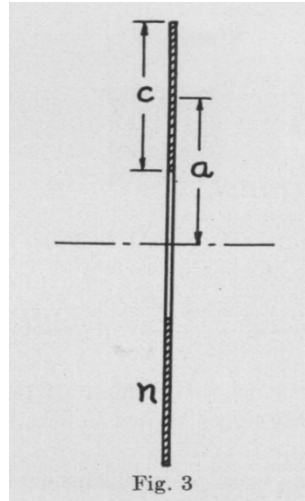


Fig. 4.6: Single layer coil geometry for Wheeler's spiral inductance calculation [19]

Fig. 4.7 depicts an example coil and the design parameters that are considered in this thesis, which differ from the parameters illustrated in Fig. 4.6. A couple of nuances should be noted when dealing with a spiral coil. In many cases, a spiral coil is simplified and treated as a nested set of conducting rings. However, in this inductance calculation it is treated as a true Archimedean spiral. One difference is that a cross-sectional view of the coil would depict one more wire on one side. What follows is that  $r_{inner}$  is defined by the beginning of the innermost turn to a 'center reference point'. This 'center' isn't the center of the structure for if one would

calculate the distance between this reference point and the section of the coil  $180^\circ$  across the defined starting point, one would see that it would not equal  $r_{inner}$ . Only spiral coils of integer valued turns are considered in this document.  $r_{outer}$  is defined by the reference point to the center of the last turn of the coil. ‘w’ is the conductor diameter, and ‘s’ is the spacing between adjacent conductors measured from inner edges. For ease of calculation and to accommodate the parameters this thesis finds useful during the construction of spiral coils, Eq. 4.6 has been modified and explained below.

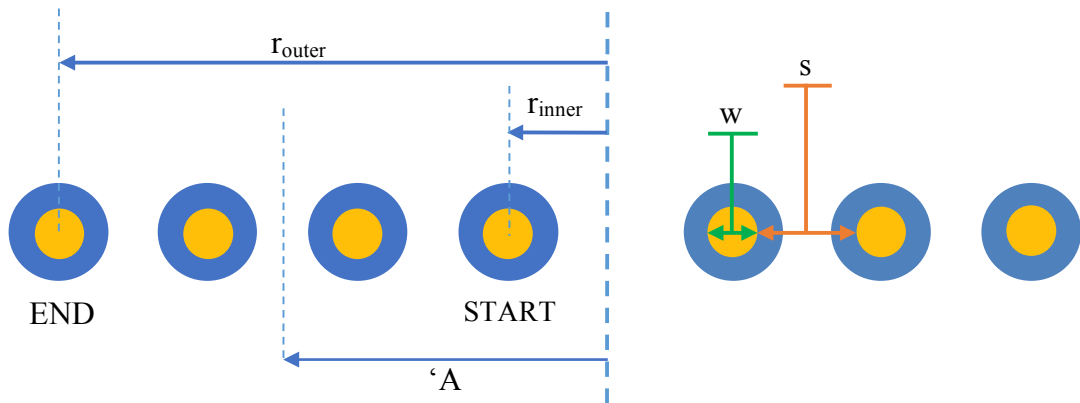


Fig. 4.7: Example 3-turn spiral coil depicting parameters of interest  
(yellow is copper wire, blue is wire insulation)

Given these parameters, define ‘ $D_i$ ’, inner diameter of the spiral coil, as Eq. 4.7, then ‘a’ and ‘c’ in Wheeler’s formula can be defined as Eq. 4.8. Finally, these definitions transform Eq. 4.6 into Eq. 4.8.

$$D_i = 2 * \left[ \frac{D_o}{2} - N(w + s) \right] \quad (\text{Eq. 4.7})$$

$$A = \frac{D_i + N(w + s)}{2} \quad \text{and} \quad c = r_{outer} - r_{inner} \quad (\text{Eq. 4.8})$$

$$L = \frac{A^2 N^2}{30A - 11D_i} * 10^{-6} \quad (\mu\text{H}) \quad (\text{Eq. 4.9})$$

A MATLAB function has been created to implement the equations used derive the inductance of a spiral coil:

## *Spiral\_Inductance*

### Inputs:

- Do:** Outer diameter of the coil (inches)
- N:** Number of turns comprising the coil
- d\_wire:** The diameter of the wire (inches)
- ca:** Ratio of the pitch over the diameter of the wire

### Outputs:

- L:** The Inductance of the coil (Henries)

#### **4.1.4 Experimental Confirmation of Theoretical Calculations**

The cylindrical coil inductance values differed by very little; less than 6% error was observed for all coil configurations. Thus, the design algorithms for cylindrical coil inductance work for a large range of inductors and produce very low error, making them fit for predicting values during the design process. Fig. 4.8 displays the error as a function of the amount of turns on each coil.

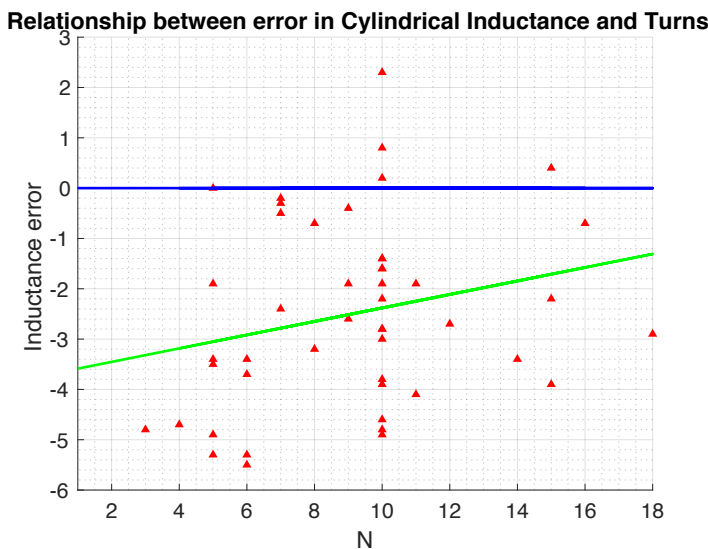


Fig. 4.8: Error in inductance as a function of number of turns for cylindrical coils

Each red triangle represents a coil with a unique coil geometry; unique number of turns, wire diameter, coil diameter, or c/a. The blue line represents zero error between theoretical and measured values and the green line was created using a linear regression model on the points of error.

The error in theoretical and measured values for the spiral coil inductance was less than 10% in most cases, with few outliers less than 15%. Thus, the design algorithms for spiral coil inductance work for a broad range of coils and produce low error as well! Fig. 4.9 displays the

error as a function of the amount of turns on each coil. The total data regarding the inductance of all constructed coils can be found in Appendix A.

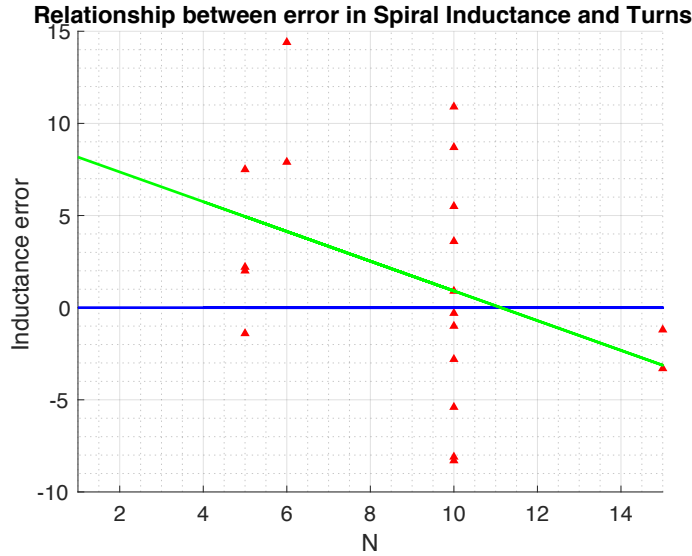


Fig. 4.9: Error in inductance as a function of number of turns for spiral coils

## 4.2 Resistance of Coils

One model for the losses in a coil of wire with both skin and proximity effects is a set of  $N$  parallel cylindrical wires, each carrying the same total current,  $I$ , Fig. 4.10 [16]. The radius of each wire is  $a_w$ , the center-to-center spacing is  $2c$ , the wire-to-wire gap is  $g$ , and the overall length of the coil is  $l$ . The coil of interest is thus represented by the series connection of  $N$  parallel wires, where the length of the system of  $N$  parallel wires is the coil circumference,  $2N\pi a_c$ . If each wire resistance per unit length,  $R_{cw}$ , is uniform for the whole coil and the coil radius is  $a_c$ , then the total coil resistance  $R_c$  becomes:

$$R_c = 2\pi a_c N R_{cw} \quad (\text{Eq. 4.10})$$

A useful metric to describe the relative distance between adjacent turns of a coil is ‘c/a’ or the center-to-center spacing over the radius of the wire. Its minimum value is 1, as this corresponds to a tightly wound coil where adjacent turns are all but ‘touching’ each other. ‘c/a’ will be employed in the design algorithms discussed later and throughout this document as a description of how tightly coils are wound.

In this section, coil resistances as a function of frequency are illustrated and visually analyzed for the severity of ‘skin’ and ‘proximity’ effect. A method of calculating DC, skin, and complete high frequency resistance of coils is then described. MATLAB implementations that performs these calculations given the physical parameters for spiral and cylindrical coils are presented as well. Lastly, the MATLAB design algorithms will be confirmed via experimental designs and the measurements. A high degree of accuracy means these tools could aid in the precise prediction of values integral to efficiency and can assist in producing better 4-coil designs.

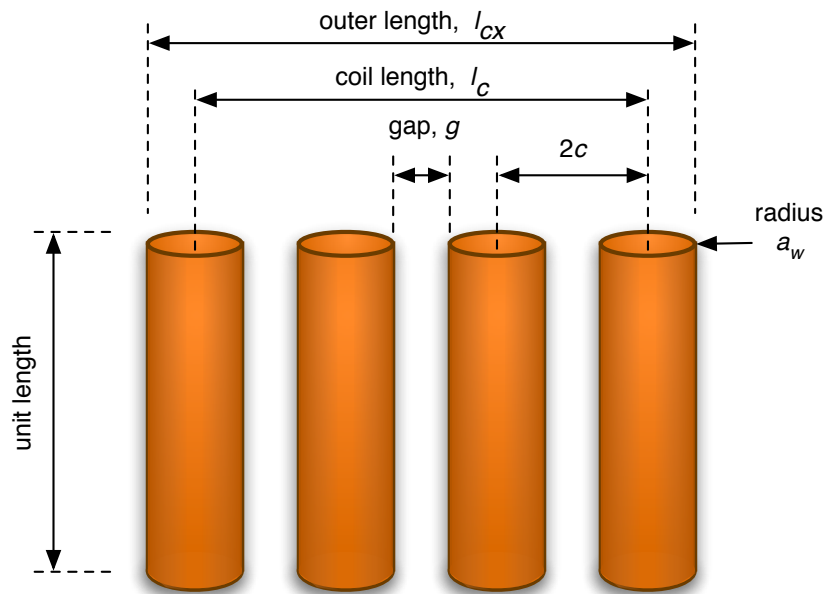
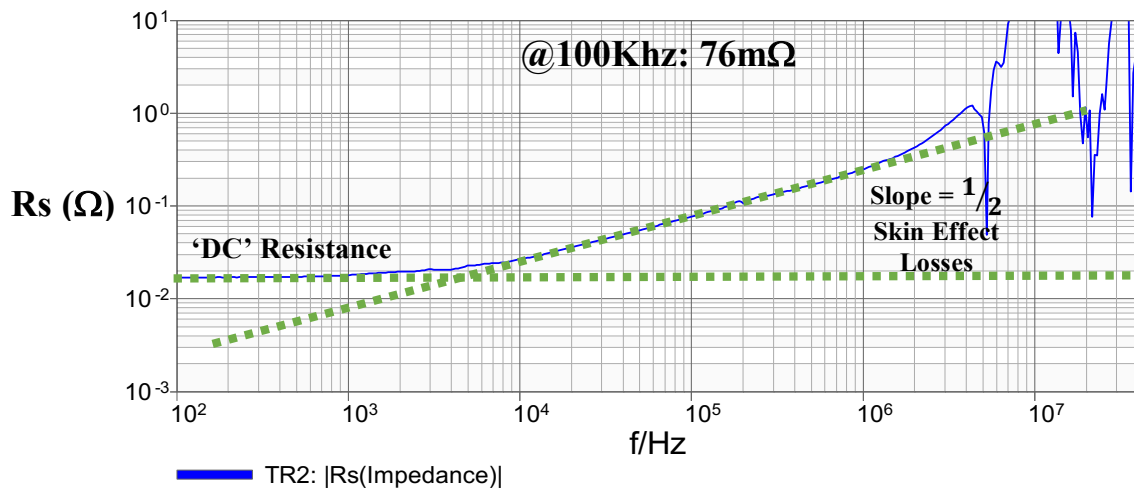


Fig. 4.10 Configuration for  $N = 4$  parallel wires, each carries equal current

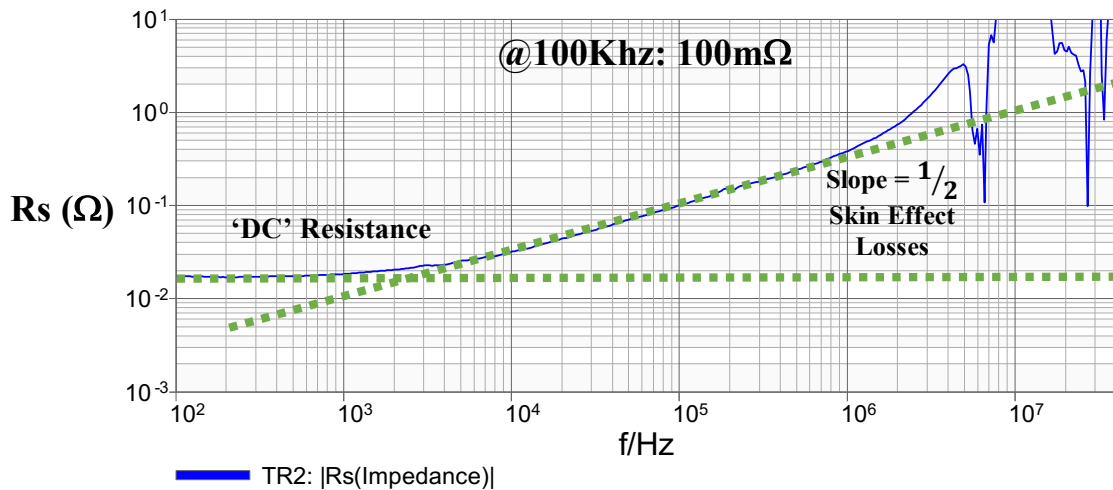
#### 4.2.1 Measuring Resistance

When measuring resistance, two values are recorded, the value measured at DC voltage, the DC-resistance, and another at 100kHz to measure the severity of the skin and proximity effect. Although the Bode100 doesn’t allow the user to make DC measurements, 1 HZ measurements are available and it is low enough so that skin effect is negligible. Fig. 4.11a displays the resistance of a #10 gauge 10-turn cylindrical coil with a  $c/a$  ratio of 2.5. Note, impedance plots of cylindrical or spiral coils will differ by absolute value, but not very much in shape; the general trends in slope will be observed in any coil topology involving solid round copper wire. Up until 4kHz, the resistance remains steady at 18mΩ. At 4kHz, high frequency phenomena take effect

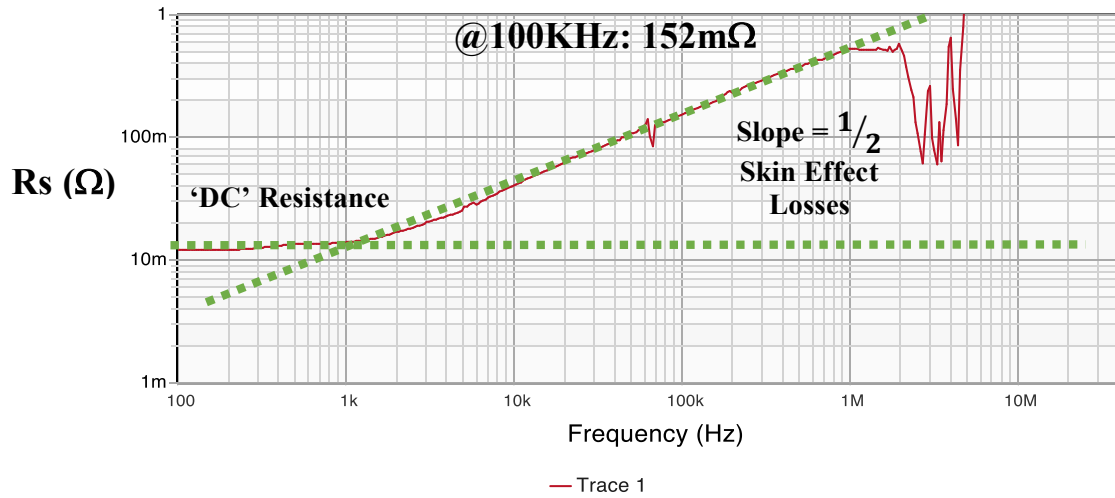
and the resistance increases at a rate equivalent to the reciprocal-root of the frequency:  $\frac{1}{\sqrt{f}}$  (the dashed green line over the plot increases at the same rate). Once in the megahertz regime, the coil's parasitic capacitance becomes significant enough to alter its total impedance and resistance in this range become increasingly difficult to measure. This thesis will concern itself with frequencies below a megahertz. Figs 4.11a, 4.11b, 4.11c display the series resistance of the same cylindrical coil, but with varying  $c/a$  of 2.5, 1.5, and 1.15. Notice the dc-resistance remains the same for all plots, and the curves follow the same 'reciprocal-root of the frequency' increase. However, due to the heightened proximity effect, the plotted values are greater than in Fig. 4.11a: 76mΩ vs 100mΩ vs 150mΩ. Through comparison measurements like these, one can measure the severity of the proximity effect as a function of  $c/a$ .



4.11a: Bode100 resistance plot for coil of  $c/a = 2.5$



4.11b: Bode100 resistance plot for coil of  $c/a = 1.5$



4.11c: Bode100 resistance plot for coil of  $c/a = 1.15$

#### 4.2.2 Bulk Volume Conductivity

The DC Resistance for a conductor can be calculated using the canonical resistance formula, Eq. 4.11, where  $\rho$  is the intrinsic resistivity of the material (in this case copper),  $L$  is the total wire length, and  $A$  is the cross-sectional area of the conductor.

$$R = \frac{\rho L}{A} \quad (\text{Eq. 4.11})$$

Since  $\rho$  is a property of the material and can be gleaned from online resources, there are two quantities needed to be calculated:  $L$  and  $A$ .

The length of a cylindrical coil can be found by assuming the solenoid to be a stack of rings with each ring sharing the same coil diameter. The total length is the added circumference of all the rings. Calculations considering the coil pitch have shown negligible differences in resistance. The length of a spiral coil can be computed by calculating the length of an equivalent Archimedean spiral. In the case of coils implemented with round wire,  $A$  is simply calculated as the cross-sectional area of the wire.

#### 4.2.3 Skin Effect

The ‘skin’ effect is a well-documented phenomenon that results from current being confined near the outer surface of the wire. The surface resistance,  $R^S$ , of the wire at high frequencies is determined by  $d_s$ , the ‘skin-depth’, for currents in the wire and the wire material conductivity,  $\sigma$ ,

and Eq. 4.12. The skin-depth of a wire with a certain conductivity, running a certain frequency,  $\omega$ , can be calculated using Eq. 4.13. Thus, a wire of radius  $a_w$ , has a wire resistance per unit length due to the skin effect of  $R_{skin}$ , Eq. 4.14. As a result, the skin effect is a frequency dependent characteristic and will cause the dc-resistance to increase by the square-root of frequency. Fig. 4.12 displays the high-frequency current distribution in the cross-sectional area of a wire and the physical manifestation of skin depth

$$R^S = \frac{1}{\sigma d_s} \quad (\text{ohm for a square area}) \quad (\text{Eq. 4.12})$$

$$d_s = \sqrt{\frac{2}{\omega \mu \sigma}} \quad (\text{m}) \quad (\text{Eq. 4.13})$$

$$R_{skin} = \frac{R^S}{2\pi a_w} = \frac{1}{2\pi a_w} \sqrt{\frac{\omega \mu}{2\sigma}} \quad (\text{ohm/m}) \quad (\text{Eq. 4.14})$$

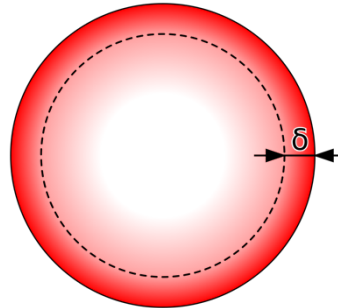


Fig. 4.12: Current distribution in round wire due to skin effect

#### 4.2.4 Proximity Effect for Coil Windings

The ‘proximity’ effect is a less-studied characteristic of coils whose exact effect on resistance is usually ignored or treated qualitatively by empirical relations during a design process. When the separation between adjacent parallel wires is large enough, then there’s negligible proximity effect and only skin effect determines the total resistance of the set of wires. Denote this resistance as  $R_o$ , Eq. 4.15. When the additional influence of the proximity-effect is included (when adjacent wires are spaced close enough) then we define the total wire resistance per meter of the system of N series-connected parallel wires to be,  $R_T$ , and hence we define the added resistance per unit length of the system of N wires due to the proximity effect,  $R_p$  (Eq. 4.16).  $R_p$  can be normalized by the non-proximity effect resistance,  $R_o$ , to get a non-dimensional

measure of the impact of the proximity effect for N parallel wires, Eq. 4.17. A simple calculation of the total normalized resistance per unit length of the set of N wires,  $\frac{R_T}{R_o}$  can be found from the previous equation, Eq. 4.18. Finally, the total wire resistance per unit length of the system of wires can be found, Eq. 4.19. Notice, when there is no proximity effect,  $R_p$  is zero and  $R_T = R_o = NR_{skin}$ , which corresponds to Eq. 2.2.5.

$$R_o = NR_{skin} = N \frac{R^S}{2\pi a_w} \quad (\text{Eq. 4.15})$$

$$R_p = R_T - R_o \quad (\text{Eq. 4.16})$$

$$\frac{R_{prox}}{R_o} = \frac{R_T - R_o}{R_o} = \left( \frac{R_T}{R_o} - 1 \right) \quad (\text{Eq. 4.17})$$

$$\frac{R_T}{R_o} = \left( \frac{R_{prox}}{R_o} + 1 \right) \quad (\text{Eq. 4.18})$$

$$R_T = \left( \frac{R_{prox}}{R_o} + 1 \right) R_o = \left( \frac{R_{prox}}{R_o} + 1 \right) NR_{skin} = \left( \frac{R_{prox}}{R_o} + 1 \right) N \frac{R^S}{2\pi a_w} \text{ (ohm/m)} \quad (\text{Eq. 4.19})$$

For coils composed of the N series-connected parallel wires depicted in Fig. 4.10, where the coil radius is  $a_c$ , the total high-frequency coil resistance,  $R_{coil}$ , becomes:

$$R_{coil} = 2\pi a_c R_T = \left( \frac{R_p}{R_o} + 1 \right) N \frac{R^S}{2\pi a_w} 2\pi a_c = N \left( \frac{R_p}{R_o} + 1 \right) \left( \frac{a_c}{a_w} \right) R^S \quad (\text{ohms}) \quad (\text{Eq. 4.20})$$

As discussed in section 2.3, there has been previous work done on the effective resistance of adjacent conductors due to the proximity effect of high frequency currents. The value of interest is the  $R_p/R_o$  value, or the added resistance due to proximity over the resistance neglecting proximity, the skin effect resistance. This factor increases as the number of parallel conductors in a system increase, as well as when the distance between adjacent conductors is decreased.

Smith [16] has provided a method of calculating  $R_p/R_o$  for round wire using integral equations that are solved numerically. The approach to analytically solve for the added losses by the proximity effect was adopted by Shatz and Cooke to calculate an extended range of turns and

wire spacings. The proximity effect is quantified by evaluation of resultant re-distributions of circumferential currents when there are  $N$  parallel round wires. The proximity effect in this situation produces an additive component to the net resistance of the wires, and is evaluated as a function of the separation between wires normalized by the wire radius. Large number of  $R_p/R_o$  values for different parallel conductors and spacings were obtained with this method. However, for other values, MATLAB's interpolating and extrapolating functions and their 'PCHIP' feature or 'Piecewise Cubic Hermite Interpolating Polynomial' were used. Fig. 4.13 depicts a 3D plot of the  $R_p/R_o$  factor vs number of turns and  $c/a$ , the pitch over the wire diameter. These values are also represented in a table via MATLAB called 'Prox'.

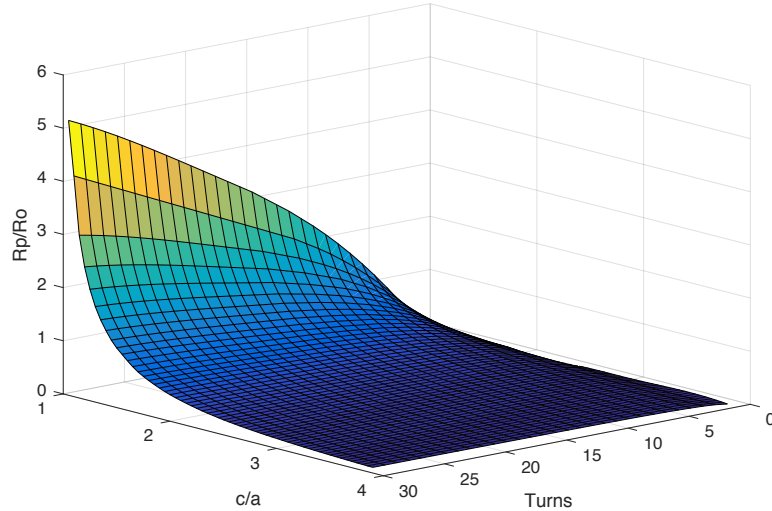


Fig. 4.13: Surface plot of  $R_p/R_o$  as a function of  $c/a$  and number of turns

Table 4.1:  $R_p/R_o$  Table for limited geometric quantities

c/a	Number of Turns										
		10	11	12	13	14	15	16	17	18	19
1.5	0.903	0.946	0.988	1.022	1.055	1.089	1.114	1.138	1.163	1.187	1.212
1.55	0.823	0.860	0.897	0.926	0.955	0.984	1.005	1.026	1.047	1.067	1.088
1.6	0.753	0.786	0.818	0.843	0.869	0.894	0.912	0.931	0.949	0.968	0.986
1.65	0.692	0.721	0.750	0.772	0.794	0.816	0.833	0.850	0.866	0.883	0.900
1.7	0.638	0.664	0.690	0.710	0.729	0.749	0.764	0.778	0.793	0.807	0.822
1.75	0.591	0.614	0.637	0.655	0.672	0.690	0.703	0.715	0.728	0.741	0.753
1.8	0.549	0.570	0.590	0.606	0.622	0.638	0.649	0.660	0.672	0.683	0.694
1.85	0.511	0.530	0.548	0.563	0.577	0.591	0.602	0.612	0.622	0.632	0.642
1.9	0.477	0.494	0.511	0.524	0.537	0.550	0.559	0.568	0.578	0.587	0.596
1.95	0.446	0.462	0.478	0.489	0.501	0.513	0.521	0.530	0.538	0.546	0.555
2	0.419	0.434	0.448	0.459	0.469	0.480	0.488	0.495	0.503	0.510	0.518
2.05	0.394	0.408	0.421	0.431	0.441	0.450	0.457	0.464	0.471	0.478	0.485
2.1	0.371	0.384	0.396	0.405	0.414	0.423	0.429	0.436	0.442	0.448	0.454
2.15	0.350	0.362	0.373	0.381	0.390	0.398	0.404	0.409	0.415	0.421	0.427
2.2	0.331	0.342	0.352	0.360	0.367	0.375	0.380	0.386	0.391	0.397	0.402
2.25	0.314	0.323	0.333	0.340	0.347	0.354	0.359	0.364	0.369	0.374	0.379
2.3	0.298	0.307	0.315	0.322	0.329	0.335	0.340	0.345	0.349	0.354	0.359
2.35	0.283	0.291	0.299	0.305	0.312	0.318	0.322	0.327	0.331	0.335	0.340
2.4	0.269	0.277	0.284	0.290	0.296	0.302	0.306	0.310	0.314	0.318	0.322
2.45	0.256	0.263	0.270	0.276	0.282	0.287	0.291	0.295	0.298	0.302	0.306
2.5	0.244	0.251	0.258	0.263	0.268	0.274	0.277	0.281	0.284	0.288	0.291

Each resistance function will call a script that produces the  $R_p/R_o$  table, *Prox*, which will be used in the final calculation of the resistance by selecting the correct  $R_p/R_o$  value given the amount of turns, c/a of the coil, and ‘proximity’, a value indicating the desired calculation of resistance with proximity effect. The MATLAB implemented functions are:

#### *Cylindrical\_Resistance*

##### Inputs:

- Freq:** Frequency of the current
- Do:** Outer diameter of the coil
- N:** Number of turns comprising the coil
- dw:** Diameter of the wire
- ca:** Pitch to wire diameter
- Proximity:** Binary value enabling the proximity effect.

##### Outputs:

- R:** The Resistance of the cylindrical coil

#### *Spiral\_Resistance*

##### Inputs:

- Freq:** Frequency of the current
- Do:** Outer diameter of the coil
- N:** Number of turns comprising the coil
- dw:** Diameter of the wire
- ca:** Pitch to wire diameter
- Proximity:** Binary value enabling the proximity effect.

##### Outputs:

- R:** The Resistance of the spiral coil

#### 4.2.5 Experimental Confirmation of Theoretical Calculations

In order to confirm the validity of the presented design algorithms and software implementations, over 50 designs were constructed and evaluated via the OMICRON Bode100 instrument. These tests reveal if the algorithms are a viable predictor of real performance. Experiments not only check the relationship of the formulas; they also aid in debugging the programs for correctness. Due to the large amount of gathered data, Appendix B contains all the information collected from the constructed designs including physical geometry, theoretical resistance, and measured resistance. The theoretical values were obtained using the MATLAB functions described in this chapter. A lack of exact agreement doesn't deem these algorithms fruitless, rather, estimates on the general trend of error can also provide qualitative insight to these parameter values.

Cylindrical coil resistance calculations exhibited noticeable error. To quantify deviations from theoretical values and to gain insight, a plot of the error as a function of  $c/a$  is shown in Fig. 4.14.

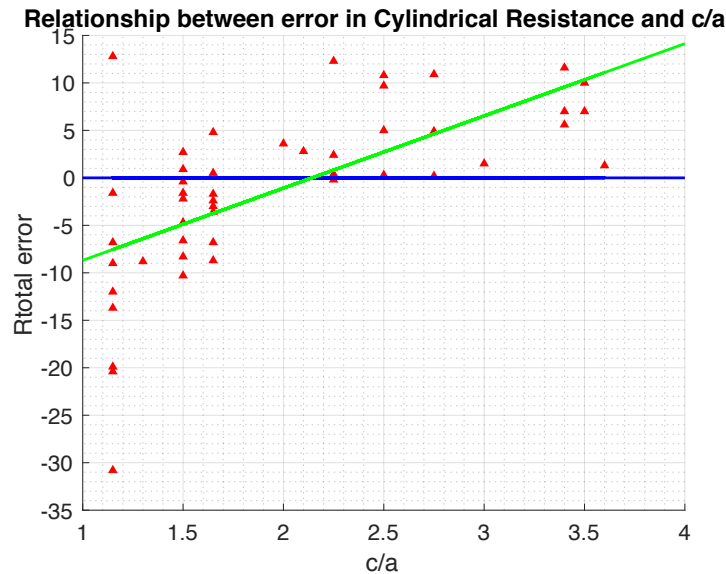


Fig. 4.14: Error in resistance as a function of ' $c/a$ ' for cylindrical coils

Each red triangles represents a coil with a unique coil geometry; unique number of turns, wire diameter, coil diameter, or  $c/a$ . The blue line represents zero error between theoretical and measured values and the green line was created using a linear regression model on the points of error. Although there is some error on either end of the spectrum, the key takeaway is that from the range of  $c/a$  of 1.5 to 2.5, the average error remains less than 5%! Additionally, one can glean

qualitative insight with Fig. 4.14 and claim that if  $c/a > 2$  then a resistance of higher magnitude would be observed in measurements and if  $c/a < 2$  then a lower resistance would be observed. Minor error can be attributed to the difficulty in constructing these coils with perfectly uniform spacing. Thus, the algorithm for cylindrical coil resistance produces minimal error in the range  $1.5 < c/a < 2$  and increases on either extreme of  $c/a$ .

Spiral coil resistance theoretical calculations also exhibited some errors. A plot of the error as a function of  $c/a$ , for spiral coils, similar to Fig. 4.14, is shown in Fig. 4.15. Evidently, the model works marginally well as a predictor. However, there are a number of reasons for the disparities that open up possibilities for future work. The proximity effect has been calculated for a set of straight parallel conductors all carrying current in the same direction; however, in a spiral coil the magnetic field is very different at the inner turns compared to that near the outer turns, hence the proximity effect will differ. Note the values in Fig. 4.15 are greater than predicted, this is consistent with the magnetic field at the inner wires being somewhat greater than that estimated from the parallel wire approximation. Finally, constructing spiral coils was found to be more difficult since unlike the cylindrical case, the windings were not held by a form to a defined radius. Hence, spiral constructions with uniform spacings and perfectly curved windings are hard to achieve without more sophisticated and specialized coil forming hardware.

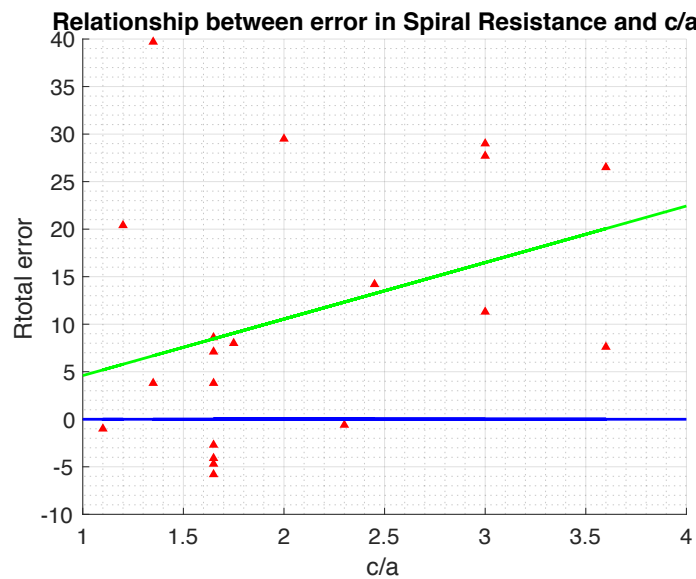


Fig. 4.15: Error in resistance as a function of ' $c/a$ ' for spiral coils

### 4.3 Coil Quality Factor, $Q$

The quality factor,  $Q$ , of a coil is a metric for the relative amount of loss that occurs in a coil with inductance  $L$ . It is the ratio of the magnitude of the reactive impedance,  $\omega L$ , to the effective series resistance of the coil winding,  $R_c$ :

$$Q = \omega \frac{L}{R_s}$$

If inductance  $L$  and resistance  $R_c$  are constant, then  $Q$  would increase linearly with frequency. However, as seen above in Section 4.1, coil inductance stays nearly constant with frequency. On the other hand, as seen in Section 4.2, coil resistance changes with frequency due to the skin and proximity effects. Fig. 4.16 displays a plot of  $Q$  measured by the Bode100 for a coil of 10-turns with an outer diameter of 6.4 inches and a c/a of 1.5. Two dashed blue lines are shown on the plot. The first shows the linear dependence of  $Q$  on  $\omega$  due to  $L$  and  $R_c$  being constant. The second depicts the ‘reciprocal-root’ relationship between  $Q$  and  $\omega$  as the skin effect increases.

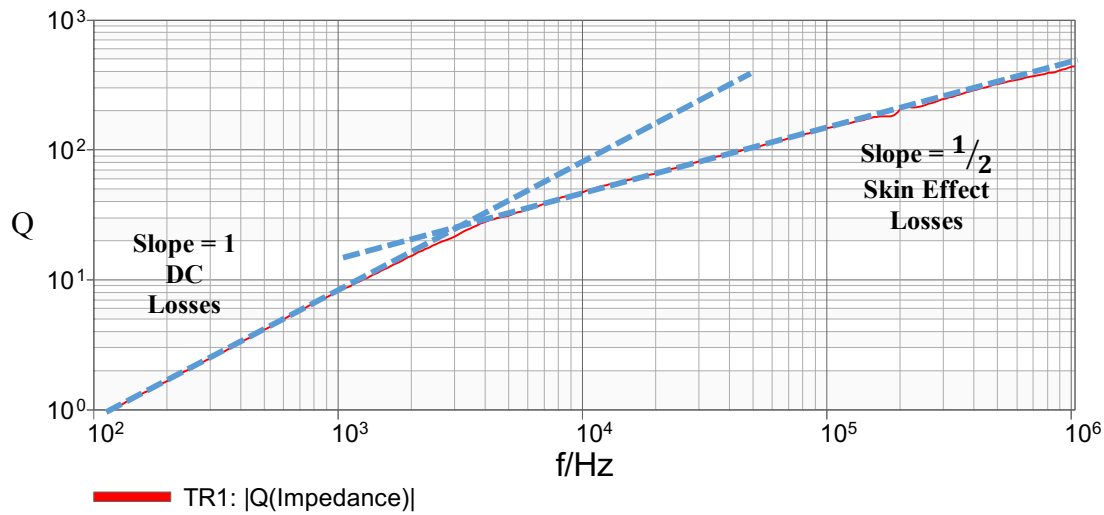


Fig. 4.16: Example Bode100  $Q$  measurement plot

It is desirable to evaluate the preferred wire sizes and spacing between turns for a wire-wound inductive coil structure that maximizes the quality factor of that coil for high-frequency applications. When wire sizes and spacings are too small, inductance is maximized but so is the resistance due to proximity effect. Conversely, when wire sizes and spacings are made large, then the resistance and inductance both decrease due to inhibited proximity effect and result in a

longer, loosely self-coupled coil. Now that algorithms for calculating high frequency resistance and inductance of spiral and cylindrical coils have been developed, one can find values for  $Q$  for an arbitrary coil with these geometries. Appendix C shows the theoretical and measured  $Q$  for a number of constructed coils.

## 5. Magnetic Coupling Between Pairs of Coils

While the previous section provided an analysis of the inductance and resistance of high-frequency individual coils, this section will discuss the behavior and interaction of two coils in proximity to each other. Isolated, coils possess a self-inductance; however, when two are brought close enough together they experience a mutual inductance. This occurs when a time-varying current is flowing through one coil and another coil is placed in its vicinity. The ensuing time-varying magnetic flux produced by the first coil, by Faraday's law, will induce a time-varying current in the second coil. This means the magnetic flux from one coil is *coupled* to the other. However, in typical cases the total flux produced by the first coil doesn't couple 100% to the second, therefore the fraction of magnetic flux generated by the first coil that links to the second is known as the *mutual magnetic coupling coefficient* or ' $k$ '. It is a quantity that only applies to a pair of coils. When the entire magnetic flux produced by one coil links with another coil, it is said that the mutual magnetic coupling between the coils is 100% or  $k=1$ . Fig. 5.1 is a representation of two coupled coils.

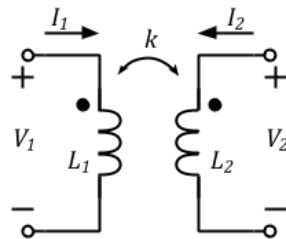


Fig. 5.1: An equivalent circuit representation for 2 coupled coils

The mutual magnetic coupling of the coils play a significant role in achieving high efficiency as it is a representative of the amount of energy transfer among coils. Fig. 2.6 also depicts the dependency of efficiency in resonant systems on the coupling of coils as a function of coupling coefficient,  $k$ . Thus, it is desirable to accurately predict the  $k$  value among pairs of coils in order to predict the efficiency of plausible designs. Subsection 5.1 will discuss how to measure the coupling coefficient experimentally. Subsection 5.2 will discuss implemented design algorithms for theoretically calculating  $k$  for spiral and cylindrical coils. Subsection 5.3 will show example calculations using the developed MATLAB design programs. Finally, subsection 5.4 will provide experimental confirmation of the MATLAB functions by comparing their results against manually constructed pairs of coils.

## 5.1 Measuring Magnetic Coupling

This subsection will discuss the measurement of  $k$  among two coils by first deriving the necessary equations and then the physical implications that result. A lumped Pi-equivalent circuit model for a pair of coupled coils with coupling represented by mutual inductance,  $M$ , is illustrated in Fig. 5.2.

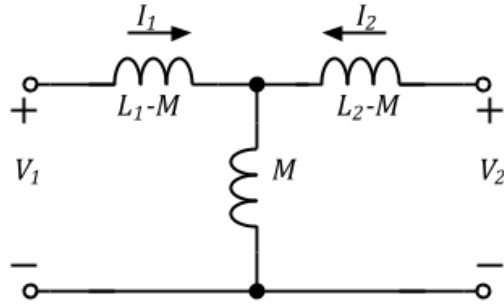


Fig. 5.2: An equivalent circuit representation for 2 coupled coils using their ideal lumped equivalent models

The terminal equations that describe the coupled coils are:

$$V_1 = j\omega(L_1 I_1 + M I_2)$$

$$V_2 = j\omega(M I_1 + L_2 I_2)$$

where  $M$  is the mutual inductance between the windings and where  $L_1$  and  $L_2$  are the respective individual inductance values of the two coils separately. If the windings on the second coil are shorted, then  $V_2 = 0$  and  $I_2$  becomes:

$$I_2 = \frac{-M I_1}{L_2}$$

and thus, under these same conditions,  $V_1$  is:

$$V_1 = I_1 * j\omega \left( L_1 - \frac{M^2}{L_2} \right)$$

$V_1$  resembles the impedance equation for an inductor with an inductance corresponding to the value in parenthesis. This corresponds to the effective inductance seen by the first set of terminals when the second set is shorted,  $L_s$ , or the *shorted-inductance*:

$$L_s = \left( L_1 - \frac{M^2}{L_2} \right) \quad (\text{Eq. 5.1})$$

Now, using the definition of  $k$  (Eq. 5.2) and Eq. 5.1, Eq. 5.3 can be derived and reveals the relationship of the coupling coefficient  $k$  to the inductances of the coils of interest.

$$k = \frac{M}{\sqrt{L_1 L_2}} \quad (\text{Eq. 5.2})$$

$$k^2 = \frac{M^2}{L_1 L_2}$$

$$k^2 = \frac{L_2(L_1 - L_s)}{L_1 L_2} = 1 - \frac{L_s}{L_1}$$

$$k = \sqrt{1 - \frac{L_s}{L_1}} \quad (\text{Eq. 5.3})$$

where  $L_1$ , defined as the individual inductance values of first coil, can now also be defined as the inductance measured at the first coils terminals when the second coil is open, the *open-inductance*. While  $L_s$  is the inductance measured at the first coils terminals when the second coil is shorted, the *shorted inductance*.

These calculations imply that two measurements are needed to calculate the coupling coefficient for a pair of fixed spaced coils: one inductance measurement with the second coil open, and another inductance measurement with the second coil shorted. Fig. 5.3 displays an experimental setup for calculating the coupling factor between two 6-turn coils. Notice in the left image, the second coil is open to produce a measurement of  $L_1$ . Alternatively,  $L_1$  could have been determined by removing the second coil from the first coil's vicinity and obtaining an inductance measurement of the first. The image on the right displays the experimental setup for the measurement of  $L_s$  with the second coil shorted.



Fig. 5.3: Experimental setup for measuring the coupling coefficient between a pair of separated coils. The left image is the setup for  $L_1$ . The right image is the setup for  $L_s$ .

## 5.2 Calculating Mutual Magnetic Coupling

In this section, a method for calculating the magnetic coupling between two coils is described and a design algorithm implemented in MATLAB is presented. The methods employed are based upon established formulas from the literature. This analysis follows the method developed by Neumann[20] and Duarte[21]

Magnetic coupling is primarily a geometry driven problem with slight dependence upon the conduction properties of the winding material, thus the geometric details of the coil structures are carefully identified. A good degree of accuracy will enable these calculations to aid in the prediction of power transfer efficiency and can lead to better designs.

### 5.2.1 Cylindrical Coils

The mutual magnetic coupling coefficient,  $k$ , between two cylindrical coils is calculated in this section and is extended to spiral coils in a following section. The coupling coefficient  $k$  is determined from a calculation of the mutual magnetic inductance that couple the two coils,  $M$ , and the definition of  $k$ , where  $L_1$  and  $L_2$  are the respective individual inductance values of the two coils separately, Eq. 5.2.

The geometry for two coaxial circular coils of  $N_1$  and  $N_2$  turns, radii of  $r_1$  and  $r_2$ , with turn- to-turn pitches of  $P_1$  and  $P_2$ , respectively, is depicted in Fig. 5.4. All coil positions are

referenced to the *center of the conductors*. [Note, these coil lengths,  $x_{1,2}$ , use the wire centers whereas the coil lengths,  $l_c$ , in the inductance calculations use outer edges]

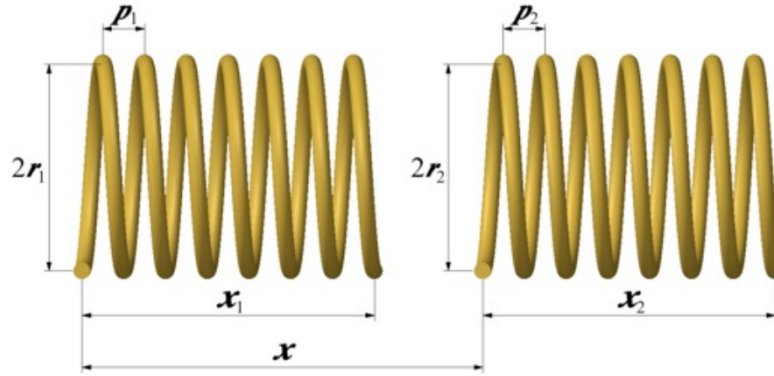


Fig. 5.4: Two coaxial coils of radius  $r_1$  and  $r_2$ , respectively

The ‘offset’ position ‘ $x$ ’ of the second coil can be less than the first coil length ‘ $x_1$ ’, so that the coils may be partially or totally nested and the solution method here remains valid. It is assumed that the coil pitch values,  $P_1$  and  $P_2$ , are much less than the coil radii values,  $r_1$  and  $r_2$ . Hence the coils can be approximated as two stacks of  $N_1$  and  $N_2$  rings. Each ring is spaced by the wire center-to-center pitch distances  $P_1$  and  $P_2$ , respectively, Fig. 5.5.

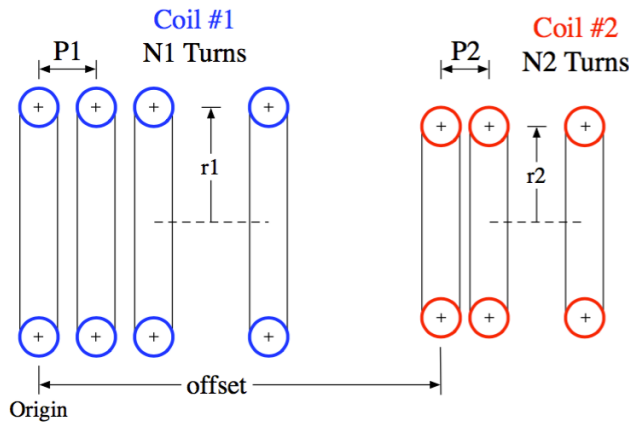


Fig. 5.5: Stacked ring-conductors representation of two coils

It is further assumed that the current is symmetric in each ring and hence the ring current is represented as a filamentary ring conductor in the center of each ring, and so the ring diameters do not enter directly into the calculations. Fig. 5.6 is extended to multiple rings by

linear summation of the mutual inductances between each pair of loops. The integration around the rings results in Elliptical functions of the first and second kind,  $K(m)$  and  $E(m)$ , respectively.

The substitution of (4) in (3) results in

$$M = \frac{\mu}{4\pi} \iint_0^{2\pi} \frac{ab \cos(\phi - \phi')}{a^2 + b^2 + d^2 - 2a \cos(\phi - \phi')} d\phi d\phi'. \quad (5)$$

The integral in (5) can be rewritten using elliptic integrals, yielding

$$M(m) = \frac{2\mu\sqrt{ab}}{m} \left[ \left(1 - \frac{m^2}{2}\right) K(m) - E(m) \right], \quad (6)$$

where  $K(m)$  and  $E(m)$  are the elliptic integrals of first and second kind, respectively, and  $m$  is defined as

$$m = \sqrt{\frac{4ab}{(a+b)^2 + d^2}} \quad (7)$$

assuming values between 0 and 1.

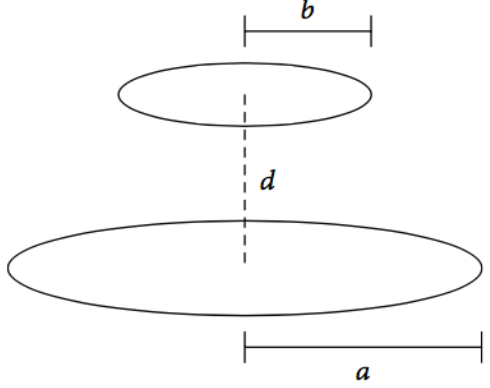


Fig. 5.6: Structure and calculation for two coaxial rings offset by ‘ $d$ ’ [20]

The calculation first determines the amount of mutual magnetic coupling,  $M_{ni}$ , associated with each possible pair of ring-turns, turn ‘ $n$ ’ on coil #1 and turn ‘ $i$ ’ on coil #2. The total mutual inductance between the pair of coils,  $M$ , is the summation of all the  $M_{ni}$  values.

The ‘origin’ for the relative position of the two coils in the implemented calculation is the left-most turn of the first coil as depicted in Fig. 5.5, and the axis is the center of the coils. The coaxial coils are ‘offset’ by a distance ‘ $x$ ’ that is the distance to the closest turn of the 2<sup>nd</sup> coil from the origin of the first coil. All these dimensions are input in units of inches in the MATLAB program, and converted to the needed SI units inside the program.

Internally, the calculation uses two coefficients: ‘ $m$ ’ and ‘ $d$ ’. The coefficient  $m$  is dependent upon the coil radii and separation distance,  $d$ , and is evaluated with Eq. 5.4. The coefficient  $d$  is the separation distance between two-coupled rings, and changes for each selected ring-pair,  $n$  and  $i$ , (from coil 1 and coil 2, respectively) and the pitch values of the two coils, by Eq. 5.5. The inductance between two rings (1 and 2) is thus defined by Eq. 5.6, where the elliptic functions  $K(m)$  and  $E(m)$  are the elliptic integral of the first kind and second kind respectively.

$$m = \sqrt{\frac{4r_1 r_2}{(r_1 + r_2)^2 + d^2}} \quad (\text{Eq. 5.4})$$

$$d = |offset - (n - 1)p_1 + (i - 1)p_2| \quad (\text{Eq. 5.5})$$

$$M(m) = \frac{2\mu}{m} \sqrt{r_1 r_2} \left[ \left(1 - \frac{m^2}{2}\right) K(m) - E(m) \right] \quad (\text{Eq. 5.6})$$

Hence by summation the total mutual inductance between two coils is:

$$M = \sum_n \sum_i M_{ni} \quad (\text{Eq. 5.7})$$

The sequence for the calculation is to select the first ring of coil 1 ( $n=1$ ) at the origin and to cycle through all  $i$  rings in coil 2, then repeat again for the next ring ( $n=2$ ) of coil 1 and again with each of the coil 2 rings, etc. until all ring pairs have calculated  $M_{ni}$ , and when added they form the total mutual inductance between the two coils,  $M$ .

The value of the resultant coupling coefficient  $k$  between coils 1 and 2 is calculated from the definition (Eq. 5.2). Note mutual magnetic coupling coefficients between coils that are displaced so as to be non-coaxial, and for coils that are also tilted at an angle relative to one another are available in the literature, but are not included here, since there seems to be no advantage to employ such shifts in the design of fixed structures. Rather, non-coaxial coil coupling is of use for systems where the coils are free to move relative to each other, such as in wireless power transfer systems.

The MATLAB function that calculates the mutual magnetic coupling among a pair of cylindrical coils by following the explained algorithm, where ‘coil 1’ and ‘coil 2’ can be arbitrarily chosen to be whichever coil but must remain consistent throughout the parameter inputs, is:

### *Cylindrical\_Coupling*

#### Inputs:

**Distance:** The offset value depicted in Fig. 5.5 (inches)

**r1:** Outer radii of the coil 1 (inches)

**r2:** Outer radii of the coil 2 (inches)

**L1:** Inductance of the coil 1 (Henries)

**L2:** Inductance of the coil 2 (Henries)

**N1:** Number of turns of coil 1 (Integer)

**N2:** Number of turns of coil 2 (Integer)

**Dw1:** Wire diameter of coil 1 (inches)

**Dw2:** Wire diameter of coil 2 (inches)

**CA1:** Ratio of pitch to wire diameter of coil 1

**CA2:** Ratio of pitch to wire diameter of coil 2

**Output:**

Mutual Magnetic Coupling Factor  $k$

When manipulating the parameter values, users may accidentally input arguments that produce non-realizable coil configurations. For example, if the coupling for two loops with the same coil radius is desired and the distance between them is set to 0, the user is effectively asking for the coupling of coils that are in the same space. To resolve this potential issue, an error message is produced, 'Unrealizable Geometry: Overlapping Coils Detected', whenever the calculated mutual inductance is detected to be incorrect for realizable coils. The user must be completely aware of the generated pair of coils and their positions in space.

### 5.2.2 Spiral Coils

Calculation of mutual magnetic coupling between spiral coils follows the same procedure. The geometry for two coaxial circular coils of  $N_1$  and  $N_2$  turns, radii of  $r_1$  and  $r_2$ , with turn- to-turn pitches of  $P_1$  and  $P_2$ , respectively, is depicted in Fig. 5.7. All coil positions are referenced to the *center of the conductors* as the case with cylindrical coils.

Since a side view of two co-axial planar coils appears as two sets of wires in their corresponding plane positions, the ‘offset’ value is the center –to-center distance between these two planes. As well as in this scenario, if the coils are appropriately sized (one entirely outside the other), the offset position of the second coil can be 0, so that the coils may be nested and the solution method here remains valid. It is assumed that the coil pitch values,  $P_1$  and  $P_2$ , are much less than the coil radii values,  $r_1$  and  $r_2$ . Hence the coils can be approximated as two nested structures of  $N_1$  and  $N_2$  rings. Each ring is spaced by the pitch distances  $P_1$  and  $P_2$ , respectively, Fig. 5.7.

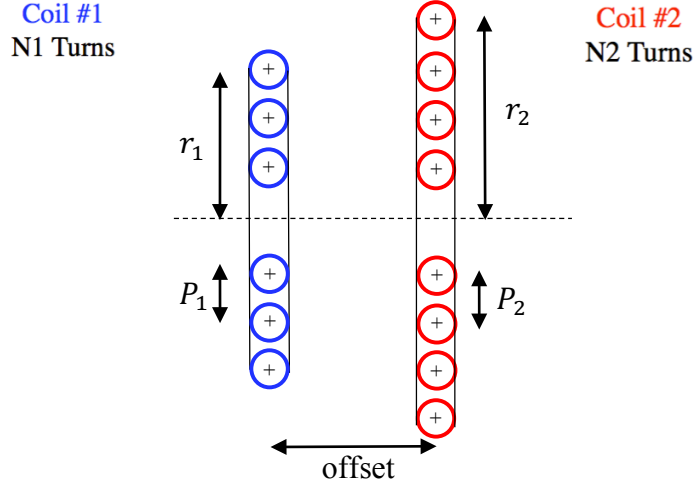


Fig. 5.7: Nested ring-conductors representation of two spiral coils

It is further assumed that the current is symmetric in each ring and hence the ring current is represented as a filamentary ring conductor in the center of each ring, and so the ring diameters do not enter directly into the calculations. Now, during the calculation of mutual inductance among nested rings, instead of the separation distance,  $d$ , varying for every ring-to-ring calculation via  $m$  (Eq. 5.4),  $r_1$  and  $r_2$  are going to be varying. As noted earlier, non-coaxial coil coupling is of use for systems where the coils are free to move relative to each other, such as in wireless power transfer systems and won't be studied in this thesis.

The MATLAB function that calculates the mutual magnetic coupling among a pair of spiral coils by following the explained algorithm, where ‘coil 1’ and ‘coil 2’ can be arbitrarily chosen to be whichever coil but must remain consistent throughout the parameter inputs, is:

### *Spiral\_Coupling*

#### Inputs:

- Distance:** The offset value depicted in Fig. 4.2.2.4 (inches)
- ro1:** Outer radii of the coil 1 as defined by  $r_1$  in Fig. 5.7 (inches)
- ro2:** Outer radii of the coil 2 as defined by  $r_2$  in Fig. 5.7 (inches)
- L1:** Inductance of the coil 1 (Henries)
- L2:** Inductance of the coil 2 (Henries)
- N1:** Number of turns of coil 1 (Integer)
- N2:** Number of turns of coil 2 (Integer)
- Dw1:** Wire diameter of coil 1 (inches)
- Dw2:** Wire diameter of coil 2 (inches)
- CA1:** Ratio of pitch to wire diameter of coil 1
- CA2:** Ratio of pitch to wire diameter of coil 2

#### Output:

Mutual Magnetic Coupling Factor  $k$

As when users input arguments in the cylindrical coil coupling algorithm, a potential issue is the creation of an unrealizable geometry by the over lapping or close spacing of loops. If the program detects an unrealizable geometry an error message is produced, 'Unrealizable Geometry: Overlapping Coils Detected', and will halt the output response. The user must be completely aware of the generated pair of coils and their positions in space.

### 5.3 Theoretical Magnetic Coupling of Nested Coils

The developed design algorithms can predict the coupling relationship between two arbitrary coaxial cylindrical and spiral coils. With it, plausible coil arrangements for power transfer can be studied and evaluated without the need for manual construction. For example, one topology worth considering involves the use of nested coils. Consider: is coupling greater if a smaller coil is nested inside a bigger, or the opposite scenario? Two results using the *Cylindrical\_Coupling* function for nested cylindrical coils, with one longer than the other, is depicted in Fig. 5.8. In the left image, Fig. 5.8a, the longer coil has a coil diameter of 9 inches and the shorter coil is made larger in diameter, 11 inches, so that it can slide 'over' the longer coil. In Fig. 5.8b, the shorter coil was made smaller in diameter, 7 inches, so that it can slide 'inside' the longer coil, still 9 inches.

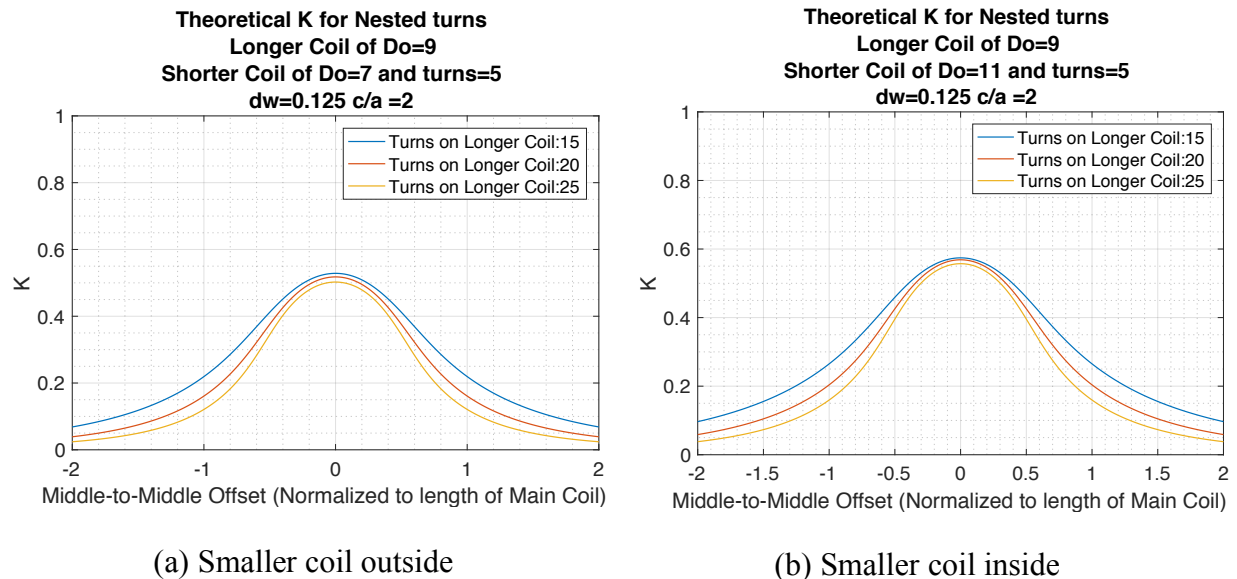


Fig. 5.8 Theoretical  $k$  values for nested coils of varying lengths

The horizontal axis is the relative position of the centers of the two coils, normalized by the length of the longer coil. Here the longer coil is varying from 15 to 25 turns in 5-turn

increments, while the smaller is fixed at 5-turns. Both are made from #8 gauge solid wire. When the shorter coil is centered *over* the center of the longer coil, and the longer coil is 15 turns, the coupling coefficient is a maximum at 0.57. When the shorter coil is centered *within* the longer coil the coupling coefficient is a maximum at 0.53. An even greater difference between maximum k values occurs when the longer coil's turn number is increased.

#### 5.4 Experimental Confirmation of Theoretical Results

To confirm the validity of the presented design algorithms and software implementations, 32 variations of coil pairs have been selected, constructed, and their coefficients evaluated. These tests were used to confirm the algorithms are a viable predictor of actual performance.

Experiments not only check the validity of the formulas; they also help aid in debugging the programs for correctness (something is clearly wrong when theoretical values deviate by 200%). Inductance values were measured at 100kHz via the OMICRON Bode100 instrument. Table 4.1 shows the measured and theoretical coupling coefficient for a pair of #12 gauge, normalized gap spacing between turns,  $g/dw$ , of 1.65, 12-turn coils from a distance of .25 inches to a distance of around 15 inches. The measured value was obtained with the procedure described in subsection 5.1 and the theoretical value was obtained through the *Cylindrical\_Coupling* function. Most error can be attributed to the difficulty of physically constructing ‘perfect’ structures, as wire-to-wire spacing wasn’t exactly uniform among all adjacent turns. Despite the error in construction, most resultant coupling error wavered around 5%, and increases as the coils were further separated. This is likely because as the amount of coupling becomes smaller, the two inductances,  $L_s$  and  $L_o$ , begin to converge until it becomes very difficult for the Bode100 device to detect a difference.

Other tests were made with #12 gauge coils and #8 gauge coils with different outer diameters, 8.75~ and 12~ inches, different normalized gap spacing, 1.65 and 2.05, and varying turn numbers. For the #12 gauge wire, 2, 12, and 24-turn coils were paired up and tested. The coils were all placed coaxially at various selected distances. The results are tabulated in Table 4.2. The first column,  $N1$ , represents the number of turns on the first coil while the second column,  $N2$ , represents the number of turns on the second coil. The third column is the distance between their centers in inches. The #8 gauge coils were 1, 3, and 10 turns and the results are tabulated in Table 4.3. Note, in arrangements where adjacent coils become nested, the outer

coil's diameter increases marginally. Notice there is a very good correlation between the calculated and measured results over a broad range of geometric conditions, making this design algorithm useful for accurate coil coupling predictions in many arrangements.

Table 5.1:  $k$  values for two #12 gauge 12-turn coils with coil pitch=.132

Distance (in)	Lo	Ls	K-meas.	K-theory
.25	51.40	.39.58	0.48	0.45
0.5	51.50	43.06	0.41	0.39
0.75	51.50	44.56	0.37	0.35
1	51.50	45.80	0.33	0.31
1.5	51.50	47.47	0.28	0.26
2	51.48	48.97	0.22	0.21
2.5	51.52	49.76	0.19	0.18
3	51.49	50.23	0.16	0.15
4	51.53	50.86	0.11	0.11
5	51.49	51.13	0.084	0.080
6	51.55	51.34	0.064	0.061
7	51.54	51.42	0.050	0.047
8	51.51	51.44	0.039	0.037
9	51.49	51.44	0.033	0.029
10	51.55	51.53	0.022	0.024
11.6	51.56	51.54	0.017	0.017
13.2	51.56	51.55	0.015	0.013
14.7	51.56	51.57	0.013	0.010

Table 5.2:  $k$  values for two #12 gauge 2/12/24-turn coils with coil pitch=.132

N1	N2	Distance	K-meas.	K-theory
2	2	3.4	.17	.16
2	2	.25	.7	.72
2	2	1.35	.34	.32
2	2	1.9	.31	.28
2	24 (nested inside)	1.4	.55	.55
2	12 (nested inside)	.75	.78	.79
2	12 (nested inside)	.7	.68	.68
2	12	.95	.59	.59

Table 5.3:  $k$  values for two #8 gauge 1/3/10-turn coils with coil pitch=.256

N1	N2	Distance	K-meas.	K-theory
3	3	3.3	.23	.234
3	10	1.66	.57	.56
1	1	2.8	.23	.21
1	10	1.4	.58	.56
1	1	2.3	.28	.25
1	10 (nested inside)	1.15	.65	.63

## 6. Magnetic Coupling Dynamics in Multi-Coil Systems

Chapter 5 discussed the inductive coupling interaction that occurs between a pair of mutually linked coils. Now that the interaction of a pair of coils is understood, this chapter will discuss the complex interaction within multi-coil systems and develop the 4-coil transformer device.

Subsection 6.1 will introduce the 4-coil transformer system starting from a number of coils in close proximity to each other to the full model that is designed and constructed in this thesis. Subsection 6.2 will discuss important design parameters in building 4-coil systems and subsection 6.3 will examine coupling coefficients produced experimentally by assembling a number of example devices.

### 6.1 4-Coil Transformer

With the objective of efficiently transferring power without a magnetic core to guide the magnetic flux between coupling coils, consider a pair of coupled resonant coils. Now, add two more coils, one to couple energy into and the other to couple energy out-from the resonant-pair. These two added coils may also be utilized for impedance matching and step-up/step-down capabilities. The added ‘drive’ coil, identified as coil 1, is inductively coupled to the first coil of the resonant pair. The added ‘load’ coil, identified as coil 4, is inductively coupled to the second coil of the resonant pair. In total, there are four coils used with the objective of transferring power to the load. However, the coupling is not so simple. Due to the coil positions, all coils are coupled to all other coils and there is substantial interdependence of coil coupling that needs to be considered in overall transformer performance.

Since coils in resonance transfer energy to each other more efficiently, resonant coils 2 and 3 can be tuned to the frequency of interest by connection of the appropriate resonant capacitor. This enables a designer to decide and alter the resonating frequency of these coils via an external element. What has been effectively created is a 4-coil transformer system!

The 4-coil system consists of a source voltage with source impedance, two resonant coils denoted as ‘primary’ and ‘secondary’, and a load coil connected to the output load impedance, Fig. 6.1. The coils have been renamed to Coils 1 to 4 and the translation is shown in Fig. 6.1. Each coil is represented by its lumped series inductance resistance circuit equivalent. The resonant coils include their coil and a parallel-connected lumped capacitor. When an HF signal powers the drive coil, the resulting magnetic field excites the primary resonant coil, which stores

energy in the same manner as an LC tank. The drive coil's magnetic field also influences the secondary resonant coil and the load coil (though not to the same degree). The key interaction occurs between the two resonant coils which, act as ideal high- $Q$  resonators and work to propagate the energy between them. The secondary resonant coil is then inductively coupled to the load coil where power will be transferred over to the loading device. For a set of  $N$  coils in close proximity to each other there will be  $(N-1)$  factorial coupling coefficients that describe the overall magnetic linkages between all the coils. Therefore, because there are 4-coils in this system, there are 6 coupling coefficients that are determined by the geometry of each coil and their relative position to one another:  $K_{12}, K_{23}, K_{34}, K_{13}, K_{24}, K_{14}$ . Each  $K_{xy}$  refers to the coupling coefficient between Coil-X and Coil-Y. Fig. 6.1 depicts this lumped equivalent circuit and the corresponding magnetic coupling coefficients. There is a plethora of design options in physically placing the four coils in these systems. The next section will give a brief overview of the topological options and the ones chosen for this thesis.

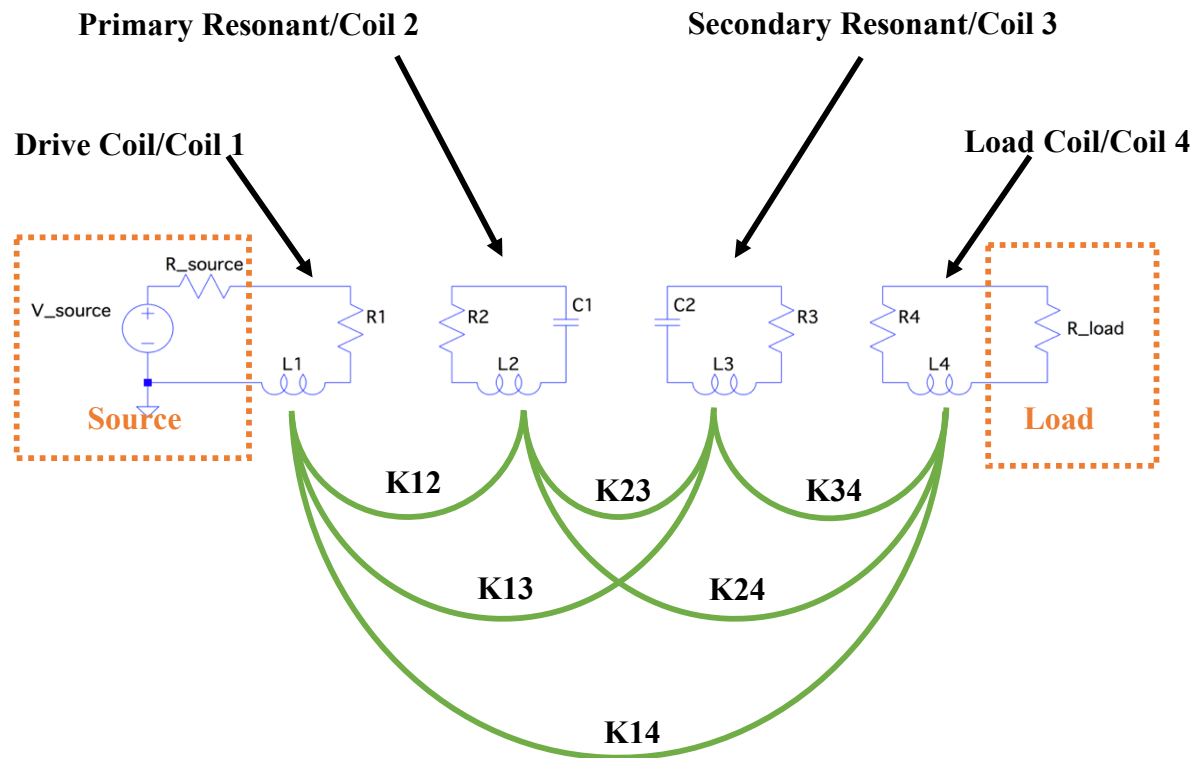


Fig. 6.1 High-level schematic of 4-coil coreless transformer. There are four enumerated coils names that refer to the four coils of the system. The drive and load side are labeled in orange. The coupling coefficients and their linkages are shown in green.

## 6.2 Topological Choices

The 4 coils can be positioned in space in a multitude of ways. The resonant coils can be placed outside of the drive and load coils, or nested within their respective drive/load coil, or all coils can even be nested inside of each other. With many designs to choose from, what are the benefits to these designs and what is the goal of the entire system? This section will run through some topological decisions that intuitively lead to higher efficiency systems.

As stated earlier, all coils are coupled in the 4-coil system and the goal is to transfer power efficiently from the drive coil to the load coil. It is desirable to have coil 1 highly coupled to coil 2, so the resonant coil can receive energy from the drive coil (by having a higher  $k$  value associated with their coupling). The same goes for coil 3 and coil 4. The load coil extracts energy from the secondary resonant coil. To enhance coupling, the literature suggests that the coils should be nested within each other. It was shown in chapter 5 that if two coils are nested within each other, then higher theoretical  $k$  values can be achieved if the longer coil is nested within the shorter coil. Consider the drive and load coils to be smaller than their respective resonant coils and thus, consider wrapping the drive/load coils around their respective resonant coils. Fig. 6.2 depicts the arrangement.

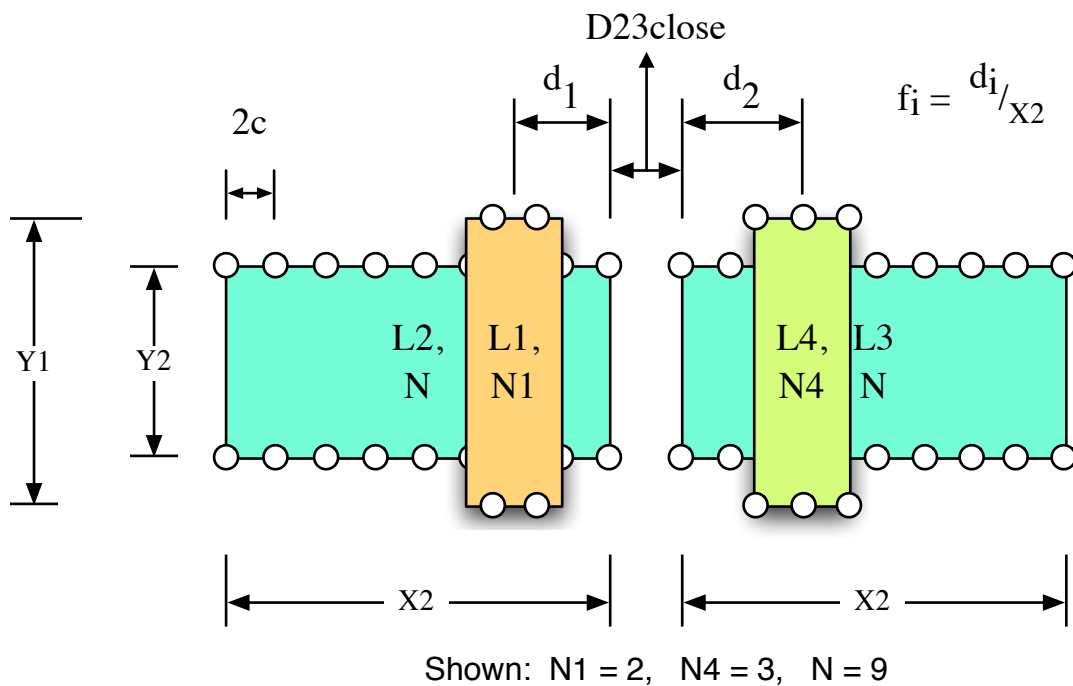


Fig. 6.2 Diagram of the 4-coil system with nested coils.

It has been noted that the positions where the load and drive coils are wrapped around their resonant coil is important to high efficiency operation. To better quantify this variation of the topology, normalized scaling parameters  $f1$  and  $f2$  have been defined. They correspond to the fractional position of the drive and load coils normalized by the length of their corresponding resonant coil. Starting from the turn ***closest to the center*** of the arrangement, the  $f1$  and  $f2$  values are the center position of the drive and load coils divided by the length of their respective resonant coils. Therefore, an assembly with  $f1=.5$  and  $f2 =1$  means the drive coil is centered upon the center of the primary resonant coil and the load coil is centered upon the turn furthest away from the primary resonant coil. In Fig. 6.2 these  $f$  values are approximately  $f1 = 0.3$  and  $f2 = 0.35$ .

All subsequent 4-coil designs in the thesis will follow this construction scaling. The next subsection will discuss the construction of these transformer systems and display some examples with accompanying information about the coils used and the calculated vs theoretical  $k$  values.

### **6.3 Coupling Coefficients Dynamics**

Two example configurations (with variations in  $f1$  and  $f2$  values) have been constructed and evaluated for inductance and their 6 coupling coefficients. As stated in chapter 5, the coupling coefficient is a parameter defined by each pair of coupled coils with all other coils in the vicinity set open-circuited. This method was used to theoretically calculate and experimentally measure all the coefficients.

#### **6.3.1 Symmetric Drive and Load Coils**

Table 6.1 displays the physical construction of a symmetric 4-coil transformer system defined as configuration #1, describes the coils involved, and shows the coupling coefficients for a range of  $f1$  and  $f2$  values. There is high enough agreement between the calculated and theoretical inductance values that error bars aren't necessary.

**Table 6.1**



**CONFIGURATION #1 (all distances in inches)**

**Drive Coil/ Coil 1: 6 turn, L = 13.75uH, Do = 9.25, dw = .125, ca = 2**

**Primary Resonant/ Coil 2: 18-turns, L = 73uH, Do = 8.75, dw = .125, ca = 2**

**Secondary Resonant/ Coil 3: 18-turns, L = 73uH, Do = 8.75, dw = .125, ca = 2**

**Load Coil/ Coil 4: 6 turns, L = 13.75uH, Do = 9.25, dw = .125, ca = 2**

Coupling Between Coil 1 and Coil 2				
Coupling Parameter	f = .25		f = .5	
	Theory	Measured	Theory	Measured
K12	.77	.765	.82	.807

Coupling Between Coil 2 and Coil 3				
Coupling Parameter	Distance = .75			
	Theory		Measured	
K23	.251		.253	

Coupling Between Coil 3 and Coil 4				
Coupling Parameter	f = .25		f = .5	
	Theory	Measured	Theory	Measured
K34	.77	.75	.82	.8

Coupling Between Coil 1 and Coil 3				
Coupling Parameter	f = .25		f = .5	
	Theory	Measured	Theory	Measured
K13	.127	.138	.178	.180

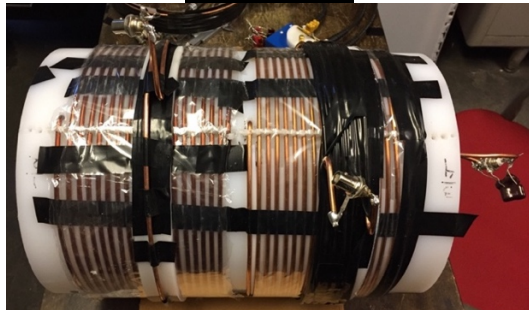
Coupling Between Coil 2 and Coil 4				
Coupling Parameter	f = .75		f = .5	
	Theory	Measured	Theory	Measured
K24	.26	.288	.184	.182

Coupling Between Coil 1 and Coil 4						
Coupling Parameter	f = .25		f = .5		f = .75	
	Theory	Measured	Theory	Measured	Theory	Measured
K14	.279	.29	.133	.126	.072	.071

### 6.3.2 Asymmetric Drive and Load Coils

Table 6.2 describes the coils involved in configuration #2. This arrangement is asymmetric, and the number of turns on the drive coil differs from the number of turns on the load coil. There is sufficient agreement between the calculated and theoretical inductance values that error bars aren't necessary.

**Table 6.2**



**CONFIGURATION #2 (all distances in inches)**

**Drive Coil/ Coil 1:** 1 turn, L = .750uH, Do = 9.25, dw = .125, ca = 2

**Primary Resonant/ Coil 2:** 18-turns, L = 73uH, Do = 8.75, dw = .125, ca = 2

**Secondary Resonant/ Coil 3:** 18-turns, L = 73uH, Do = 8.75, dw = .125, ca = 2

**Load Coil/ Coil 4:** 6 turns, L = 13.75uH, Do = 9.25, dw = .125, ca = 2

Coupling Between Coil 1 and Coil 2				
Coupling Parameter	f = .25		f = .5	
	Theory	Measured	Theory	Measured
K12	.77	.765	.82	.807

Coupling Between Coil 2 and Coil 3		
Coupling Parameter	Distance = .75	
	Theory	Measured
K23	.251	.253

Coupling Between Coil 3 and Coil 4				
Coupling Parameter	f = .25		f = .5	
	Theory	Measured	Theory	Measured
K34	.77	.75	.82	.8

Coupling Between Coil 1 and Coil 3				
Coupling Parameter	$f = .25$		$f = .5$	
	Theory	Measured	Theory	Measured
K13	.127	.138	.178	.18

Coupling Between Coil 2 and Coil 4				
Coupling Parameter	$f = .75$		$f = .5$	
	Theory	Measured	Theory	Measured
K24	.26	.288	.184	.183

Coupling Between Coil 1 and Coil 4						
Coupling Parameter	$f = .25$		$f = .5$		$f = .75$	
	Theory	Measured	Theory	Measured	Theory	Measured
K14	.279	.29	.133	.126	.072	.071

## 7. Coreless Transformer Design Overview

Chapter 6 discussed the assemblage of coils and topologies that have the potential to be highly efficient 4-coil transformers. Before designing the individual coils for a given inductance, resistance, and the specific topology to achieve the best coupling configuration, system specifications must be established to define the constraints of the overall design. The system in this thesis consists of driving circuitry, the 4-coil transformer, and a load impedance.

The intention of this thesis is to show an approach to accurately designing one of these transformers. Therefore, 100W has been chosen to be the device power specification as a small-scale demonstration of successful construction. If the coils are meant to consume a percentage of the input power as heat, then the 100W power specification characterizes the physical geometries of the coil (number of turns, wire diameter, etc). The next chapter will discuss the methodology of deciding among all the possible designs that fit 100W by analyzing the relative spatial positions of the coils.

Subsection 7.1 will examine the design choices that enable the system to run at 100W specification and how the physical dimensions of the coils are affected. Subsection 7.2 will provide an overview of the measurement tool in regards to power efficiency and the necessary adjustments needed to correct the output under certain measurement conditions. Finally, subsection 7.3 will deal with the implications of using a half-bridge inverter to power the system.

### 7.1 100W Design Choices

Given a 100W specification, there are many ways to split up the power at the output into voltage and current. For convenience, it has been decided that 40V at 2.5A will be the desired output voltage and current values. Given the 100W constraint, this sets the resistor output to  $16\Omega$ .

Therefore, the load resistor of the system will be fixed at  $16\Omega$ .

All the coil geometries are impacted by the 2.5A output current specification. Since heat loss in the windings is a component of the overall loss and thus a factor in power efficiency, the transformer coils must be built such that heat loss is a small fraction of the power. Because heat loss is generated by the resistive elements in the coils, this constrains the amount of material that composes the coils. Due to proximity effect, not only is the length of wire to create a coil an important factor in the heat loss calculation, but so is the amount of turns and the spacing

between them. Two coils of similar wire length may have substantially different resistance and Q values due to the amount of turns and spacing between adjacent turns. Thus, the heat loss limit also effects the geometry of the coils. To aid in obtaining a number of coils that fit the winding loss specification, a MATLAB script was built, *Possible\_Coils.m*, using the design algorithms developed in Chapter 4 and 5. It evaluates the inductance, Q, and power loss in coils of varying c/a and coil turn numbers for different frequencies. *Possible\_Coils.m* allows the user to set these parameters:

Inputs:

- Current:** The current expected in coils (amps)
- Freq:** Frequency of operation (Hertz)
- Ca:** c/a values of interest (matrix of rational numbers)
- Do:** Outer Diameter of coils (inches)
- N:** Number of turns on the coils (matrix of integer)
- Dw:** Wire diameter of the coils (inches)
- Llow:** Lower Bound for Inductance (Henries)
- Lhigh:** Upper Bound for Inductance (Henries)

The program runs through every coil specified by the user settings and evaluates its inductance, resistance, Q, and power loss given the maximum current. It then plots two scatter plots, one for Q and another for inductance. Each point represents a coil and is augmented with its c/a value followed by its power loss in watts. Fig. 7.1 depicts the coils that fit the constraints of coil diameters equal to 10 in, wire diameters of .3 in, current of 2A, c/a varying from 1.5 to 2, inductance from 50uH to 60uH, and operating frequencies of 100kHz and 300kHz. The user settings that produced the plots are given to the left. Changing the frequency won't change the distribution of coils, but will provide the user insight into the achievable values of Q and power loss. This method allows for convenient prediction of coils that are good candidates for transformer design. Now that a number of agreeable coil geometries are known, the next engineering challenge is figuring out how to position them in space to maximize the efficiency of the system via coupling parameters. This will be discussed in Chapter 8.

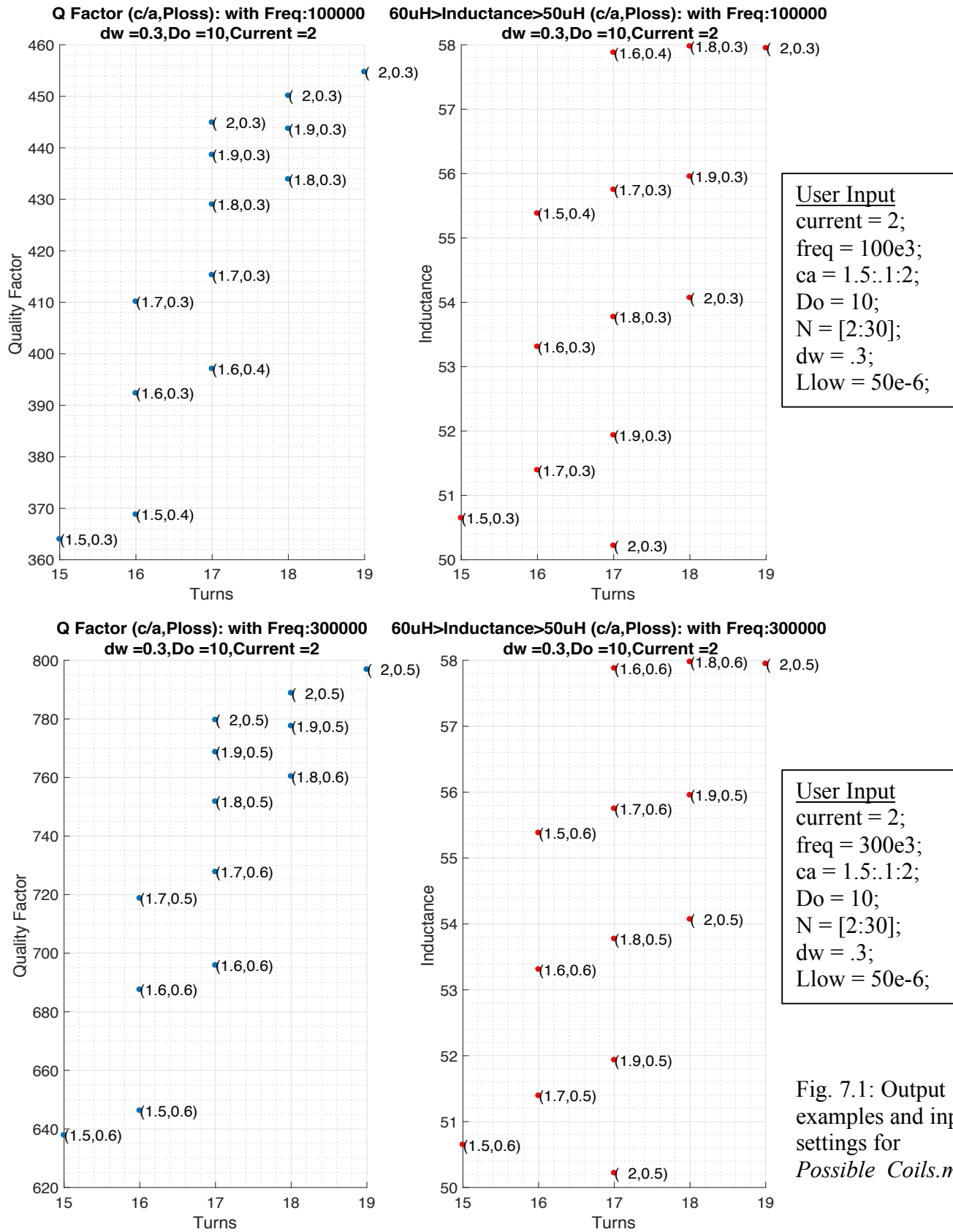


Fig. 7.1: Output examples and input settings for *Possible Coils.m*

## 7.2 Impact of Resonant Capacitors

Although proper coil selection is paramount to efficient design due to minimization of losses and frequency of operation, selecting the right capacitors are also important to further benefit the efficiency of design. A resonant coil (coil and capacitor) acts as a series RLC circuit and at the resonance frequency has a  $Q$  of the following:

$$Q = \frac{\sqrt{L/C}}{R}$$

Thus, for higher  $Q$  values, it is preferable for the capacitor to be of smaller magnitude. Additional appealing capacitor characteristics include, low series resistance, low tolerance values, and high self-resonance. A series resistance presents additional losses to the resonant coils, which will increase damping in the frequency response. An example plot of the series resistance of a 10nF capacitor is shown later in table 10.1. As capacitance increases, so too does its losses, a trend in capacitor selection. However, a simple method of achieving low losses is to place capacitors in parallel with each other, essentially connecting their ESRs in parallel, and thus reducing the total effective series resistance. Low tolerances are necessary for maintaining the capacitance values over time and preventing the resonance frequency from drifting. High self-resonance will ensure the capacitors operate at their nominal values for a long span of frequency and will never resonate at frequency regimes of operation. Capacitors also play a role in tuning the resonators since they take part in the resonance frequency. Capacitors are vital components in the transformer model and should be taken into consideration during design to guarantee high efficiency.

## 7.3 Data Collection

In designing this power transfer system, the figure of merit is the power efficiency. This section will discuss how the circuits in this thesis will be evaluated for power efficiency.

### 7.3.1 Power Efficiency and S-Parameter Analysis

The 4-coil system can be considered as a two-port network where the input source terminals and output load terminals act as the two ports. Therefore, one can analyze the system using 2-port scattering and reflection parameters. The magnitude of the transmission coefficient,  $S_{21}$ , can be

used to measure power transfer efficiency. The  $S_{21}$  parameter is calculated as in [22] and is given by:

$$S_{21} = 2 * \frac{V_{load}}{V_{source}} \sqrt{\frac{R_{Source}}{R_{Load}}}$$

If the load and source impedance are equal then in an ideal, 100% efficient system the load voltage would be half the source voltage. Thus,  $S_{21}$ 's maximum value is 1. Consider  $S_{21}^2$ , given as:

$$S_{21}^2 = 4 * \left. \frac{V_{load}^2}{V_{source}^2} \right|_{R_{Source} = R_{Load}}$$

Here, one can see that  $S_{21}^2$  is a ratio of squared voltages. Therefore, under the condition that the source and load impedance are equal, it is a measure of the power ratio from output to input [23]. The Bode100 can directly measure the  $S_{21}$  parameter from the physical circuit and uses the following configuration to achieve it, Fig. 7.2:

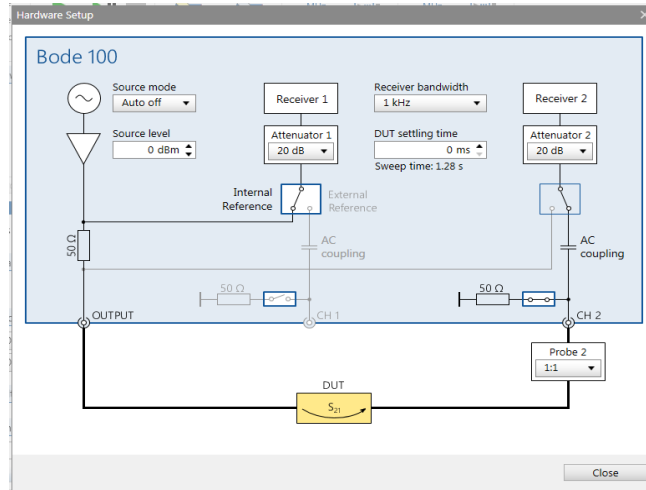


Fig. 7.2: Bode100 circuit configuration for  $S_{21}$  transmission coefficient measurement.

One set of voltage probes measures the source voltage *before* the source resistance and another measures the voltage *at* the load resistance. The Bode100's input and output impedances are fixed 50 Ω, thus the  $S_{21}$  measurement made with it provides an accurate measurement of power transfer efficiency. However, when operating the Bode100 with an unmatched source and load resistance, a few corrections have to be made to arrive at the right output. This is because

the device calibration assumes a matched impedance system. Appendix D discusses the adjustments required to calculate the proper output plots.

#### 7.4 Power Amplifier Drive Circuitry

Drive circuitry in the form of a power amplifier is necessary for applying the input power to the transformer. Powered by a DC voltage, the amplifier is driven by a frequency generator and applies a switched voltage waveform to the transformer via the drive coil. The basic amplifier topology consists of four transistors in the H-bridge configuration [23] working as on-off switches, which allows the transmitter to receive a square-wave AC voltage signal with no DC component.

The H-bridge works by turning on pairs of diagonally opposed switches while keeping the other pair off. The transistors function as switches, meaning that they are ideally either fully on or fully off with no time in between. Using Fig. 7.3, switches A turn on and B off to bring  $V_{cc}$  to the transmitter during the first half of the cycle. During the second half, switches B turn on and A off such that the voltage across the transmitter is now  $-V_{cc}$ . Making sure that switches A and B are on for equal time periods is important to prevent application of DC voltages to the drive coil.

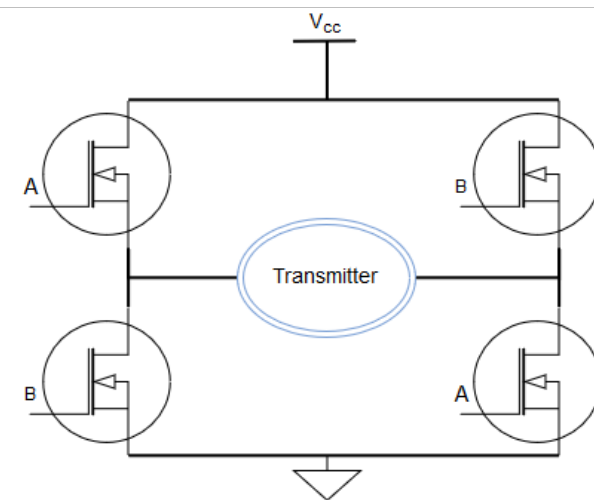


Fig. 7.3: High-level schematic depicting the operation of the H-bridge circuit [23]

The output of the H-bridge has a low impedance ( $< 1\text{ohm}$ ) and thus the source impedance of input voltage to the drive coil of the transformer will have a low impedance in simulation efforts. The H-bridge circuit employed in testing the 100W model coreless transformer was

developed in a prior thesis by Lukashov [23]. Figure 7.4 displays a labeled top view of the amplifier PCB. The schematic for the H-bridge can be found in Appendix E.

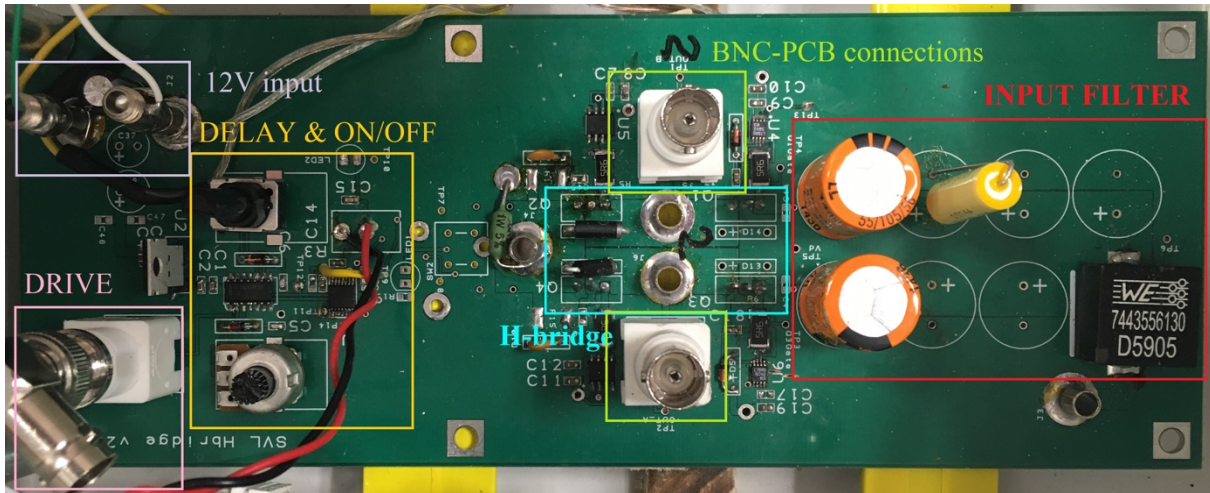


Fig. 7.4: Top view of amplifier PCB [23]

## 8. System Design Program using MATLAB and LTSpice

In the 4-coil transformer system many parameters are inter-related. Seldom can one change a single parameter value without affecting a couple others. For example, a change in inductance of one coil will alter its magnetic coupling to every other coil and thus change the output efficiency. Therefore, it is desirable to create simulations that are in agreement with the experimental results. LTspice is a tool that can be used to implement these simulations. By itself, LTspice offers a powerful toolset for composing netlists and simulating circuits under different conditions. However, manual manipulation of a multitude of LTspice netlists can be very time consuming, especially when a small amount of variation guides each change. Such manual manipulation would occur for every configuration that would be evaluated. A change in one value leads to re-calculation of all contingent values, which requires the use of the MATLAB-coded design algorithms explained earlier.

Therefore, it is desirable to combine MATLAB parameter calculations, alterable parameters, and high volume LTspice automation to get rid of the tedious manual value changing that often results in these situations. Furthermore, specific value changing of one parameter, such as coupling coefficients or inductance, might lead to topologies that are physically unrealizable given our spatial and geometric constraints. One would like to evaluate simulations associated with systems that one can actually build. Therefore, for the purposes of this thesis, a joint MATLAB-LTspice utility has been developed to ease the communication between these programs. By using the design algorithms discussed in Chapter 4, a user can input the physical quantities that describe the coil arrangement of interest and the program will output  $S_{21}$  transfer efficiency outputs determined by LTspice simulation. This program can aid design immensely by providing an accurate prediction based on first order changes to the system. Second order changes like inductance are the result of first order changes like changing the wire diameter of a coil.

This section provides documentation for a method to couple operation of MATLAB and LTspice to automate circuit design and analysis. This procedure allows the user to automate batch netlist production of 4-coil transformer systems by selecting physical parameter variations through a manually created template netlist. Once all the LTspice circuit files (.cir) are generated, a MATLAB issued command-prompt command is then executed to run LTSpice's

simulator sequentially on all generated circuits. Output data is saved in files with LTSpice's default encrypted '.raw' format. MATLAB is then used to plot resultant output values over a set of user input parameter values (described later). The MATLAB code of all the programs will be located in Appendix E.

### 8.1 Configuration and LTspice Schematic

The template for the LTspice 4-coil coreless transformer model is depicted in Fig. 8.1. The drive coil is defined by the circuit elements *Ldrive* and *RdcDrive*. The resonant coils are defined by their respective circuit elements *LmagX*, *RdcX*, and *CX*. The load coil is defined by the circuit elements *Lload* and *RdcLoad*. The drive and load resistor are defined as *RSOURCE* and *RLOAD*. The three 'extraneous' resistors 'R\_extraX' are necessary for LTspice to run simulations but don't effect the results, they are large and represent the air gap impedances between coils. Note, only the drive and load coils are directly grounded; the resonant coils are not. Finally, the two 'fictitious' voltage sources to the left are used as 'dummy' variables needed to plot the values of the source and load resistances. This is useful for calculations of  $S_{21}$ . Since LTspice doesn't allow direct plotting of component values, a workaround of generating a voltage of the same numerical value as the resistors is used. All coupling parameters are shown and the '.ac' spice directive describes the range of small signal AC analysis to be conducted: in this case 1000 points within every octave between 10KHz and 1.5MHz. MATLAB alters the values in the circuit via the '.param' LTspice statement. The next section will discuss the structure of the program.

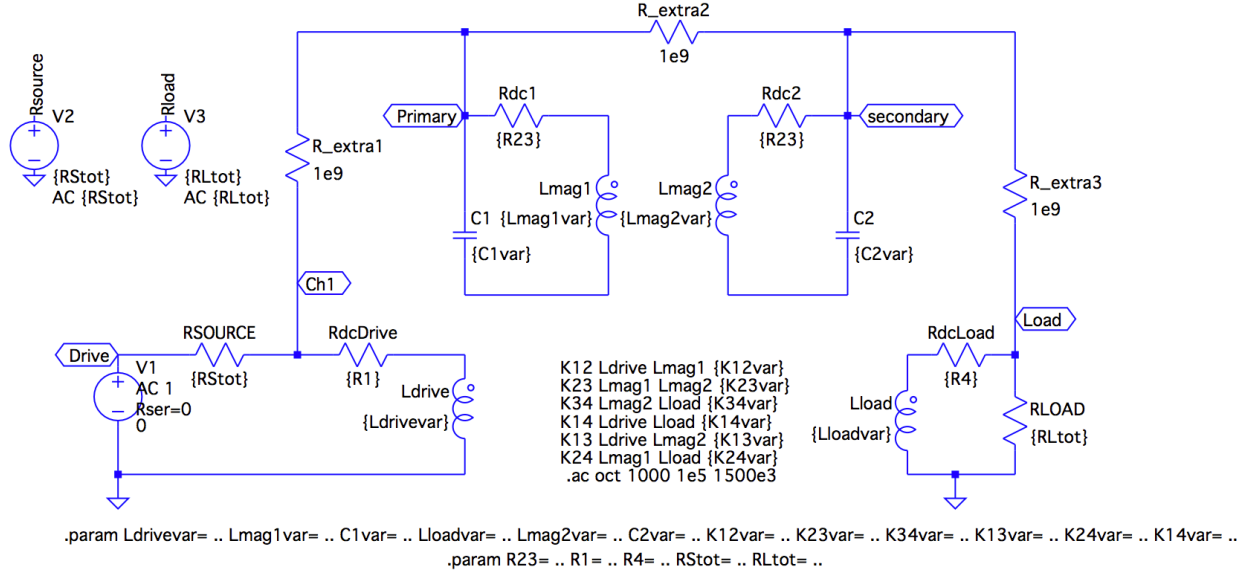


Fig. 8.1: LTspice Schematic of a 4-Coil double resonant transformer. Note, all the values for parameters are in brackets. This allows them to be manipulated by the ‘.param’ line (located in the bottom of the image). MATLAB alters the parameter values via this line. Extraneous resistors represent air gap impedances and their presence is necessary but has no impact, thus they’re large.

## 8.2. Structure of Program

The method by which MATLAB can activate and control a LTspice circuit simulation program is presented here. There are 5 components to the process. After these are presented, an example that goes through the process is given.

### Overview of System:

0. Directory Management
1. Cylindrical\_Coil\_Simulator.m
2. Master.m
3. SpiceModel.m
4. Evaluation.m
5. Plotting
6. An Example Run

#### 8.2.1 Directory Management

Throughout this chapter there will be mention of certain directories. This section of the document is intended to clarify the directory hierarchy and detail how directories will be mentioned. The directory with all the MATLAB files (Master scripts and accompanying functions) will from here on be known as the ‘MAIN’ directory. Along with the MATLAB files,

there will be a folder called ‘SpiceModels’. This directory will hold all the generated netlists and output data from simulations.

### ***8.2.2 Cylindrical\_Coil\_Simulator.m***

*Cylindrical\_Coil\_Simulator.m* is the script that is run to operate the whole procedure. The first section allows the user to input a number of parameters that will define the overall geometry of the system. Fig. 8.2 illustrates the allowed input parameters. Coils and suffixes 1, 2, 3, and 4 correspond to the drive, primary, secondary, and load coils respectively. For the rest of this chapter, MATLAB variables will be in **bold** while scripts and functions will be in *italics*. The physical parameters are listed as (all values are scalar quantities unless otherwise specified):

**dw:** The wire diameter; held uniform over all coils (inches)

**D<sub>02</sub>:** Outer diameter of the primary resonant coil (inches)

**ca:** The pitch over the wire diameter of each winding; held uniform among all coils

**N<sub>1</sub>:** Number of turns on the drive coil; held for all simulations

**N<sub>4</sub>:** Number of turns on the load coil; held for all simulations

**f<sub>1</sub>:** A matrix that determines the fractional distances of the primary resonant coil, starting from its winding closest to the secondary resonant coil, where the middle of the drive coil will be placed upon.

**f<sub>2</sub>:** A matrix that determines the fractional distance of the secondary resonant coil, starting from its winding closest to the primary resonant coil, where the middle of the load coil will be placed upon.

**N<sub>main</sub>:** A matrix quantity defining the turns of the resonant coils that will be simulated through.

**D<sub>23close</sub>:** A scalar value determining the distance between the closest turns of the resonant coils (center-to-center)

**R<sub>source</sub>:** Value of the source resistance (ohms)

**R<sub>load</sub>:** Value of the load resistance (ohm)

**C<sub>1</sub>:** The lumped capacitance attached to the primary resonant coil (F)

**C<sub>2</sub>:** The lumped capacitance attached to the secondary resonant coil (F)

**RadialDist:** The difference in diameter between the load/drive coils and their respective resonant coil (inches)

**B<sub>1-B4</sub>:** Multiplier applied to each coil resistance.

**Proximity:** Binary value enabling the Proximity effect calculation of resistance for each coil

**PlotOption:** Value of 1 or 2 enabling a plot scheme described in a later section.

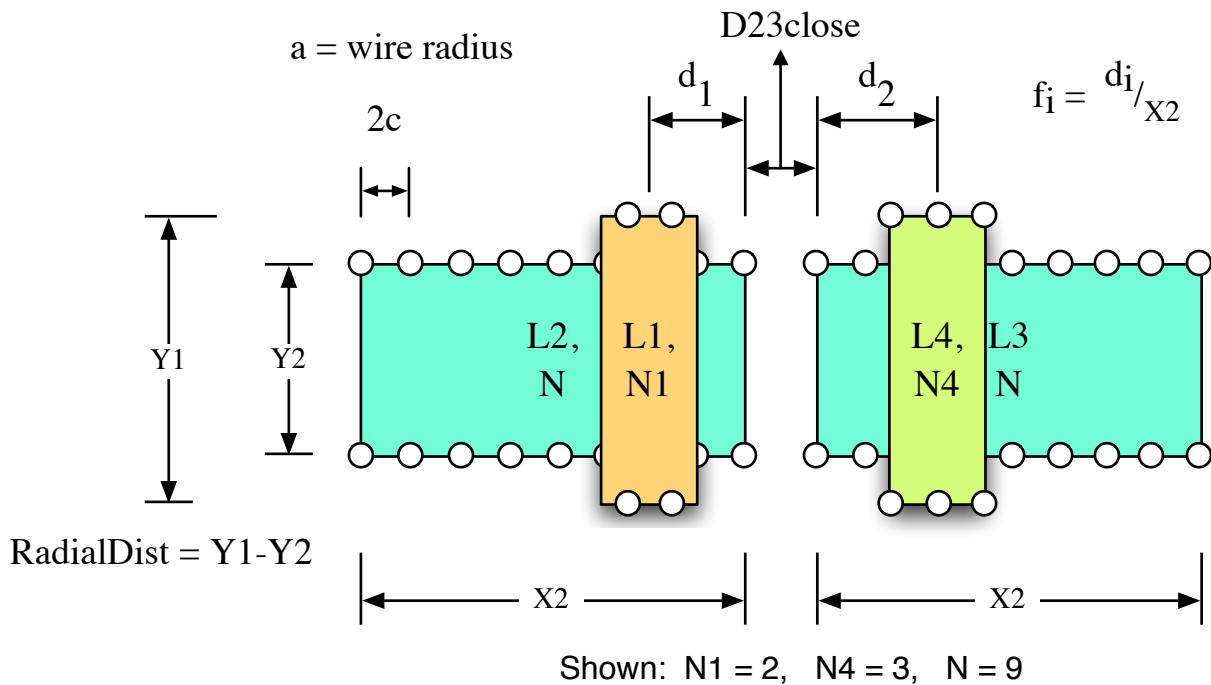


Fig. 8.2: Depicts the geometric quantities the program required as inputs and their relationship to the rest of the system.

Once the user has input their configuration, the program performs calculations to assign the rest of the coil parameters. Since the systems simulated have symmetric arrangements of resonant coils, we assign the diameter of coil 3 (the second resonant coil) to be the same diameter of coil 2 (the first resonant coil). The diameters of coils 1 and 4 are calculated by adding **RadialDist** to the diameters of coil 2,3. Next, the length and inductance of coils 1 and 4 are calculated with the *Cylindrical\_Inductance* function from Chapter 4. Finally, the program enters its main loop. The amount of iterations in this loop are determined by the number of elements in **Nmain**.

The loop begins by calculating the lengths and inductances of the resonant coils using the *Cylindrical\_Inductance* function. The amount of turns in each coil is plucked from **Nmain** and will go in sequential order once the loop is concluded. What follows is a set of two *for* loops that are determined by the elements of **f1** and **f2**. These will assign each simulation a specific **f1** and **f2** position and will iterate through all possible combinations (**f1** x **f2**). At this point, all physical quantities of a 4-coil system have been defined and all that remains is to calculate the coupling coefficients and run the simulations.

All six coupling coefficients are calculated in the subsequent lines using the *Cylindrical\_Coupling* function described in Chapter 5. The distances among coils needed for the calculations are computed with the length parameters that have been calculated for each coil thus far. Next, the program will do its final preparations for the first round of simulations by renaming component parameters used in *Master.m*, which is the script that conducts the simulations and will be explained in the next subsection. Additionally, the resistance of each coil is calculated with the *Cylindrical\_Resistance* function from Chapter 4 and is assigned variable names **Rtot1** through **Rtot4** corresponding to the 4 coils. The binary variable, **Proximity**, can be toggled to calculate high frequency resistance with proximity effect or just skin effect. It is supplied as the last argument to the *Cylindrical\_Resistance* function.

Since the program seeks to accurately calculate the maximum  $S_{21}$  value produced by each simulation and the frequency at which it occurs, it is necessary to have the right resistance values at this frequency. LTspice doesn't allow for variable frequency resistors coupled with proximity effect, so the coils are assigned resistances based upon the estimated resonance frequency of the resonant coils. Due to the frequency splitting that may occur in these systems, the first round of simulations is meant to find the frequency of peak  $S_{21}$  in order to plug it back into the resistance calculation and produce the correct resistance at the actual  $S_{21}$  peak. Therefore, after a first round of simulations, **Rtot1** through **Rtot4** are re-calculated again to the correct resistance according to the frequency corresponding to the  $S_{21}$  peak. However, this time the resistance multiplier factors **B1** through **B4** are applied to the resistances. These factors are a simple way of including the impact of coils with different resistances on the system performance without changing geometric quantities. Using factors less than 1 could simulate the effects of using different wire geometries that possess less resistivity in higher frequencies. Factors greater than 1 can account for extra losses in the system like the resistive loss in the capacitors. This new resistance is then applied for the second and final round of simulations. This concludes a set of simulations for one specific transformer geometry. Once a set of simulations are done, the next scalar **f2** value is determined, the coupling calculations are determined again, and the simulation process repeats. Once the whole **f2** matrix has been combined with an element of **f1**, the next **f1** scalar value is picked and the process repeats again. Finally, when all **f1** and **f2** combinations have been done with an element of **Nmain**, the next value of **Nmain** is chosen and the process repeats again. When the three nested loops have completed, the data is then plotted using one of the two plotting options.

This concludes the main script; the following subsections will discuss the smaller scripts that *Cylindrical\_Coil\_Simulator.m* calls.

### 8.2.3 *Master.m*

*Master.m* is the script called to start the simulation process. It first performs garbage collecting and deletes all leftover ‘.cir’, ‘.raw’, and ‘.log’ files in the “MAIN/SpiceModels” directory. These could be files left over from a previous run of the program and can potentially interfere with future calculations.

The command window displays, “Circuit Undergoing Simulation” to announce the start of model creation. The set of parameters produced in the script, *Cylindrical\_Coil\_Simulator.m*, will be placed into the function *SpiceModel.m*. The parameters undergo the renaming scheme done near the end of the previously explained script.

*SpiceModel.m* generates a netlist for each LTspice circuit condition. A name is then generated that mimics the same name of the file generated in the *SpiceModel.m* function. The name of the LTspice model is a chain of parameter values that compose the model. Next, using the MATLAB ‘system’ command, which allows one to issue commands on the command-prompt via MATLAB, the script calls LTspice to run on the recently created spice netlist. It uses the recently created name variable to specify the file. The LTspice executable is usually located in ‘C:/Program Files/LTC / LTspiceXVII/ XVIIx86.exe’. One thing to note is that on the same command line, following the LTspice command is a subsequent ‘&& ping 1.1.1.1 –n 1 –w 500> null’. This is meant to pause MATLAB before attempting to perform the next system call/LTspice simulation. It has been observed that if many calls are done back-to-back, simulation commands are dropped and errors occur. So, it’s best to give LTspice 500 ms to perform simulations between subsequent calls. The ‘500’ in ‘&& ping 1.1.1.1 –n 1 –w 500> null’ does exactly that. Once all netlists have been simulated, MATLAB displays ‘Netlist Generation/Simulation Complete’.

What follows is the penultimate step: *Evaluation.m* is called. *Evaluation.m* outputs 2 quantities: **Freq** and **S21plot**. **Freq** is the frequency value at which the  $S_{21}$  achieved a peak in this specific simulation. **S21plot** is the entire  $S_{21}$  waveform calculated by MATLAB via the voltage and current waveforms calculated by LTspice in simulation. The values are used in the plotting options described in a later subsection. When the function is done, MATLAB displays,

‘Evaluation Complete’. This concludes the operation of the script. The main functions that *Master.m* calls will be explained in detail for the remainder of this document.

#### **8.2.4 SpiceModel.m**

##### **Inputs:**

Parameter Set (Ldrive, Lmag1, C1, Lmag2, C2, Lload, K12, K23,K34, K13, K24, K14)

##### **Outputs:**

Void

This function is in charge of generating a spice netlist given a set of parameter values. First, it generates a name for the netlist it plans to create. This name is composed exactly from the parameter values input into the function. It will then open a ‘.cir’ file and first print the full path of the file. Next, the function undergoes some scoping mechanics to obtain the desired resistance values. These could’ve been passed through the function’s prototype but this method was found to be easier for quick manipulations of resistance. **Rtot1** through **Rtot4**, **Rsource**, and **Rload** are borrowed from the global scope, ‘base’. The next step is handling the text that will represent the circuit as a netlist. An LTspice netlist representing the 4-coil model in Fig. 8.1 is pasted into MATLAB with a couple exceptions. Variables of interest are appended with ‘var’ in the text file. For example, K12’s LTspice value is the variable {K12var}. This is done for all variables of interest. Next, a ‘.param’ line is inserted into the text in order to set the newly appended variables. This is where MATLAB will inject values into the file. Lastly, the waveforms to be saved are decided upon based on the labeling scheme chosen in the schematic in Fig. 8.1. If no waveforms are selected, then all voltage and current plots are saved. This option can consume a lot more memory and can cause confusion with some of the functions later in the program. Therefore, it’s best to save only the necessary signals. The program saves V(load), V(Ch1), I(r5), I(r4), V(drive), V(rsouce), and V(rload) to perform  $S_{21}$  calculations and power efficiency in MATLAB. Finally, the text (which was originally a MATLAB string array) is printed into a ‘.cir’ file. The file is then closed. The ‘.cir’ file will be located in ‘MAIN/SpiceModels/’ .

### 8.2.5 Evaluation.m

**Inputs:**

Void

**Outputs:**

Frequency of  $S_{21}$  peak value, **Freq**, and the  $S_{21}$  waveform, **S21**.

This function will use MATLAB to construct the  $S_{21}$  plot with the voltages and currents saved from LTSpice's simulation and find the frequency of maximum value. It first figures out how many '.raw' files are inside the 'MAIN/SpiceModels/' directory and iterates through all of them. In this case, there is only one, but the option has been left incase previously computed '.raw' files would like to be evaluated. For each one, it extracts the name and uses the open source function 'LTSpice2Matlab' to unpack the '.raw' file into MATLAB accessible packages.

LTSpice2Matlab is a function found on MATLAB's website. It enables unpacking of LTSpice's simulation data into MATLAB manageable portions for more powerful manipulation. The data will be saved into the 'raw\_data' variable. Next, the graph of interest, the  $S_{21}$  transmission parameter, is constructed. The 'raw\_data' has attributes that allow a user to retrieve the LTspice output data in MATLAB form. Calling 'raw\_data.variable\_mat(x,:)' will retrieve a matrix of values corresponding to the x<sup>th</sup> saved plot from the LTspice simulation. Therefore, to calculate  $S_{21}$  it is necessary to compute the following:

$$S_{21} = 2 \sqrt{\frac{R_{source}}{R_{load}} \frac{V_{load}}{V_{source}}} = 2 \frac{V(load)}{V(drive)} \sqrt{\frac{V(rsource)}{V(rload)}}$$

LTspice has its own method of saving plots that can lead to confusion. However, the methodology follows 3 simple rules:

1. Voltages are ordered in the order their nodes are introduced in the netlist; regardless of name. For example, if node 'N5' is introduced on line 1 and 'N1' is introduced on line 8, and V(N1) and V(N5) are to be saved. Then variable\_mat(1,:) will refer to 'N5' and variable\_mat(2,:) will refer to 'N1'.
2. Currents are ordered in alphabetical-numerically decreasing order. So if I(a), I(g2), and I(g5) are to be saved. Then variable\_mat(1,:) will refer to I(a), variable\_mat(2,:) will refer to I(g5) and so on.
3. Voltages are all ordered before Currents.

For the unique labeling of variables in this thesis, S21 is computed the following way, where 'raw\_data.variable\_mat(x,:)' has been substituted with 'Mat(x,:)' :

$$S_{21} = 2 \frac{V(load)}{V(drive)} \sqrt{\frac{V(rsource)}{V(rload)}} = \frac{Mat(3,:)}{Mat(1,:)} \sqrt{\frac{Mat(4,:)}{Mat(5,:)}}$$

A matrix of values corresponding to  $S_{21}$  at each point in frequency simulated is obtained. LTspice plots the absolute value of its data so the MATLAB function ‘abs’ is run on the  $S_{21}$  matrix when plotting. MATLAB now runs the ‘max’ function on the matrix and extracts the max value and index at which it occurs. The index is used to select the matching frequency from ‘raw\_data.freq\_vect’, an automatically-saved matrix from the simulation. This frequency is assigned the variable name **Freq** and is the second output of the function.

### 8.2.6 Plotting

The program offers two options for plotting useful data for design. The user has given the program two different pieces of information regarding the coil topology: constraints and variables. A constraint, like the capacitance on the resonant coils, doesn’t change through simulation. However, the number of turns each resonant coil possesses does change. Three parameters were declared variable via matrix definitions: **Nmain**, **f1**, and **f2**. Therefore, the goal is to display the relationship between the efficiency and these three variables in a digestible manner.

Plotting option #1 will display a number of figures equal to the number of elements in **Nmain** plus 1. For each value of **Nmain**, a set of plots will be generated describing the variable coil arrangement under the values of **f1** and **f2**. For example, if **f1** is a 3-element array and **f2** is a 5-element array then there will be 3 plot windows with 5 plots in each window depicting the result of all combinations. Once again, that’s for one element of **Nmain**. Throughout this iteration of plots, the ones that produced the maximum  $S_{21}$  value among their group (using the recent example, 1 plot out of the 15) will be chosen, plotted, and augmented with their corresponding (**f1,f2**) values in an additional plot figure. This is done for all elements of **Nmain**. When the program has run through all **Nmain** values, then a plot depicting the  $S_{21}$  maximum given the amount of turns on the resonant coils (values given by **Nmain**) is shown. This plot is composed of all the  $S_{21}$  peaks collected throughout all the runs and each point is detailed with the (**f1,f2**) that produced it. Therefore, one can plot for the optimal position given a set of coils and see how the position changes as the number of turns on the resonant coils change. This

plotting option can help to find the optimal number of turns on the drive and load coils and the coil positions for the highest  $S_{21}$  value.

Plotting option 2 will plot one figure. It will only consider the first element of **f1** and **f2** and all the values of **Nmain**. It will search for all the  $S_{21}$  plots associated with the first elements of the **fx** matrices for every value of **Nmain**. Then the  $S_{21}$  plots are placed on a figure. Thus, one can easily compare the effects of changing the number of turns on the resonant coils for a specific drive and load coil position. This plotting option can help to find a favorable number of turns on the resonant coils.

### 8.2.7 An Example Run

This section will walkthrough an example of a call to *Cylindrical\_Coil\_Simulator.m*. The only step (after the user has configured the proper directory hierarchy) is to input the physical quantities related to the test coil geometries. Then the user runs the script. For this example, the following values were submitted (both plotting options are considered):

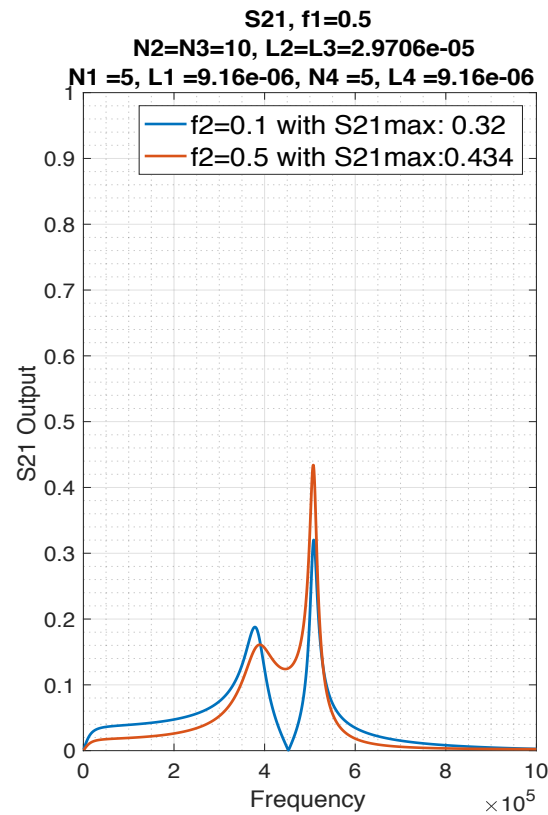
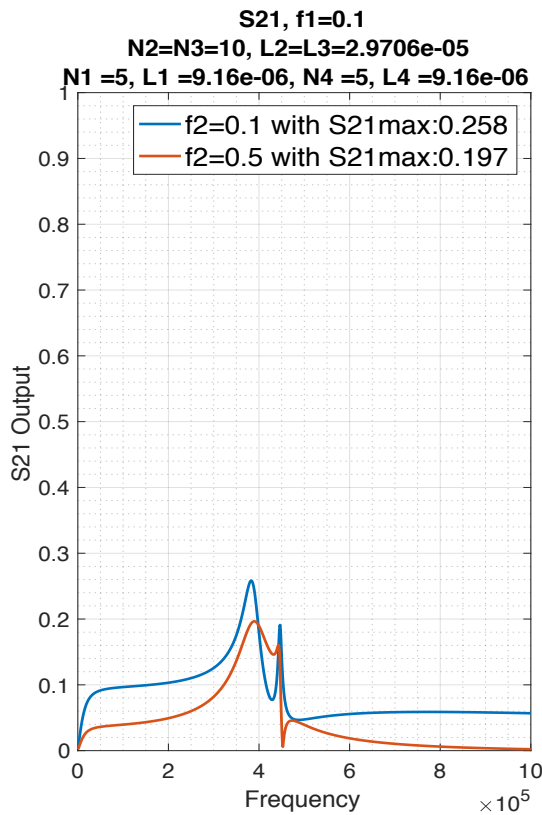
```
dw = .5;
Do2 = 10;
ca = 2;
N1 = 5;
N4 = 5;
f1 = [.1 .5];
f2 = [.1 .5];
Nmain = [10,15];
D23close = 3*dw*ca;
Rsource = 1;
Rload = 50;
C1 = 10e-9;
C2 = 10e-9;
RadialDist = 2*dw*ca;
B1 = 1;
B2 = 1;
B3 = 1;
B4 = 1;
Proximity = 1;
PlotOption = (both);
```

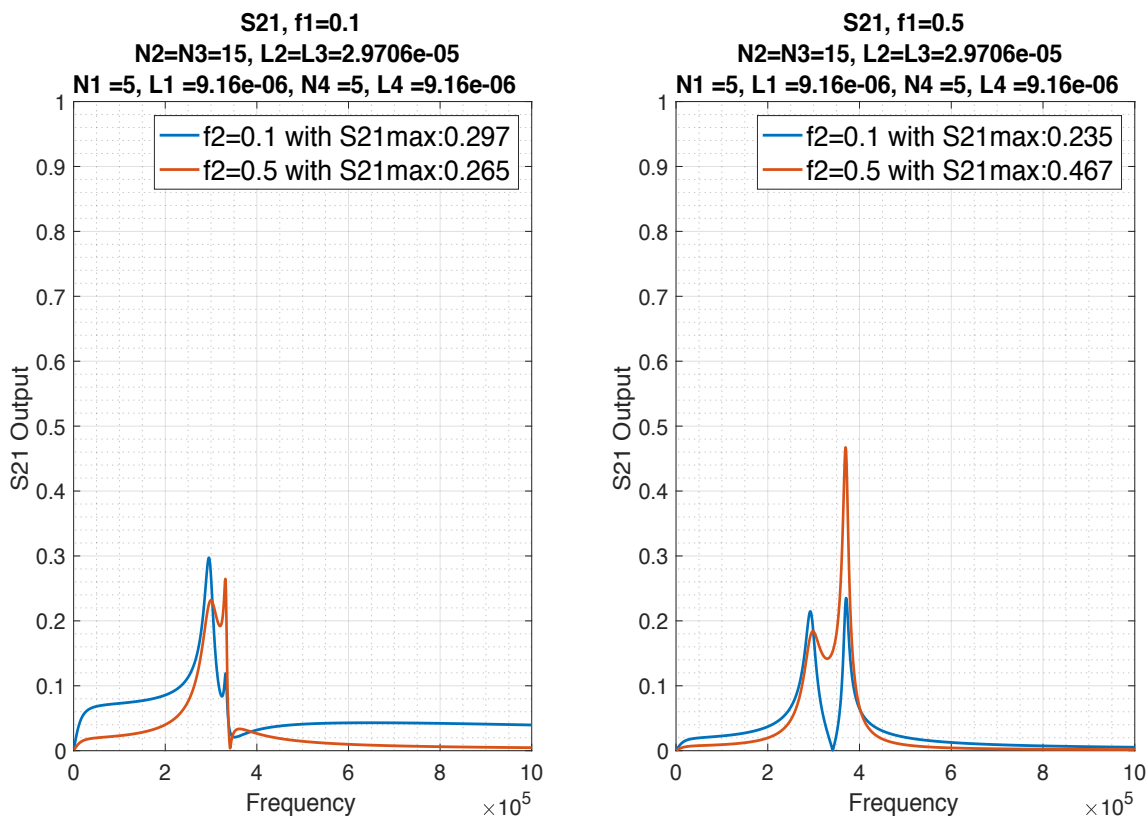
For plotting option #1, three total figures are expected, two figures containing 2 plot windows, each encompassing 2  $S_{21}$  plots for varying **f2** parameters, and the last will summarize the findings among all turns investigated. For plotting option #2, one figure will be displayed corresponding to the resonant coil turns evaluated at **f1** = **f2** = .1. **f1** and **f2** are 2-element arrays and **Nmain** is a 2-element array so there will be 8 geometries simulated, 2 simulations for each,

which makes a total of 16 simulations. MATLAB will display the following numerous times (once per simulation).

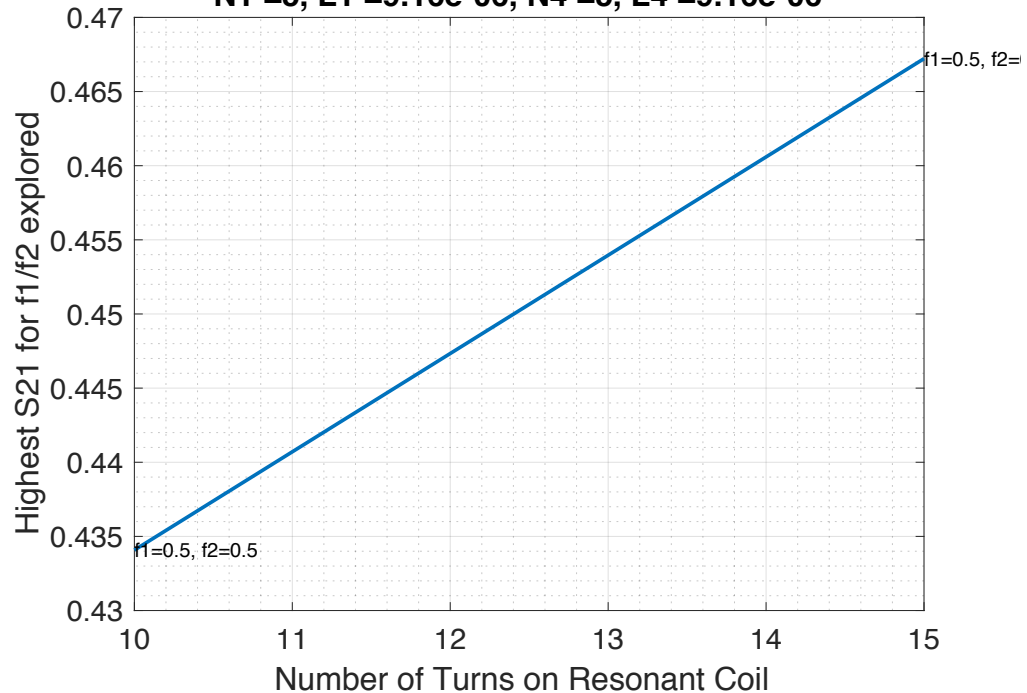
“Cleaning Complete  
 Circuit Undergoing Simulation  
 Netlist Generation/Simulation Complete  
 done  
 Evaluation Complete”

Once completed, the following figures will appear for plotting option #1. Note, this combination of parameters was not chosen for optimality, but to illustrate the program’s procedure.

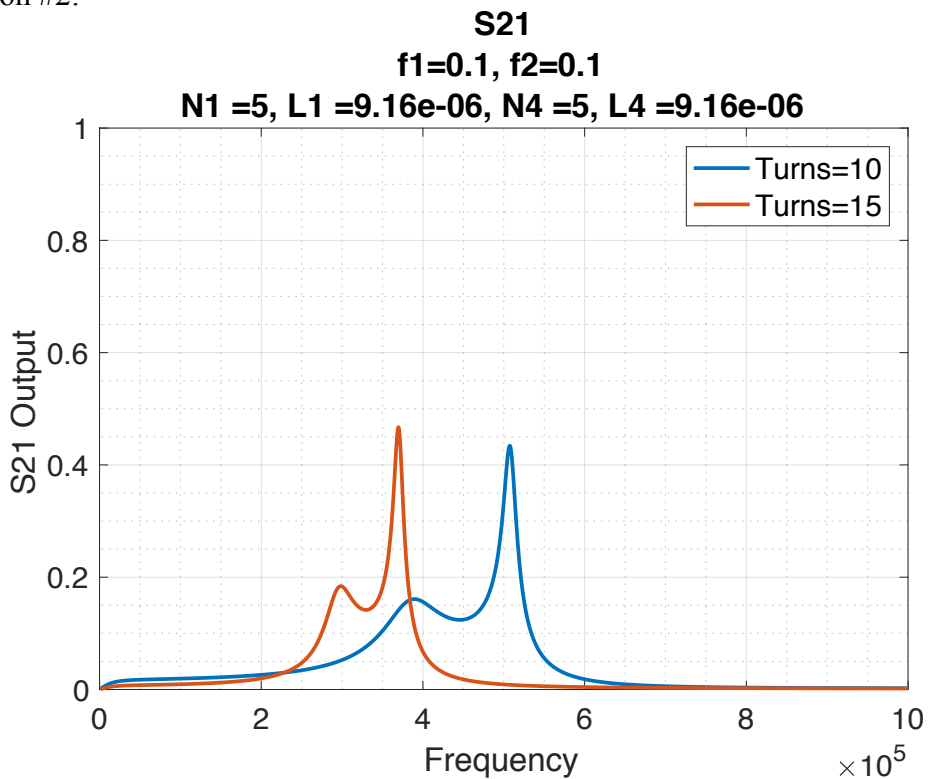




**S21 while varying turns on CYLINDRICAL resonant coils**  
**N1 =5, L1 =9.16e-06, N4 =5, L4 =9.16e-06**



Plotting Option #2:



With these plots, one can extrapolate optimal placements of load and drive coils on their respective resonant coils that would generate the highest efficiency, while at the same time analyze the system across a number of differently-wound resonant coils. The process can aid design of the 4-coil structure significantly and will be referred to in the coming chapters when discussing the device construction. Although the program looks promising, the theoretical values calculated must be confirmed by experimental breadth. This will be discussed in coming chapters. This programs operates under the assumption that the coils are all cylindrical, however, spiral coils can/and are often used in wireless transfer systems. The next section will discuss the porting of this tool into the domain of spiral coils and the adjustments needed to accommodate the changes.

### 8.3 Alternative Spiral Geometries for Simulation

For this thesis, cylindrical coils were implemented in the constructed 4-coil structures, however, this does not have to be the only geometry used. Spiral coils are also good candidates for efficient transformer design. To aid the assembly of spiral 4-coil systems, the joint MATLAB-

LTspice program can be altered in a few ways. The first of which is the list of input parameters the user determines. Here's the spiral coil parameter list that deviates from the cylindrical (all values are scalar unless otherwise specified):

**dw:** The wire diameter; held uniform over all coils (inches)

**ca:** The pitch over the wire diameter of each winding; held uniform among all coils

**N1:** Number of turns on the drive coil; held for all simulations

**N4:** Number of turns on the load coil; held for all simulations

**D01:** Outer diameter of the drive coil (inches)

**D02:** Outer diameter of the primary resonant coil (inches)

**D03:** Outer diameter of the secondary resonant coil (inches)

**D04:** Outer diameter of the load coil (inches)

**D12:** A matrix deciding the varying distance between drive and primary coils (inches)

**D23:** The distance between resonant coils (inches)

**D34:** A matrix deciding the varying distance between secondary and load coils (inches)

**Nmain:** A matrix quantity defining the turns of the resonant coils that will be simulated through.

**Rsource:** Value of the source resistance (ohms)

**Rload:** Value of the load resistance (ohms)

**C1:** Lumped capacitance attached to primary resonant coil (F)

**C2:** Lumped capacitance attached to secondary resonant coil (F);

**B1-B4:** Multiplier applied to each coil resistance.

**Proximity:** Binary value enabling the Proximity effect calculation of resistance for each coil

**PlotOption:** Value of 1 or 2 enabling a plot scheme described in a later section.

Special precautions must be taken when designing an assembly of spiral coils because the simulator won't operate if there is an overlap in coils. For example, if **D12** was chosen to include 0, this means that the drive and primary coil are nested at some point. If the primary resonant coil had too many turns such that some of them physically overlapped with the drive coil nested inside of it, then an unrealizable coil arrangement will be synthesized and erroneous values will be output. Therefore, if D12 or D34 include 0, the program calculates the inner radii of the largest resonant coils in line for simulation (the largest value in the Nmain matrix) and will compare it to the outer radii of its respective drive/load coil. If the coils overlap, no simulations will run and an error statement will be displayed in MATLAB, "ERROR: OVERLAPPING NESTED COILS: adjust riXmin", where 'riXmin' refers to the minimum inner radii of either coil 2 (X= 2) or coil 3 (X=3) .

In these simulations, the values that are going to be varied between runs are the elements of **Nmain**, so in different simulations, the number of turns on the primary and secondary coils will vary. The next deviations from the cylindrical simulator are the design algorithms that determine the resistance, inductance, and coupling of each coil. The spiral coil simulator will use its respective functions: *Spiral\_Inductance* for inductance, *Spiral\_Resistance* for resistance, and *Spiral\_Coupling* for the coupling coefficients. The procedure exactly mimics the procedure for cylindrical topologies except instead of the concept of **fX** matrices; there are instead the **D12** and **D34** matrices. Two simulations are run per 4-coil geometry, one to assess the right peak frequency and another to adjust the resistance for that peak. The *Master.m* script is also called to run the simulations. For the following coil ensemble, the subsequent plots are produced.

```

dw = .5;
ca = 2;
N1 = 4;
N4 = 4;
Do1 = 5;
Do2 = 10;
Do3 = 10;
Do4 = 5;

D12 = dw*ca*[1 5];
D23 = 2*dw*ca;
D34 = dw*ca*[1 5];

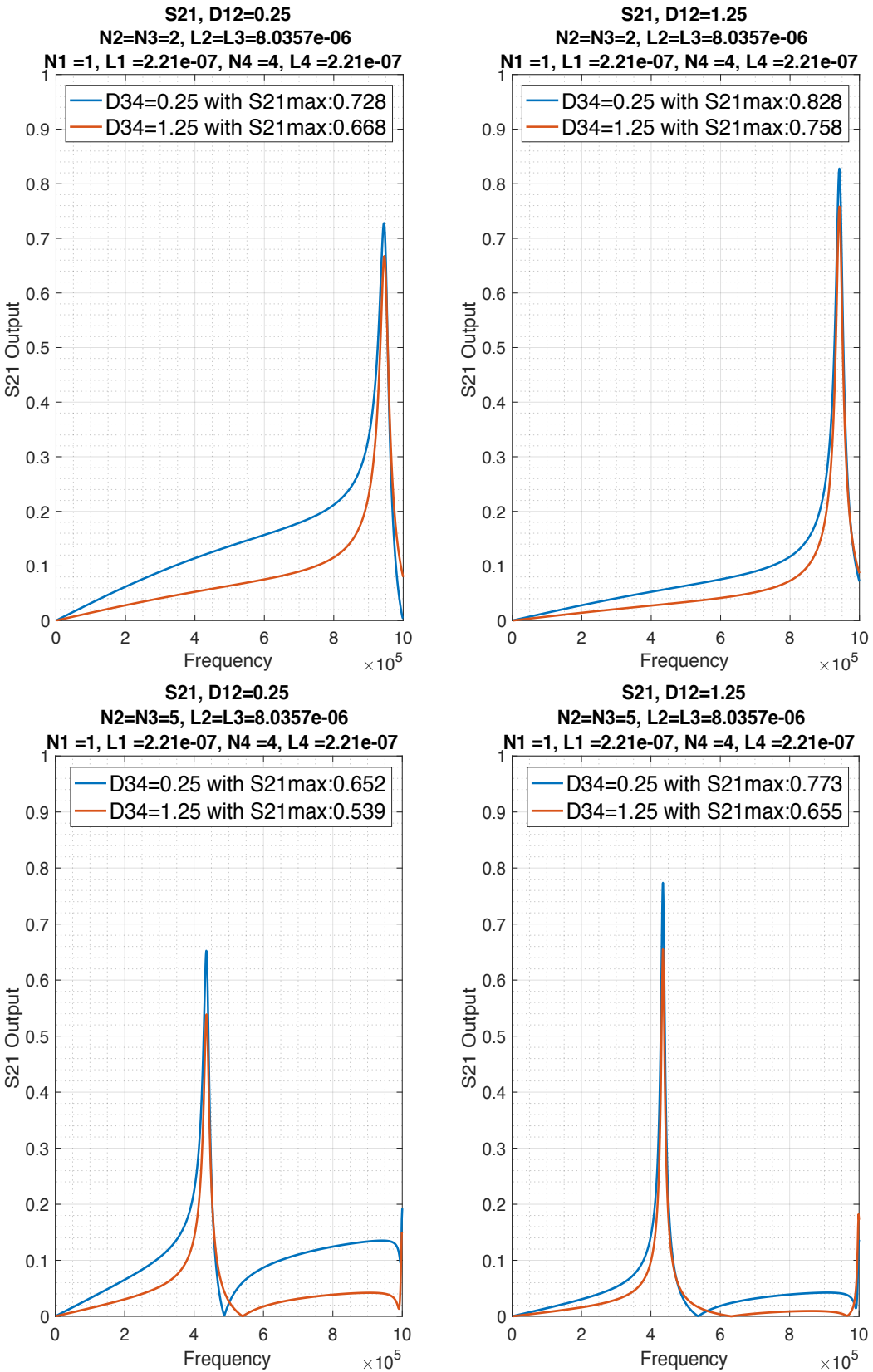
Nmain = [2 6];
Rsource = 1;
Rload = 50;

C1 = 10e-9;
C2 = 10e-9;

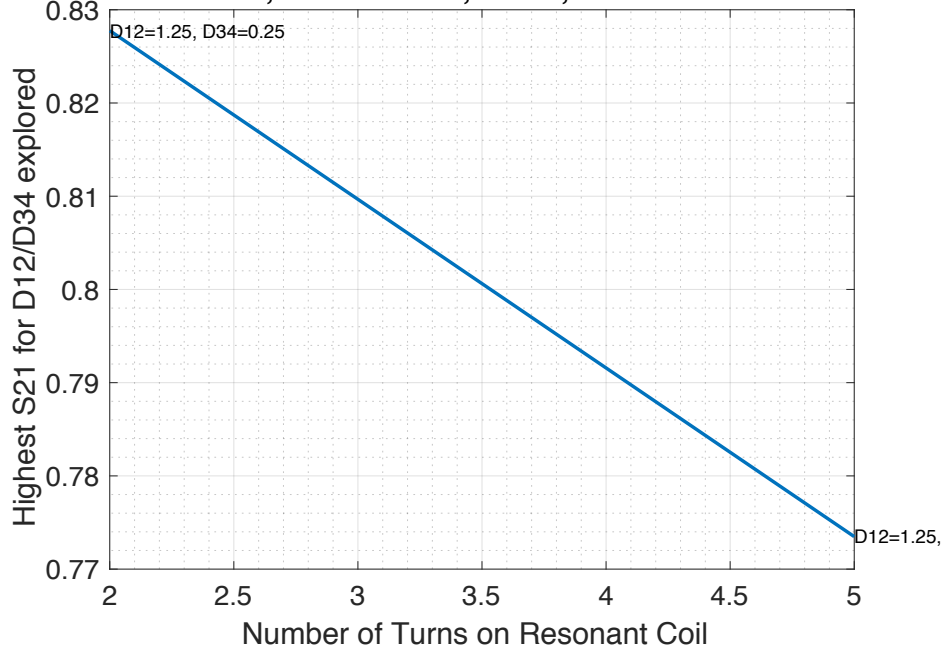
B1 = 1;
B2 = 1;
B3 = 1;
B4 = 1;
Proximity = 1;
PlotOption = (both);

```

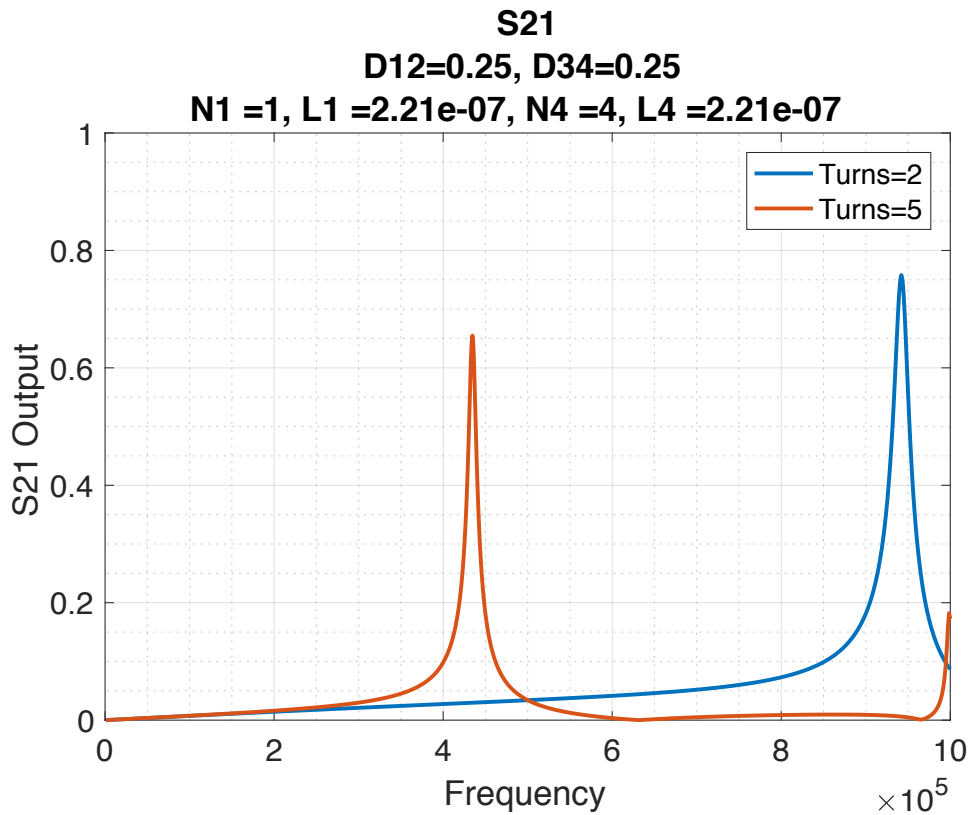
Plotting Option #1:



**S21 while varying turns on CYLINDRICAL resonant coils**  
**N1 =1, L1 =2.21e-07, N4 =4, L4 =2.21e-07**



Plotting Option #2:



## 9. Experimental Validation of Design Methodology

The previous chapter discussed the MATLAB-LTspice linked program for the simulation of the 4-coil coreless resonant transformer. The program takes the basic input quantities related to the physical properties of the coils involved and yields the calculated output efficiency metric,  $S_{21}$ , plots for the selected transformer designs. Validation of the simulation program for accuracy is achieved by constructing real 4-coil systems, measuring their efficiency, and comparing them to the simulation results. This chapter provides experimental validation of the program in order to detect the level of error between the real measurements and simulated values. Subsection 9.1 will present the coils used in this exploration, details about their structure, and their Bode100  $S_{21}$  parameter measurements. It will also display the inputs to the MATLAB program and the simulation outputs that are meant to replicate the experimentally measured  $S_{21}$  results.

Subsection 9.2 will discuss the disparity between the measured and simulated values.

### 9.1 Transformer Topologies Explored and Compared

Three different coil configurations will be tested. They vary in wire diameter, c/a, symmetry of load and drive coils, and source and load resistances. Their physical characteristics are shown in Tables 9.1-3 and are accompanied with their images and output  $S_{21}$  waveforms. The first of the configurations will have the load and drive coils positioned outside and adjacent to the resonant coils, not nested! For these tests the center-to-center wire distance between the two resonant coils, **D23**, is varied. The system is symmetric, so the distance from the load to the secondary resonant coil is the same as the distance from the drive to the primary resonant coil. Fig. 9.1 displays the output waveforms for  $S_{21}$ , peak values, the 6 coupling coefficients, and the distances of interest. The latter two configurations will have coils placed in a manner described in Chapter 6, with the resonant coils nested within their respective load or drive coil. The positions where the load or drive coils are placed upon their resonant coils will be altered per measurement. The details of their layout will be shown in Fig. 9.2 and 9.3. Note, configuration #3 has an unmatched resistor combination, thus the method demonstrated in Appendix D is implemented to correct the Bode100 plots. In the following subsections, each simulation and measurement pair will be considered an experiment. The varied variable in each experiment will be in bold for every experimental setup and simulation setting. From these figures, it is apparent that the simulation outputs are highly consistent with their experimental measurements.

### 9.1.1 Experiment 1: Changing the Distance Between Resonant Coils



Coil Configuration #1: $d_w = .08$ in, $R_s = 50$ , $R_l = 50$					
Component	# of Turns	Outer Diameter	Inductance	c/a	Capacitance
Drive Coil	1	8.75 in	.750uH	-	-
Primary Coil	12	8.75 in	51uH	1.6	4.4nF
Secondary Coil	12	8.75 in	51uH	1.6	4.4nF
Load Coil	1	8.75 in	.750uH	-	-

#### Measured Configuration #1:

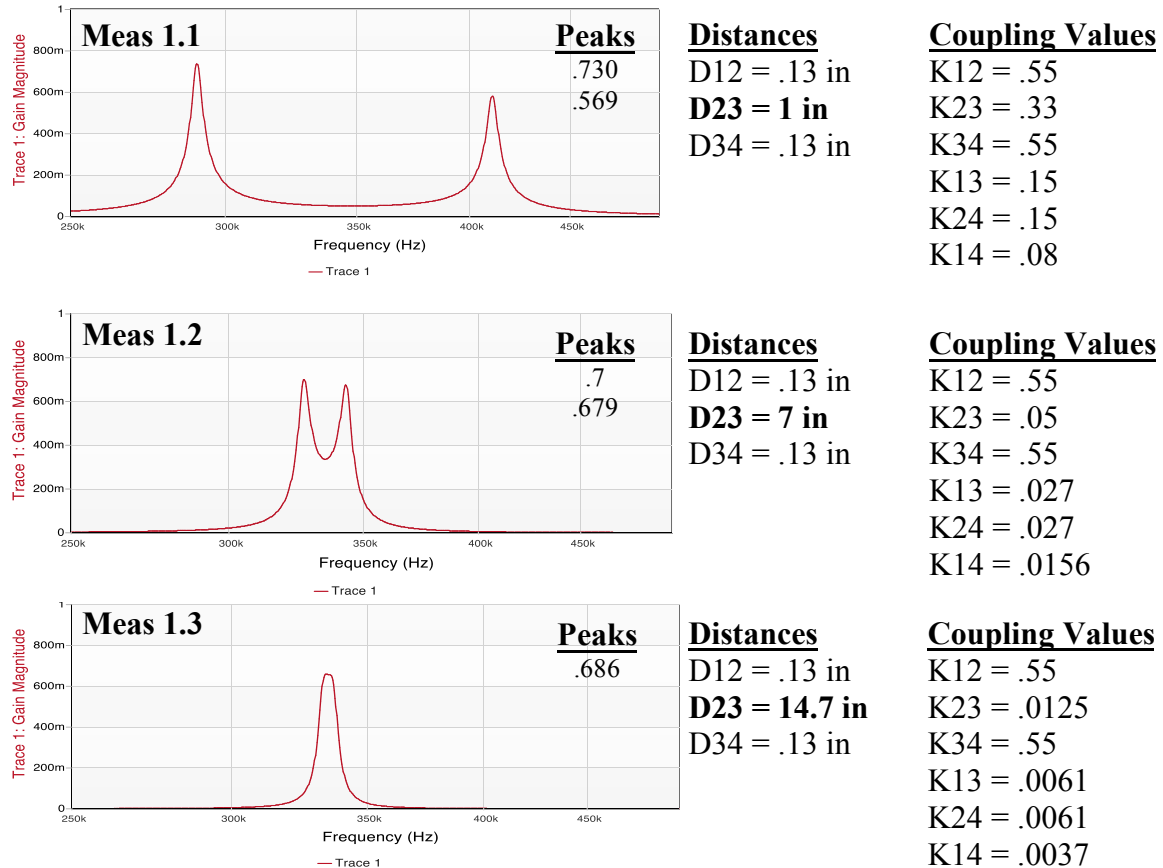
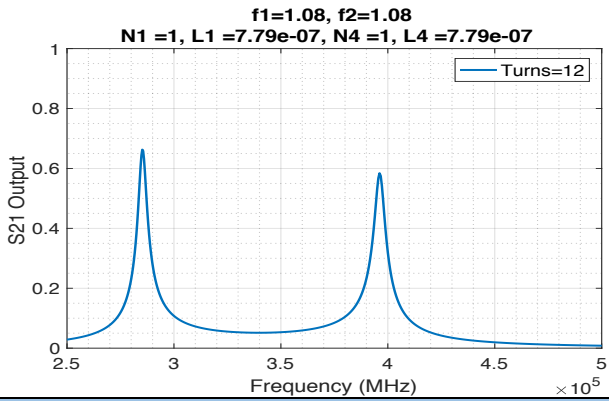
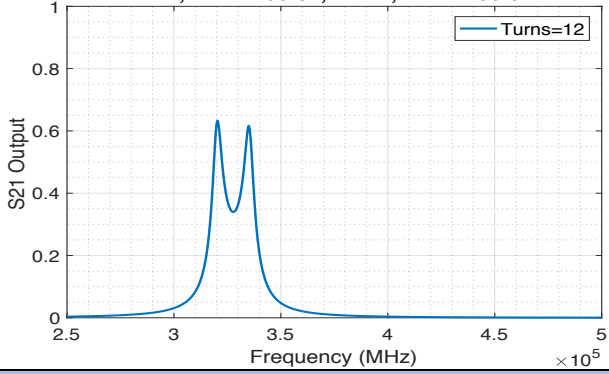
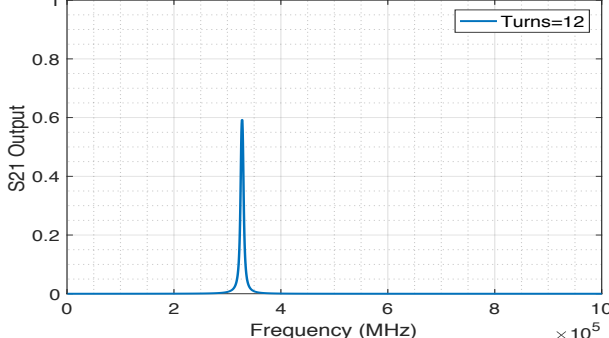


Fig. 9.1 Bode100 S21 measurements and construction details for configuration #1

## Calculation Configuration #1:

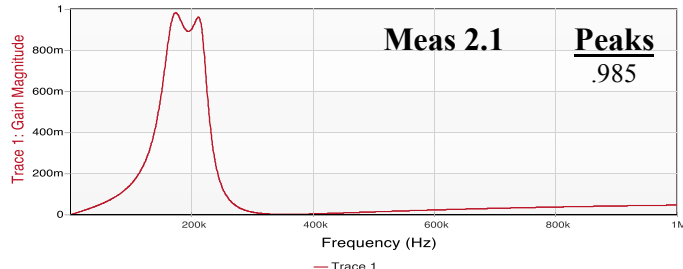
Table 9.1: CONFIGURATION #1		
Simulation 1.1		
Input Settings	Output Plot	Plot details
dw = .08; Do2 = 8.75; ca = 1.6; N1 = 1; N4 = 1; f1 = [1.08]; f2 = [1.08]; Nmain = [12]; <b>D23close = 1;</b> Rsource = 50; Rload = 50; C1 = 4.4e-9; C2 = 4.4e-9; RadialDist = 0;	<p style="text-align: center;"><b>S21</b>  <b>f1=1.08, f2=1.08</b>  <b>N1 =1, L1 =7.79e-07, N4 =1, L4 =7.79e-07</b></p>  <p>The plot shows S21 Output on the y-axis (0 to 1) versus Frequency (MHz) on the x-axis (2.5 to 5). Two sharp peaks are visible at approximately 1.08 MHz, reaching an output of about 0.65. The plot is labeled "Turns=12".</p>	<b>Peak:</b> .663 <b>Coupling Parameters:</b> K12 = .52 K23 = .32 K34 = .52 K13 = .16 K24 = .16 K14 = .08
Simulation 1.2		
dw = .08; Do2 = 8.75; ca = 1.6; N1 = 1; N4 = 1; f1 = [1.08]; f2 = [1.08]; Nmain = [12]; <b>D23close = 7;</b> Rsource = 50; Rload = 50; C1 = 4.4e-9; C2 = 4.4e-9; RadialDist = 0;	<p style="text-align: center;"><b>S21</b>  <b>f1=1.08, f2=1.08</b>  <b>N1 =1, L1 =7.79e-07, N4 =1, L4 =7.79e-07</b></p>  <p>The plot shows S21 Output on the y-axis (0 to 1) versus Frequency (MHz) on the x-axis (2.5 to 5). Two peaks are visible at approximately 1.08 MHz, with one slightly higher than the other. The plot is labeled "Turns=12".</p>	<b>Peak:</b> .633 <b>Coupling Parameters:</b> K12 = .52 K23 = .05 K34 = .52 K13 = .03 K24 = .03 K14 = .02
Simulation 1.3		
dw = .08; Do2 = 8.75; ca = 1.6; N1 = 1; N4 = 1; f1 = [1.08]; f2 = [1.08]; Nmain = [12]; <b>D23close = 14.7;</b> Rsource = 50; Rload = 50; C1 = 4.4e-9; C2 = 4.4e-9; RadialDist = 0;	<p style="text-align: center;"><b>S21</b>  <b>f1=1.08, f2=1.08</b>  <b>N1 =1, L1 =7.79e-07, N4 =1, L4 =7.79e-07</b></p>  <p>The plot shows S21 Output on the y-axis (0 to 1) versus Frequency (MHz) on the x-axis (0 to 10). A single sharp peak is visible at approximately 1.08 MHz, reaching an output of about 0.6. The plot is labeled "Turns=12".</p>	<b>Peak:</b> .592 <b>Coupling Parameters:</b> K12 = .52 K23 = .01 K34 = .52 K13 = .01 K24 = .01 K14 = .004

### 9.1.2 Experiment 2: Nested Coils, Symmetric Arrangement

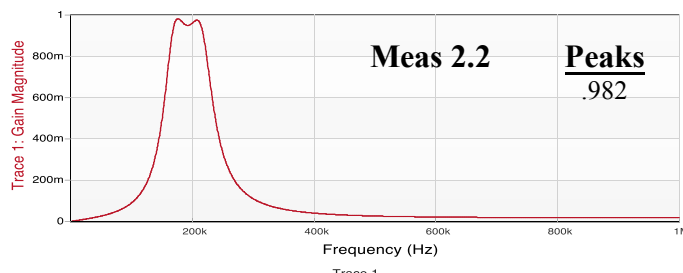


Coil Configuration #2: dw = .125 in, Rs = 50, RL = 50					
Component	# of Turns	Outer Diameter	Inductance	c/a	Capacitance
Drive Coil	6	9.25 in	13.75uH	2	-
Primary Coil	18	8.75 in	73uH	2	10nf
Secondary Coil	18	8.75 in	73uH	2	10nf
Load Coil	6	9.25 in	13.75uH	2	-

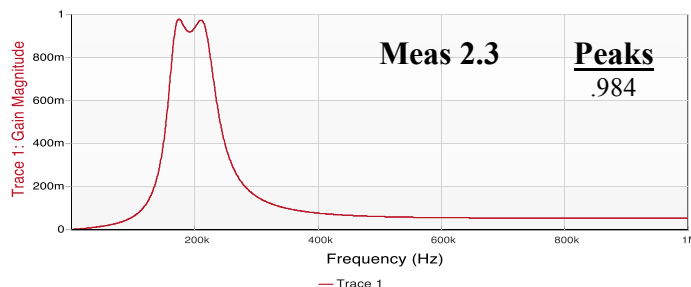
#### Measured Configuration #2:



**Distances**  
**F1 = .25**  
**F2 = .25**  
D23Close = .75      **Coupling Values**  
K12 = .77  
K23 = .25  
K34 = .77  
K13 = .28  
K24 = .28  
K14 = .29



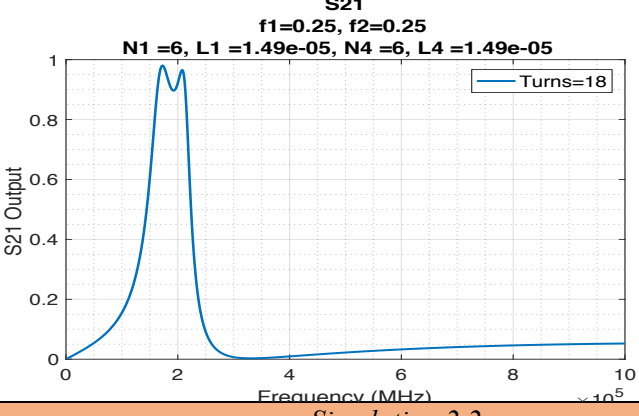
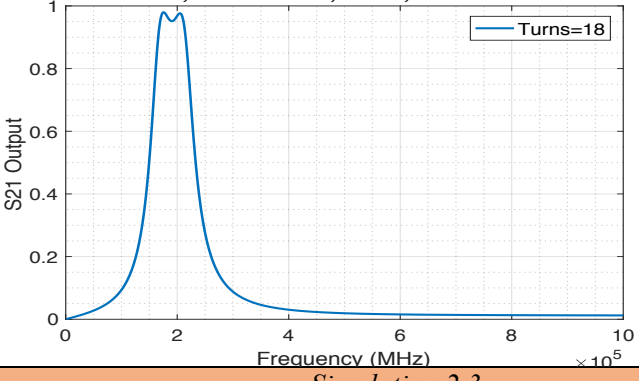
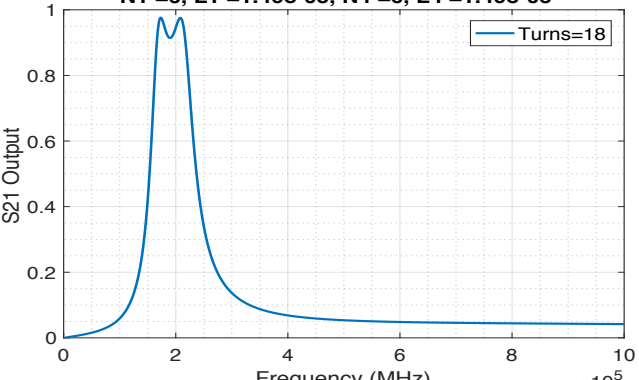
**Distances**  
**F1 = .5**  
**F2 = .5**  
D23Close = .75      **Coupling Values**  
in  
K12 = .81  
K23 = .25  
K34 = .81  
K13 = .18  
K24 = .18  
K14 = .13



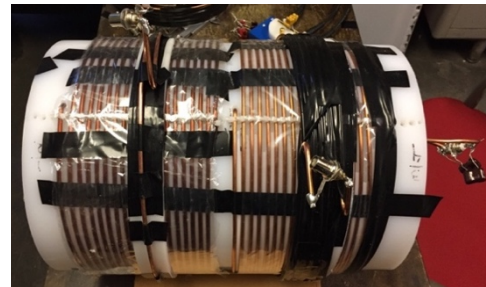
**Distances**  
**F1 = .75**  
**F2 = .75**  
D23Close = .75      **Coupling Values**  
K12 = .77  
K23 = .25  
K34 = .77  
K13 = .14  
K24 = .14  
K14 = .07

Fig. 9.2: Bode100 S21 measurements and construction details for configuration #2

## Calculated Configuration #2:

Table 9.2 :CONFIGURATION #2		
Simulation 2.1		
Input Settings	Output Plot	Plot details
dw = .125; Do2 = 8.75; ca = 2; N1 = 6; N4 = 6; f1 = [.25]; f2 = [.25]; Nmain = [18]; D23close = .75; Rsource = 50; Rload = 50; C1 = 10e-9; C2 = 10e-9; RadialDist = .5;	<p style="text-align: center;"><b>S21</b>  <b>f1=0.25, f2=0.25</b>  <b>N1 =6, L1 =1.49e-05, N4 =6, L4 =1.49e-05</b></p> 	Peak: .9818  Coupling Parameters: K12 = .71 K23 = .25 K34 = .71 K13 = .25 K24 = .25 K14 = .26
Simulation 2.2		
dw = .125; Do2 = 8.75; ca = 2; N1 = 6; N4 = 6; f1 = [.5]; f2 = [.5]; Nmain = [18]; D23close = .75; Rsource = 50; Rload = 50; C1 = 10e-9; C2 = 10e-9; RadialDist = .5;	<p style="text-align: center;"><b>S21</b>  <b>f1=0.5, f2=0.5</b>  <b>N1 =6, L1 =1.49e-05, N4 =6, L4 =1.49e-05</b></p> 	Peak: .97  Coupling Parameters: K12 = .76 K23 = .25 K34 = .76 K13 = .18 K24 = .18 K14 = .13
Simulation 2.3		
dw = .125; Do2 = 8.75; ca = 2; N1 = 6; N4 = 6; f1 = [.75]; f2 = [.75]; Nmain = [18]; D23close = .75; Rsource = 50; Rload = 50; C1 = 10e-9; C2 = 10e-9; RadialDist = .5;	<p style="text-align: center;"><b>S21</b>  <b>f1=0.75, f2=0.75</b>  <b>N1 =6, L1 =1.49e-05, N4 =6, L4 =1.49e-05</b></p> 	Peak: .9813  Coupling Parameters: K12 = .71 K23 = .25 K34 = .71 K13 = .13 K24 = .13 K14 = .07

### 9.1.3 Experiment 2: Nested Coils, Asymmetric Arrangement



Coil Configuration #3: dw = .125 in, Rs = .5, RL = 16.6					
Component	# of Turns	Outer Diameter	Inductance	c/a	Capacitance
Drive Coil	1	9.25 in	.750uH	-	-
Primary Coil	18	8.75 in	73uH	2	10nf
Secondary Coil	18	8.75 in	73uH	2	10nf
Load Coil	6	9.25 in	13.75uH	2	-

#### Measured Configuration #3:

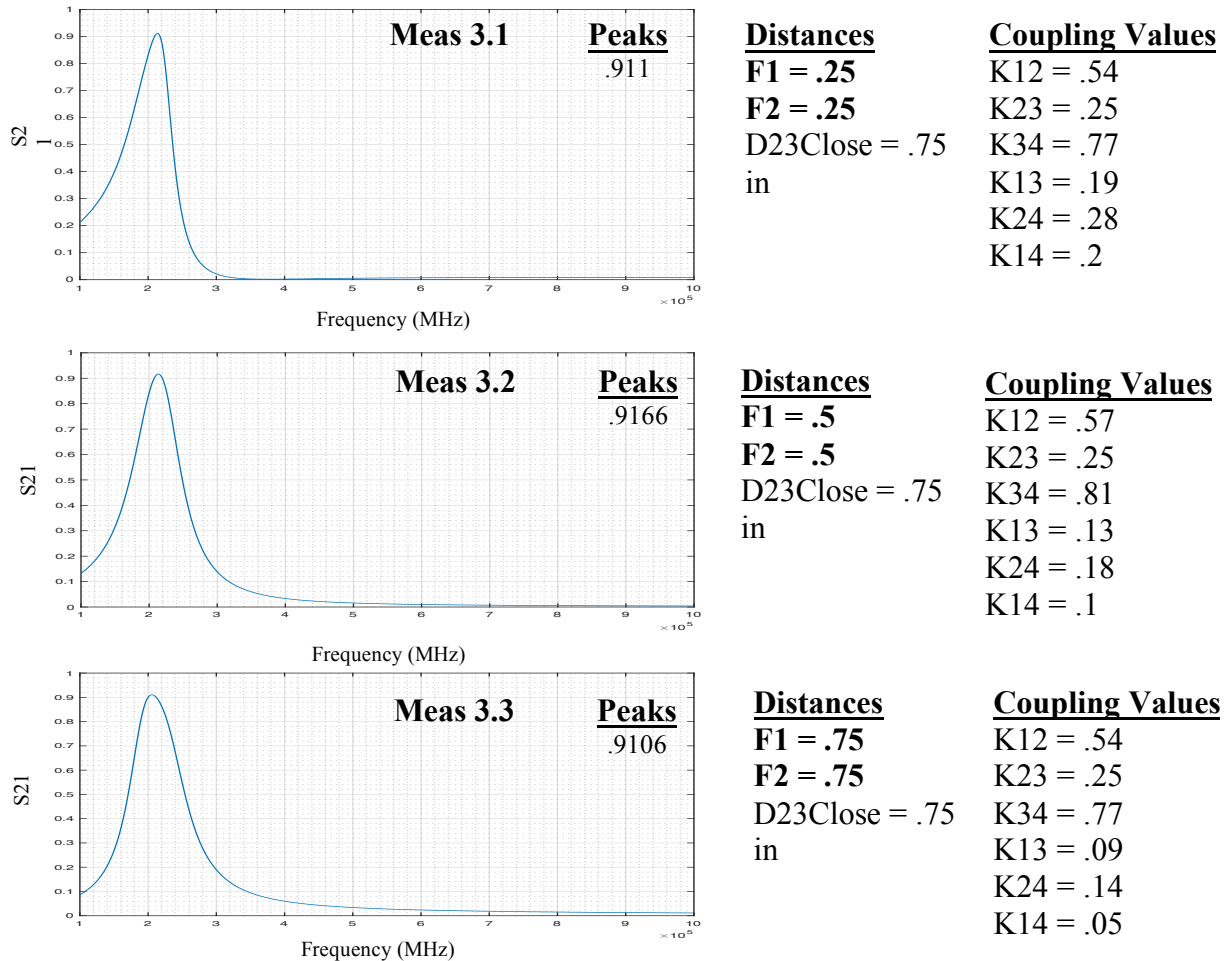
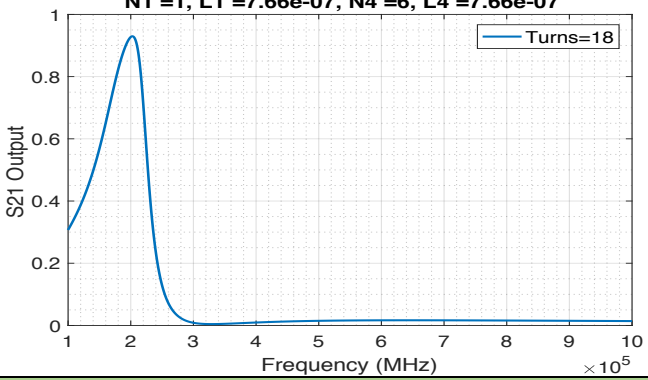
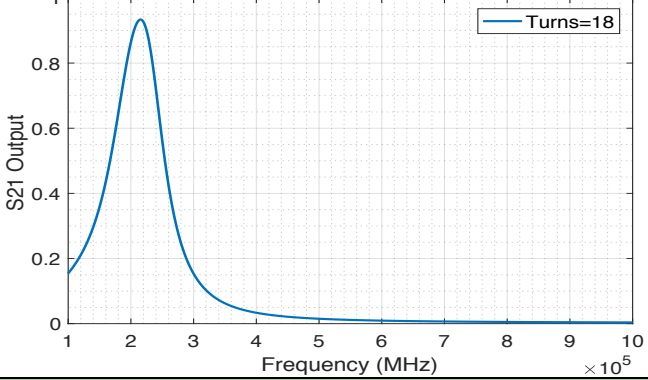
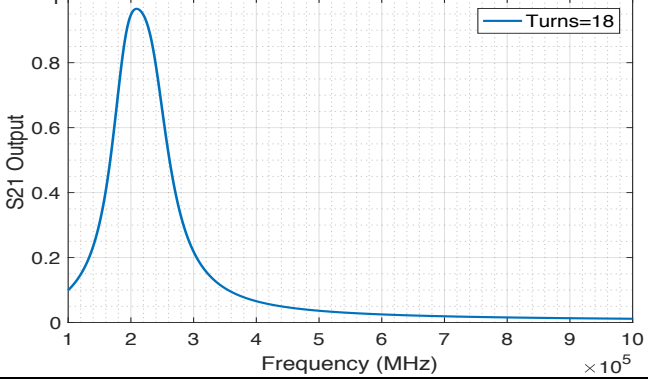


Fig. 9.3 Bode100 S<sub>21</sub> measurements and construction details for configuration #3

## Measured Configuration #1:

Table 9.3: CONFIGURATION #3

Simulation 3.1

Input Settings	Output Plot	Plot details
dw = .125; Do2 = 8.75; ca = 2; N1 = 1; N4 = 6; f1 = [.25]; f2 = [.25]; Nmain = [18]; D23close = .75; Rsource = .5; Rload = 16.6; C1 = 10e-9; C2 = 10e-9; RadialDist = .5;	<p style="text-align: center;"><b>S21</b>  <b>f1=0.25, f2=0.25</b>  <b>N1 =1, L1 =7.66e-07, N4 =6, L4 =7.66e-07</b></p>  <p style="text-align: center;">S21 Output</p> <p style="text-align: center;">Frequency (MHz) <math>\times 10^5</math></p>	Peak: 9083  Coupling Parameters: K12 = .53 K23 = .25 K34 = .71 K13 = .18 K24 = .25 K14 = .19
<b>Simulation 3.2</b>		
dw = .125; Do2 = 8.75; ca = 2; N1 = 1; N4 = 6; f1 = [.5]; f2 = [.5]; Nmain = [18]; D23close = .75; Rsource = .5; Rload = 16.6; C1 = 10e-9; C2 = 10e-9; RadialDist = .5;	<p style="text-align: center;"><b>S21</b>  <b>f1=0.5, f2=0.5</b>  <b>N1 =1, L1 =7.66e-07, N4 =6, L4 =7.66e-07</b></p>  <p style="text-align: center;">S21 Output</p> <p style="text-align: center;">Frequency (MHz) <math>\times 10^5</math></p>	Peak: .9205  Coupling Parameters: K12 = .56 K23 = .25 K34 = .76 K13 = .13 K24 = .18 K14 = .09
<b>Simulation 3.3</b>		
dw = .125; Do2 = 8.75; ca = 2; N1 = 1; N4 = 6; f1 = [.75]; f2 = [.75]; Nmain = [18]; D23close = .75; Rsource = .5; Rload = 16.6; C1 = 10e-9; C2 = 10e-9; RadialDist = .5;	<p style="text-align: center;"><b>S21</b>  <b>f1=0.75, f2=0.75</b>  <b>N1 =1, L1 =7.66e-07, N4 =6, L4 =7.66e-07</b></p>  <p style="text-align: center;">S21 Output</p> <p style="text-align: center;">Frequency (MHz) <math>\times 10^5</math></p>	Peak: .9660  Coupling Parameters: K12 = .53 K23 = .25 K34 = .71 K13 = .09 K24 = .13 K14 = .05

## 9.2 Output Plot comparison

This subsection will discuss the error in the simulation program by comparing the simulated  $S_{21}$  output results to measured values. Because the program's inputs are physical properties of the ensemble of the coils, inductance is calculated and then  $k$  parameters are evaluated. This second degree of computation may introduce more error into the final solution. The following tables display the error between  $k$  parameters for all experiments. Aside from a few outliers, the vast majority of theoretical values remained within 10% of the measured values!

Experiment #1: Error Comparison

	Experiment 1: Error in parameters (%)		
	Experiment 1.1	Experiment 1.2	Experiment 1.3
Peak	-9.18	-9.57	-14.49
K12	-5.45	-5.45	-5.45
K23	-3.03	0	0
K34	-5.45	-5.45	-5.45
K13	6.66	0	0
K24	6.66	0	0
K14	0	0	0

Experiment #2: Error Comparison

	Experiment 2: Error in parameters (%)		
	Experiment 2.1	Experiment 2.2	Experiment 2.3
Peak	-0.31	-1.22	-0.27
K12	-7.79	-6.17	-7.79
K23	0	0	0
K34	-7.79	-6.17	-7.79
K13	-10.71	0	-7.14
K24	-10.71	0	-7.14
K14	-10.34	0	0

Experiment #3: Error Comparison

	Experiment 3: Error in parameters (%)		
	Experiment 3.1	Experiment 3.2	Experiment 3.3
Peak	-0.29	0.42	6.08
K12	-1.85	-1.75	-1.85
K23	0	0	0
K34	-7.79	-6.17	-7.79
K13	-5.26	0	0
K24	-10.71	0	-7.14
K14	-5.00	-10.00	0

## 10. Final Design

Chapters 8 and 9 were dedicated to refining the design process for 4-coil transformers and have presented fragments of the complete design methodology. This chapter will review the design, construction, placement, and verification of an ‘optimized’ 4-coil transformer system. When the coils are configured to their optimal positions, the developed transformer achieves a high value of efficiency with an  $S_{21}$  parameter of .96 at 186kHz.

This chapter combines the various design methods developed in preceding chapters to produce a transformer fit for 100W. Subsection 10.1 presents the investigated range of coils that fit the power specification of the system. Subsection 10.2 provides a review of how simulating numerous coil topologies and coil placements aid in selecting an adequate set of coils. 10.3 gives an overview of the final transformer design, presenting the component resistances as functions of frequency and the computation of the 6  $k$  parameters in the system. 10.4 will compare the small signal performance of the measured transformer with its simulated equivalent system. Finally, 10.5 discusses applying power to the drive coil and running at 10W (the limit of the available high frequency load resistance).

### 10.1 Determining Appropriate Coils

Using the *Possible\_Coils.m* script, this subsection establishes a set of favorable coils for a coreless transformer design at 100W. The design considers operating frequencies between 175kHz and 225kHz. As stated in Chapter 7, it is preferable to have the resonant coil’s capacitors to be relatively small since smaller capacitors tend to have lower losses. Hence, capacitors of 10nF are used. Given the frequency range selected, the lower limit on the inductances of the coils is 40uH. As the coils get larger, they have higher inductances, but also experience higher losses. Therefore, the highest inductance achieved in the coils is really a function of power loss. The windings losses have been chosen to be 2% of the total power: 2 watts, or less. Due to this constraint, the coil inductances have been limited to 80uH. The parameters of frequency and current were input into the *Possible\_Coils.m* script for an assumed outer diameter of 8.75, a wire diameter of .125 in, and c/a values in the range of 1.7 to 2.2. These coil dimensions were chosen for power handling and construction convenience. Coils of a larger wire diameter makes the wires harder to bend but less lossy, and larger coil diameters requires less turns to achieve similar inductances. While smaller wire diameters have higher resistances and smaller coil

diameters require more turns to achieve the same inductance. Future work may explore a greater range of dimensions.

The ‘c/a’ parameter is kept constant (in the 1.7 to 2.2 range) among all the coils due to the resultant moderate proximity effect that still enables the coils to achieve high enough inductance. The algorithms for resistance are also the most accurate in that range. The results are shown in Fig. 10.1. The program results indicate that coils with turn numbers of 14 to 19 show favorable characteristics of adequate inductance and low loss. Keeping in mind that each resonant coil experiences these losses, the heat losses shown in the plots should be multiplied by 2. The possible resonant coils, especially near 18 turns have been identified by this subsection.

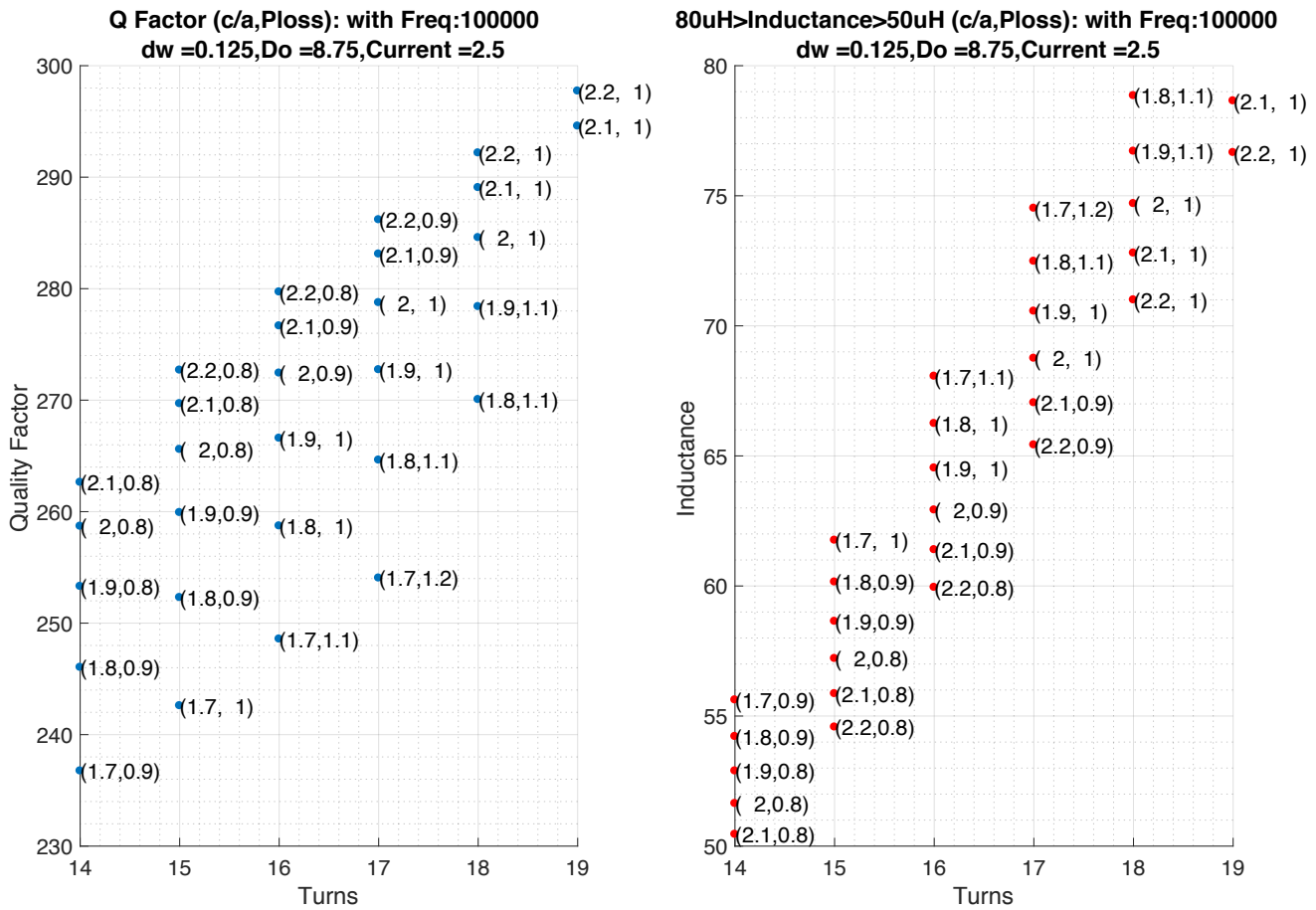


Fig. 10.1: Output plots of the *Possible\_Coils.m* script used to evaluate the range of coils that are good candidates for coreless transformer design.

## 10.2 Coil Selection from Topology and Simulation Results

Using the MATLAB simulation program, all of the coils are evaluated for an optimal number of turns as best suited for high efficiency given the load and source impedances. As discussed, the expected output voltage of the transformer will be 40 V with a current of 2.5A. Since 100W is to be transferred to the load, this restricts the load impedance to be  $16 \Omega$ . The drive circuitry, in the form of a low output impedance H-bridge inverter, will be attached to the drive coil of the system. To emulate the low impedance of the source, a .5-ohm source resistor is used in simulations. Given these parameters, the MATLAB programs were used to achieve good designs for efficiency. Here are the steps:

1. In the first step, the goal of selecting the proper number of turns for the drive and load coils is accomplished. Specific drive and load coils are evaluated by variation of  $f1$  and  $f2$  over a desired range for a set of resonant coils. Use plot option #1 to find the optimal configuration for each resonant coil within the set (defined by **Nmain**). Repeat this process for a variety of load and drive coil combinations. The final plot of each run of the script offers a final indicator of performance for the resonant coils selected.
2. The second step is used to decide an appropriate number of turns on the resonant coils and the optimal positioning of the drive and load coils. Using plotting option #2 and given the amount of turns for the load and drive coils determined in the previous step, run the simulator for the coil geometries with the *Nmain* matrix reflecting the number of turns of the resonant coils in consideration.

Implementing step 1, the MATLAB program was used to simulate the results of varying the number of turns on the load and drive coils with resonant coils ranging from 14 to 19. All these combinations were made with  $f1$  ranging between .25 and 0 and  $f2$  ranging from .75 to 1, as these configurations had the highest efficiencies observed. Combinations of drive coils having up to 3 turns and the load coils up to 8 were attempted, as going any higher for either, or reversing the ratio would result in reduced performance. The key features include keeping the peak frequencies near the desired operating frequency of 200 kHz and their corresponding  $S_{21}$  magnitude above 0.95. A drive coil of 1 turn and a load coil of 4-turns was chosen and the resulting plots are shown in Fig. 10.2. A reduced performance configuration, with a 2-turn drive and 4-turn load is shown beside it for comparison.

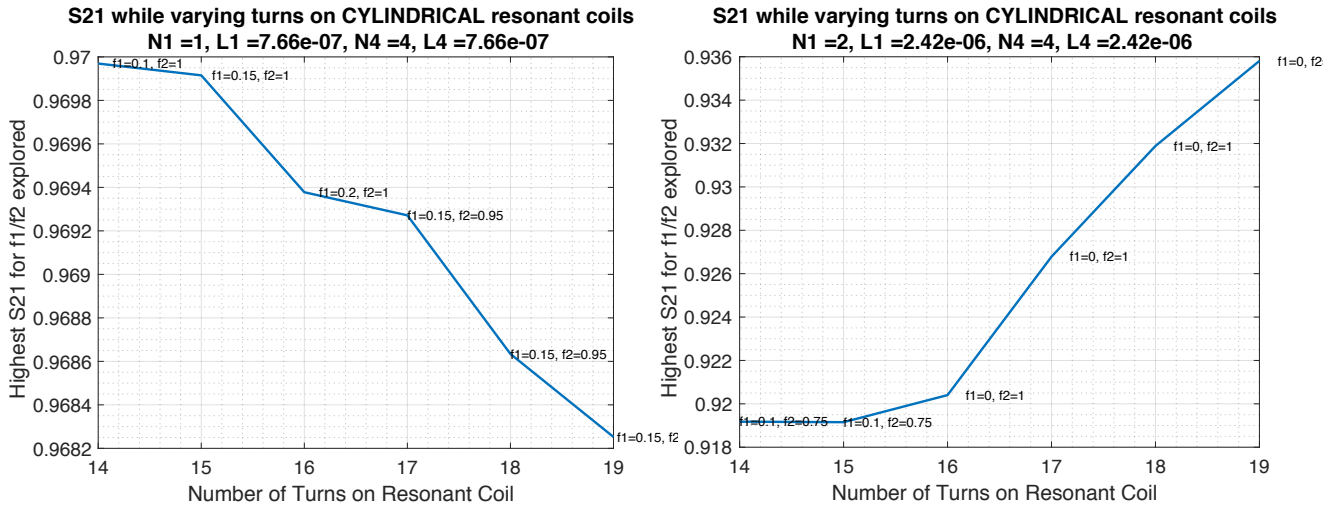


Fig. 10.2:  $S_{21}$  peak evaluation plots generated by plotting option #1. The left has a 1-turn drive coil and 4-turn load coil. The right has a 2-turn drive coil and 4-turn load coil.

Now that the drive and load coils have been decided to be 1 and 4 turns respectively, the amount of turns on the resonant coils is evaluated next and step 2 will be implemented. Using plotting option #2 and given the decided coils so far, the program will be configured to run at different  $f1$  and  $f2$  values in order to obtain adequate  $S_{21}$  values. During each run, not only does the maximum  $S_{21}$  have to be noted, but also the frequency and shape of the curves plotted. Since this is going to be driven with a power amplifier that must be tuned to the circuit, having a broader single peak is preferable than a thin spike. By running many simulations, a resonant coil of 18-turns with a spacing of  $f1 = .05$  and  $f2 = .8$  has been selected for the design due to its shape, high peak  $S_{21}$  value, and lower frequency needed to achieve its maximum value. Fig. 10.3 displays the final results with the decided  $f1$  and  $f2$  value. The choice of 18-turns was also determined with the intention of the flexibility to reduce the number of turns to achieve better designs in future work.

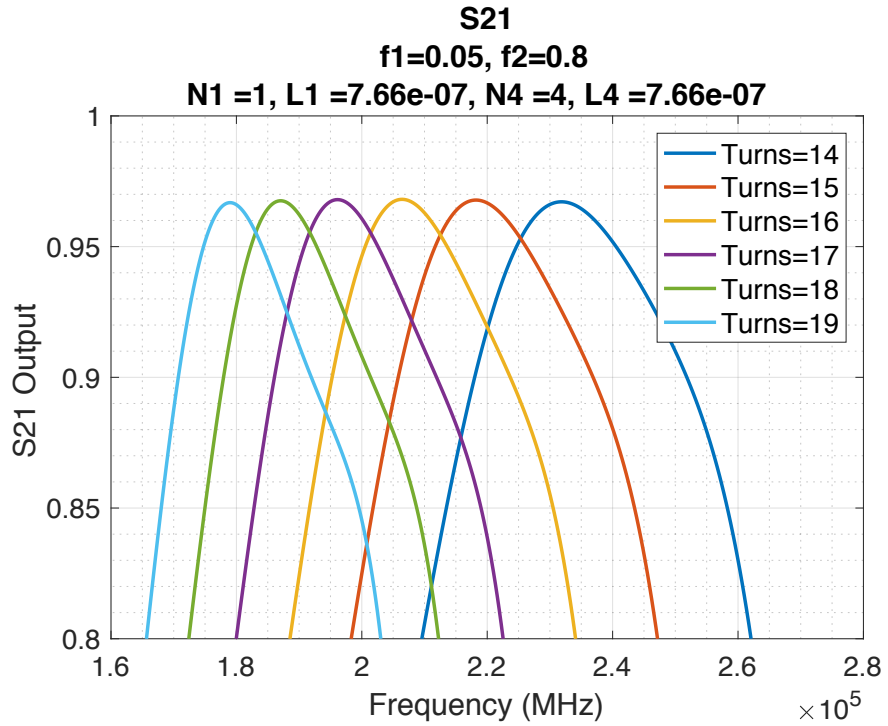


Fig. 10.3: Optimal  $S_{21}$  peaks with a 1-turn drive coil and 4-turn load coil

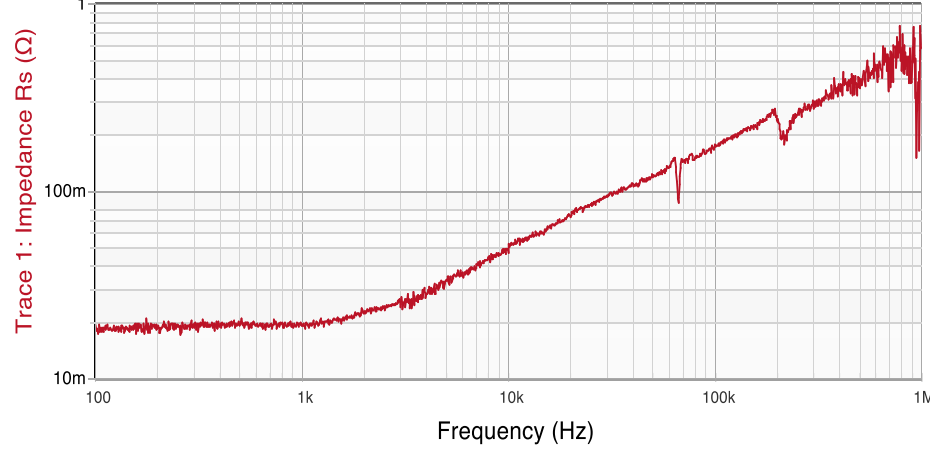
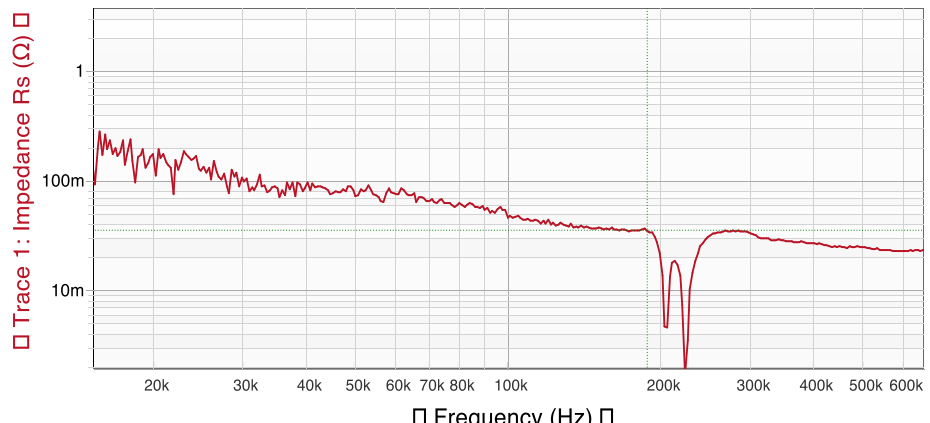
### 10.3 Final 4-Coil Transformer Design

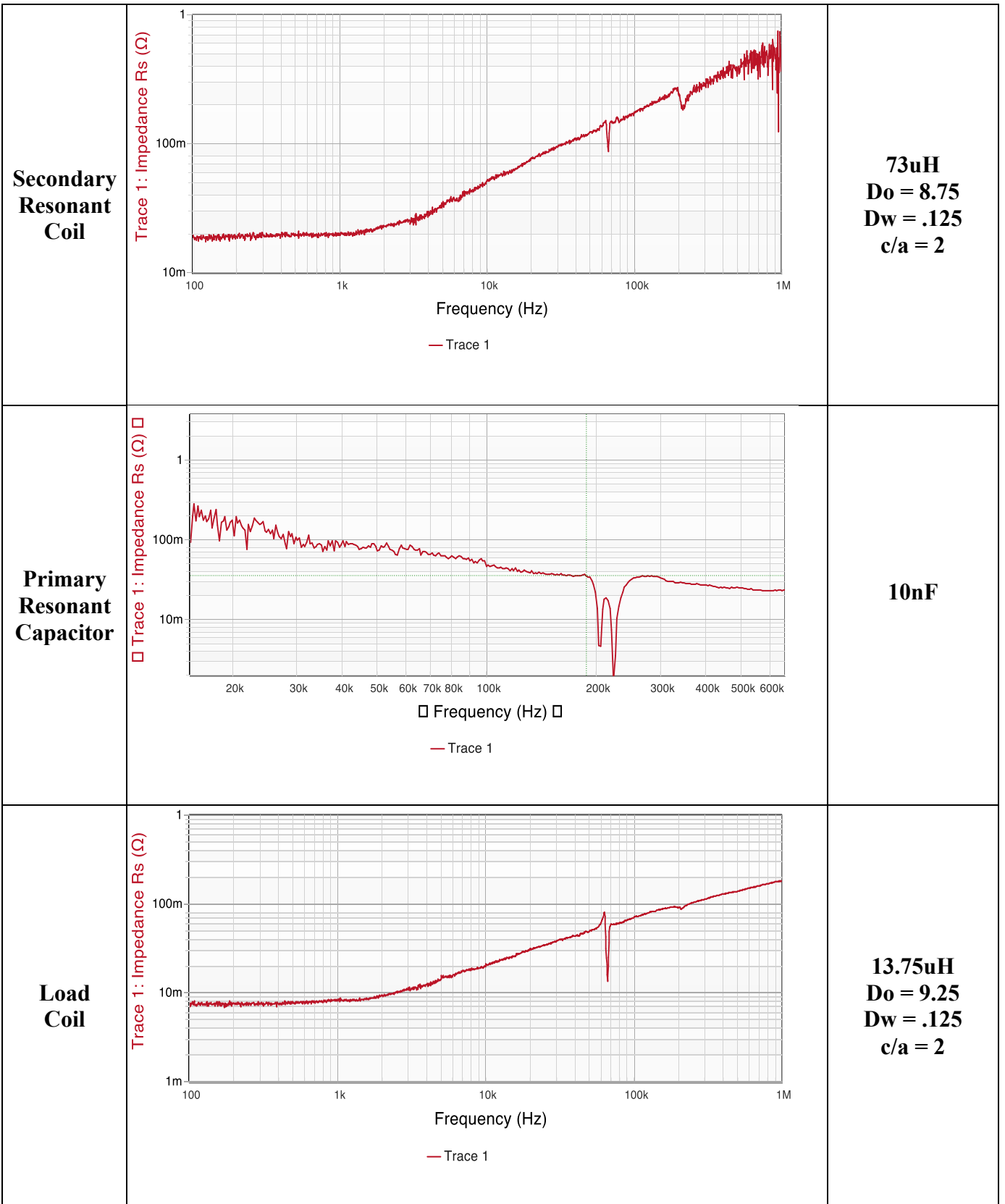
The previous section provided details about the design approach for selecting the coils used for a highly efficient coreless transformer design and the use of the approach as taken by this thesis project. It resulted with a 1-turn drive coil, two 18-turn resonant coils with 10nF capacitors, and 4-turn load coil. In this subsection, plots and details of the component values will be presented.

#### 10.3.1 Impedance

Table 10.1 displays resistance plots from 100Hz to 1MHz for each circuit component. Details of the physical parameters for each coil is presented to the right of each plot. Note, for the 1-turn coil, the Bode100 instrument isn't capable of such a low resistance measurement with high fidelity; thus, there is substantial noise in the plot. The ESRs of the capacitors were measured and represent a minor component of the losses in the resonant coils (<20%).

**Table 10.1**

<b>Drive Coil</b>	 <p>Trace 1: Impedance <math>R_s</math> (<math>\Omega</math>)</p> <p>Frequency (Hz)</p> <p>— Trace 1</p> <p>Detailed description: A log-log plot showing the impedance <math>R_s</math> of the primary resonant coil. The y-axis ranges from 10m to 1, and the x-axis ranges from 100 Hz to 1 MHz. The trace shows a low impedance of about 20m until 10 kHz, then rises to about 100m at 100 kHz, and continues to rise with some noise at higher frequencies.</p>	$.750\mu\text{H}$ $D_o = 9.25$ $D_w = .125$ $c/a = 2$
<b>Primary Resonant Coil</b>	 <p>□ Trace 1: Impedance <math>R_s</math> (<math>\Omega</math>) □</p> <p>□ Frequency (Hz) □</p> <p>— Trace 1</p> <p>Detailed description: A semi-log plot showing the impedance <math>R_s</math> of the primary resonant capacitor. The y-axis ranges from 10m to 1, and the x-axis ranges from 20 kHz to 600 kHz. The trace shows a relatively flat line around 100m until 100 kHz, followed by a sharp dip to about 10m at 200 kHz, a peak back to 100m at 300 kHz, and then a gradual decline.</p>	$73\mu\text{H}$ $D_o = 8.75$ $D_w = .125$ $c/a = 2$
<b>Primary Resonant Capacitor</b>	 <p>□ Trace 1: Impedance <math>R_s</math> (<math>\Omega</math>) □</p> <p>□ Frequency (Hz) □</p> <p>— Trace 1</p> <p>Detailed description: A semi-log plot showing the impedance <math>R_s</math> of the primary resonant capacitor. The y-axis ranges from 10m to 1, and the x-axis ranges from 20 kHz to 600 kHz. The trace shows a relatively flat line around 100m until 100 kHz, followed by a sharp dip to about 10m at 200 kHz, a peak back to 100m at 300 kHz, and then a gradual decline. A vertical dashed green line is drawn at 200 kHz.</p>	$10\text{nF}$



### 10.3.2 Coupling Coefficients

Table 10.2 displays a photo of the optimal configuration of the transformer and compares the measured coupling parameters with the values calculated in the simulation. There isn't much error in most values; K14's error can be attributed to the low inductance value that is hard to measure during coupling measurements.

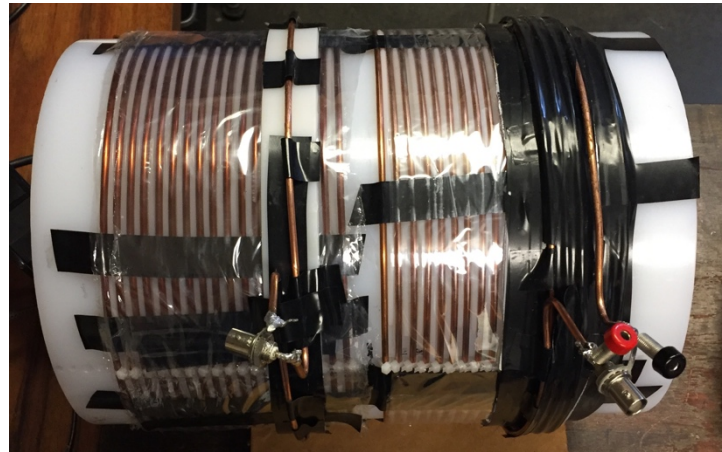


**Table 10.2**

Final Design Coupling Parameters						
	K12	K23	K34	K13	K24	K14
<b>Measured</b>	.45	.25	.68	.26	.117	.117
<b>Simulated</b>	.44	.25	.65	.26	.11	.1046
<b>Error (%)</b>	<b>2</b>	<b>0</b>	<b>4.4</b>	<b>0</b>	<b>0</b>	<b>10.6</b>

### 10.4 Measured and Theoretical Performance

The circuit components have been designed, built, and characterized for their lumped circuit equivalents. The resonant coils have been tuned to a desired frequency with capacitors of relatively minimal measured losses. The positions of all the coils are set to maximize the  $S_{21}$  parameter as per simulation. The penultimate step is to measure the performance via small signal analysis with the Bode100 instrument. After this, the drive circuitry can be applied to the drive coil and power measurement will be performed with 10W through the system. Fig. 10.4 displays the simulation results beside the measured results for frequencies up to 400kHz. The simulations

peak value is  $S_{21}=.967$ , while the measurement shows a peak value of .96: there is excellent agreement between the plots!

Lastly, a measure of how sensitive the  $S_{21}$  parameter is to perturbations in the drive and load coil positions is also desired. Fig. 10.5 shows the effect of perturbations around the optimal positions of the load and drive coils. Fig. 10.5a plots the deviations in  $S_{21}$  as the drive coil remains in optimal place and the load coil is perturbed in both directions. Fig. 10.5b shows the opposite scenario, the load coil in optimal place and the drive coil perturbed in both directions. The system is much more sensitive to moving the single turned drive coil. This should be taken into consideration when handling.

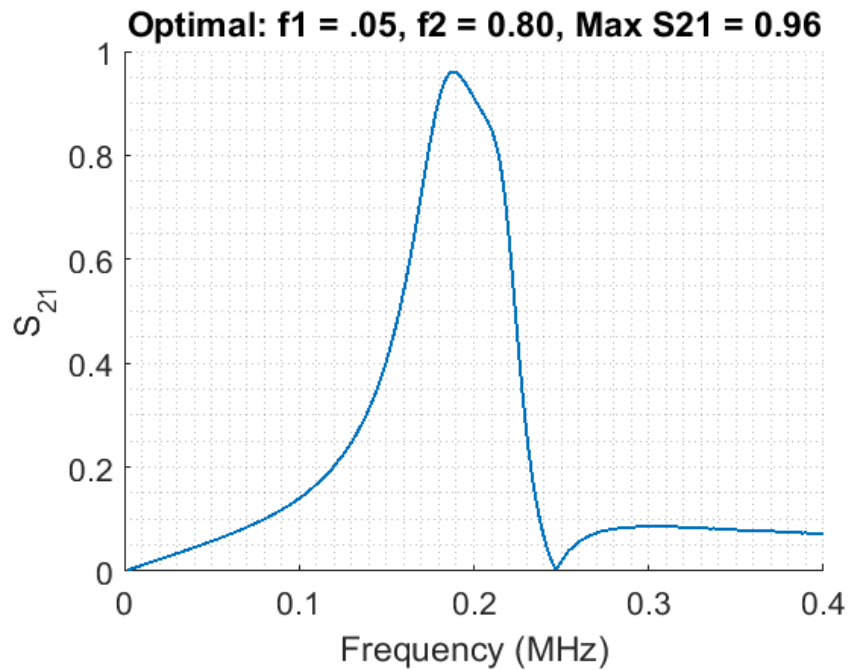
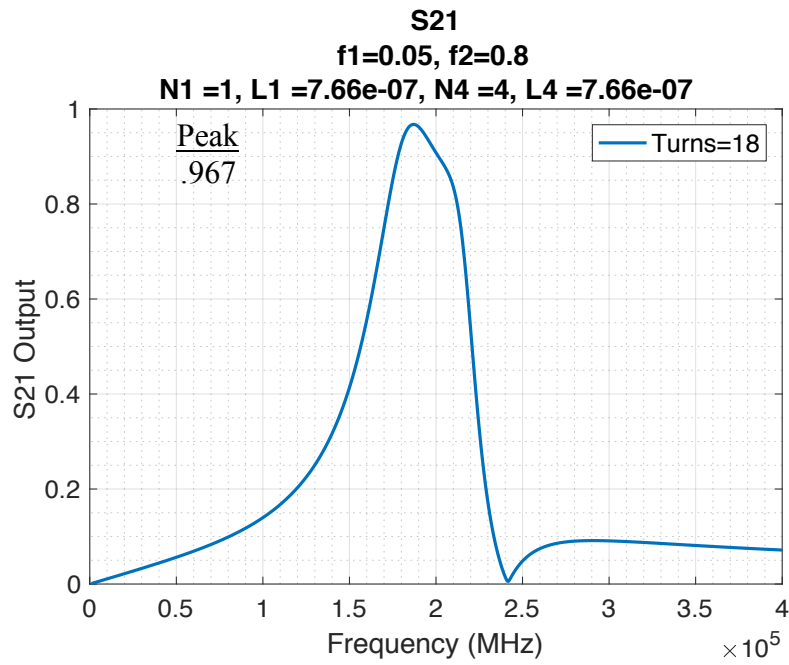


Fig. 10.4: Optimal  $S_{21}$  plots achieved with simulation (top) and measurement (bottom)

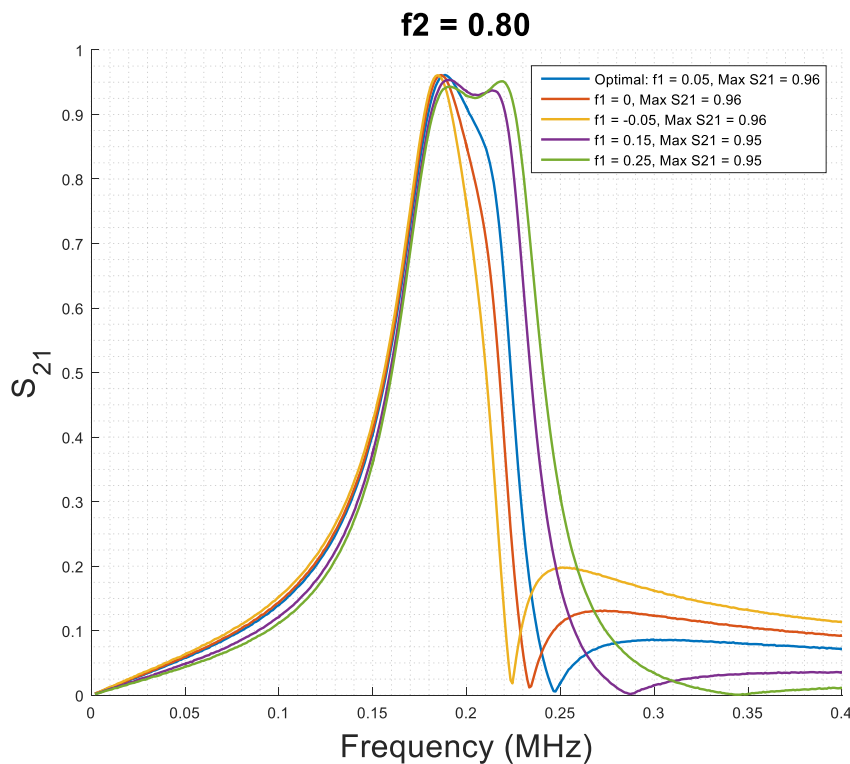
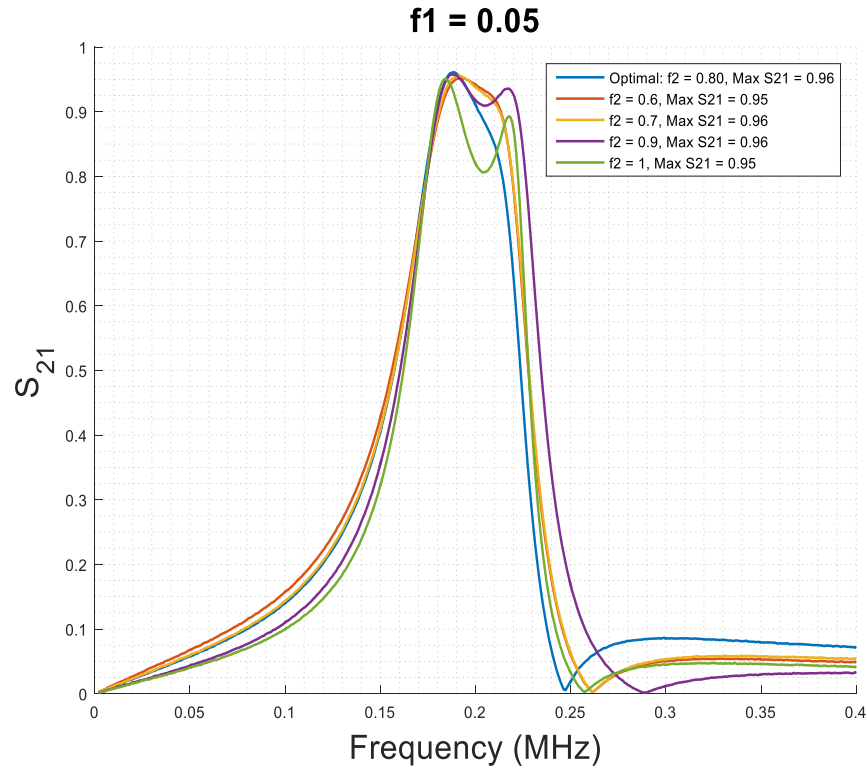


Fig. 10.5: Perturbations in  $S_{21}$  as the drive and load coils are displaced from their optimal positions. (Top) The drive coil remains static as the load coil is shifted. (Bottom) The load coil remains static as the drive coil is shifted.

## 10.5 Powering the Transformer System

The final step is to apply power to the drive coils and measure the voltage output on the load resistor. The transformer system performance was evaluated with the experimental setup displayed in Fig. 10.6. It includes an oscilloscope with a differential probe to measure the voltage across the load, PWM drive signals and power supplies for the drive circuitry, and the H-bridge directly connected to the transformer. Under these setup conditions, the entire system performed with 85% efficiency at 184kHz. However, there are a couple details to note. First, the H-bridge is driving the transformer with a square wave voltage input, a signal that has a significant amount of energy in its harmonics. Since, the transformer was designed to work for sinusoidal inputs, the harmonic components are heavily attenuated and only the fundamental is seen at the output. Additionally, the H-bridge isn't 100% efficient, and thus decreases the efficiency of the system. Given these conditions, the development team can claim that the transformer is at least 90% efficient!

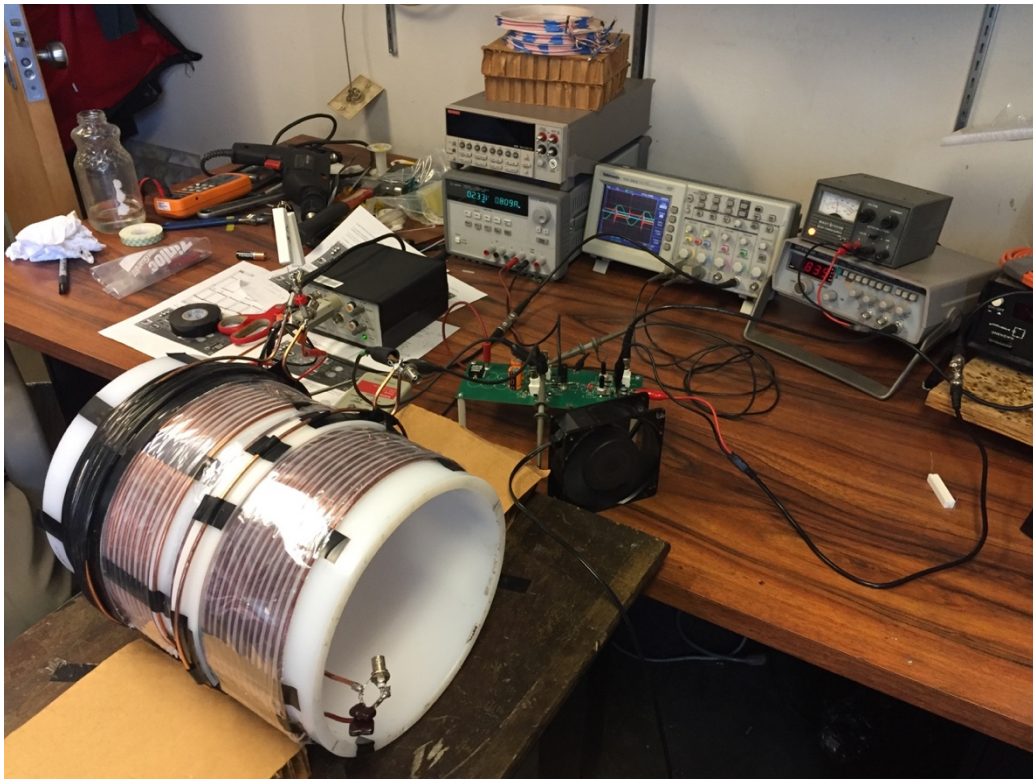


Fig. 10.6: Experimental setup to evaluate the  $S_{21}$  transmission coefficient of the system.

## 11. Conclusion

This thesis presents the theoretical foundation and methodology for designing efficient 4-coil high frequency coreless transformers from first principles and applies the procedure to construct a design for 100W example transformer. The design methodology produces accurate predictions of inductance, resistance, coupling coefficients, and  $S_{21}$  parameter values by applying software implemented design algorithms to calculate these values at high frequencies for an ensemble of coil models.

Using the simulation program, a range of spatial arrangements were explored to optimize the transformer for a criterion involving maximum efficiency achieved,  $S_{21}$  parameter shape, frequency of operation, power dissipation in the coils, size of the system, and the impedance characteristics of each coil.

Once the relative positions of the coils have been specified, the simulation then establishes high-frequency lumped circuit equivalents and implements an equivalent circuit netlist that is then simulated using LTspice as called into operation via MATLAB scripts. Simulation results are then fed to MATLAB for calculation and plotting of  $S_{21}$  parameter performance as a function of frequency. The information resulting from these simulations is shown to be valuable in the construction of efficient designs, as confirmed by a high degree of convergence of simulation with experimental manually constructed systems.

### 11.1 Summary of Operation

The example transformer is rated to run at 100W and was measured to yield a 1:2.2 voltage ratio between the high frequency AC RMS at the output terminals loaded with  $16\ \Omega$  and the DC voltage at the input of an H-Bridge drive circuit. Its output is designed to provide 40V and 2.5A and the  $S_{21}$  parameter efficiency is .96. The drive and load coils are moderately resilient to perturbations, on the order of 5% the length of their resonant coil. The transformer was designed for a single broad optimal operating frequency peak in order to simplify tuning by the driving circuitry. The total power losses were expected to be ~8% of the output at an optimal operating frequency of 186kHz. The measured  $S_{21}$  achieved 0.96 compared to the simulated value of 0.967. Even for the high efficiency values achieved, a key observation is the excellent agreement between measurement and theory associated with the various attributes that influence the

coreless transformer performance. This capability enables prediction of future coil designs with even better overall performance.

## **11.2 Further Work**

The current analysis system is a fully capable working simulator that supports the basic concept of the coreless transformer technology and has been applied to a validated example working transformer design. Although the present design works well, there are many topics that are worth future pursuit and provide opportunities for potential improvements.

### ***11.2.1 Reduced Losses with Improved Conductors***

The 100 Watt example design in this thesis was intended primarily to demonstrate the capability to predict the performance of coreless transformers based upon simulations. And this was achieved. While moderate efficiencies were demonstrated with simple small round copper wires, the losses in these coil conductors were not minimized and can be reduced. For example, larger wires or wires more suited for high frequency operation could be employed. Hence, there is the possibility to substantially improve the performance compared to the example design.

### ***11.2.2 System Scaling to 1kW***

The design methodology developed in Chapter 10 can be used for a transformer for a higher power rating, like 1kW. A design for such larger power would require a higher capacity drive circuit, but equally as important, a significant change to the construction of the coils. Larger diameter coils and wire would have to be constructed in order to increase the  $Q$  of the coils and reduce the amount of losses. Due to possibly higher voltages in the coils, either larger spacing or dielectric insulators may have to be used to avoid breakdown between coils in close proximity. At that magnitude of power, the coil losses may require enhanced cooling for sustained operation.

### ***11.2.3 Proximity Effect in Curved Windings***

As elaborated upon in Chapter 4, the theoretical calculations for proximity effect are based on a set of parallel conductors carrying the same current. Although exporting these findings to cylindrical coils proved to cause marginal error in certain regimes of  $c/a$ , there is room for

improvement. Additionally, spiral coil resistance values experienced more error in the resistance loss values. However, an analysis of the data shows that the coils that suffered such severe disparity were the harder ones to construct (i.e larger gauge, most turns, and smallest spacing). The ones that were designed well, suffered much less error. Despite this, lack of certainty may be due to limits of the parallel conductor assumption; the curvature and the winding of the coils may need to be taken into account to produce more accurate predictions of resistance.

#### ***11.2.4 Alternative wire shapes and coil geometries***

This thesis studied and utilized round wire for all theoretical and constructed coils so as to better establish reliable theoretical models. However, sparse experimentation with strip wire coils has shown a notable reduction in losses without much of an impact on inductance, thus enabling higher  $Q$  values. In cases where losses need to be minimized by the material and geometry of the wires involved, litz wire provides an alternative. Litz wire significantly reduces the high frequency resistance experienced in coils, and thus leads to higher  $Q$  values. However, there is a higher cost trade-off with litz wire that needs to be considered. Hollow round wires can also be of use when larger diameters are required to minimize losses and in situations where cooling is a priority since coolant can be passed through the interior of the hollow conductor.

Alternative coil geometries can also be explored. This thesis studied spiral and cylindrical coils but many more are available and likely experience different tradeoffs between inductance and resistance. Conical coils, where the cross section at one end of the coil can be smaller than at the other end, and multi-layered coils, where a cross sections appears to be a 2D grid of wires, can both be implemented. These designs have different calculations for inductance and coupling coefficients, but once an algorithm is generated with MATLAB, fusing the theoretical computation with the current software is possible.

#### ***11.2.5 Nested Cylindrical and Spiral Structures/ Mixed designs***

This thesis also explored transformer designs with symmetric close cylindrical coils. The variation of coil size and shape has not been fully explored. Examples include:

- a) larger diameter drive and load coils
- b) non-uniform wire diameters for all the coils
- c) mixed spiral and cylindrical designs

d) nesting coils.

Some adjustments and changes to the coupling calculator presented in this work would be necessary to more fully explore such variations.

#### ***11.2.6 Alternative Driving Methods***

Lastly, because the transformer in the thesis was constructed to have one peak frequency, a square wave drive signal that contains a moderate amount of energy in its harmonic frequencies might be suboptimal. This can introduce substantial loss into the system since the transformer losses are likely higher in those higher frequencies. To mitigate the losses, slow switching of the square wave, effectively reducing the harmonic content of the waveform, could be employed. Alternatively, other driving electronic circuits specifically arranged for the coreless transformer may provide additional means for improvement.

### **11.3 Final remarks**

The coreless high frequency transformer discussed in this document is an early stage development, yet is a promising example of novel electromagnetic engineering. It offers an opportunity for a cost effective, simple to implement, and simple to design alternative to core-type transformers. There appears to be many more possibilities to enhance the basic concepts developed in this thesis. It is the hope of the author that more ‘out of the box’ engineering ideas continue to be explored and that they may lead to a more sophisticated and efficient technological future.

## 12. Bibliography

- [1] J. W. Coltman, "The transformer [historical overview]," in *IEEE Industry Applications Magazine*, vol. 8, no. 1, pp. 8-15, Jan.-Feb. 2002.
- [2] C. Center, "History of Transformers", *Edisontechcenter.org*, 2018. [Online]. Available: <http://www.edisontechcenter.org/Transformers.html>. [Accessed: 30- Jan- 2018].
- [3] "Infrastructure Security and Energy Restoration Office of Electricity Delivery and Energy Reliability U.S. Department of Energy", Office of Electricity Delivery and Energy Reliability, 2014.
- [4] M. E. Valentinuzzi, M. H. Ortiz, D. Cervantes and R. S. Leder, "Nikola Tesla: Why was he so much resisted and forgotten? [Retrospectoscope]," in *IEEE Pulse*, vol. 7, no. 6, pp. 61-68, Nov.-Dec. 2016.
- [5] A. Bomber, "Wireless Power Transmission: An Obscure History, Possibly a Bright Future.", Portland State University, 2006.
- [6] A. Ghahary and B. Cho, "Design of a transcutaneous energy transmission system using a series resonant converter," in *Proc. 21st Ann. IEEE Power Electronics Specialists Conf.*, 1990, pp. 1–8.
- [7] S. Y. R. Hui, S. C. Tang, and H. Chung, "Coreless printed-circuit-board transformer for signal and energy transfer," *Electron. Lett.*, vol. 34, no. 11, pp. 1052–1054, May 28, 1998.
- [8] J. C. Schuder, J. H. Gold, and H. E. Stephenson, "An inductively coupled RF system for the transmission of 1kW of power through the skin," *IEEE Trans. Biomed. Eng.*, vol. 18, no. 4, pp. 265–273, July 1971.
- [9] W. H. Ko, S. P. Liang, and C. D. Fung, "Design of radio-frequency powered coils for implant instruments," *Med. Biol. Eng. Comp.*, vol. 15, pp. 634–640, 1977.
- [10] P. Bevelacqua, "Maxwell's Equations: Faraday's Law", *Maxwells-equations.com*, 2018. [Online]. Available: <http://www.maxwells-equations.com/faraday/faradays-law.php>. [Accessed: 31- Jan- 2018].
- [11] "Aerospaceweb.org | Ask Us - 400 Hz Electrical Systems", *Aerospaceweb.org*, 2018. [Online]. Available: <http://www.aerospaceweb.org/question/electronics/q0219.shtml>. [Accessed: 30- Jan- 2018].
- [12] "Large Power Transformers and the U.S. Electric Grid", Office of Electricity Delivery and Energy Reliability, 2012.
- [13] "Wireless power transfer | Wikiwand", *Wikiwand*. [Online]. Available: [http://www.wikiwand.com/en/Wireless\\_power\\_transfer](http://www.wikiwand.com/en/Wireless_power_transfer). [Accessed: 30- Jan- 2018].

- [14] M. Zargham and P. G. Gulak, "Maximum achievable efficiency in near-field coupled power-transfer systems," in *IEEE Transactions on Biomedical Circuits and Systems*, vol. 6, no. 3, pp. 228-245, June 2012.
- [15] V. Nair and J. Choi, "An efficiency enhancement technique for a wireless power transmission system based on a multiple coil switching technique", *Energies*, vol. 9, no. 3, p. 156, 2016.
- [16] G. S. Smith, "Proximity effect in system of parallel conductors", *J. Appl.Phys.*, vol.43, no. 5, p. 2196-2203, May 1972.
- [17] Bode 100 User Manual. Houston, TX: OMICRON electronics, 2010.
- [18] H. Nagaoka "The inductance coefficient of solenoids", *Journal of the College of Science, Imperial University*, vol. XXVII, article 6, Tokyo, 1909.
- [19] H. A. Wheeler, "Simple Inductance Formulas for Radio Coils," in *Proceedings of the Institute of Radio Engineers*, vol. 16, no. 10, pp. 1398-1400, Oct. 1928.
- [20] F.E Neumann, 1847 *Schr. Berliner Akad. Wiss.*
- [21] M. Duarte *et al.*, "Design and characterization of a full-duplex multiantenna system for WiFi networks," in *IEEE Transactions on Vehicular Technology*, vol. 63, no. 3, pp. 1160-1177, March 2014.
- [22] A. P. Sample, D. T. Meyer and J. R. Smith, "Analysis, experimental results, and range adaptation of magnetically coupled resonators for wireless power transfer," in *IEEE Transactions on Industrial Electronics*, vol. 58, no. 2, pp. 544-554, Feb. 2011.
- [23] S. Lukashov, "A self-tuning 100 watt wireless power transfer system", S.B., Massachusetts Institute of Technology, 2015.

## Appendix A: Inductance of Constructed Coils

### A.1 Cylindrical Coils: Coil Geometries and Inductance

Coil Geometry										Inductance		
diam.		Coil	Theory	Theory	Measured	Error	Measured	Gap		Theory	Measured	Error
Wire	Turns	Diameter	WireLength	Coil Length	Coil Length	in Length	c/a	Distance	Nagaoka	L	L	L
(inc)		(inch)	(inch)	(inch)	(inch)	(%)		(inch)	Factor	( $\mu$ H)	( $\mu$ H)	(%)
0.102	3	6.4	60.34	0.412	0.402	-2.4	1.5	0.1	0.1169	3.4	3.2	-4.8
0.102	4	6.4	80.45	0.562	0.552	-1.8	1.5	0.09	0.1574	5.5	5.2	-4.7
0.102	5	6.35	99.76	0.572	0.582	1.7	1.15	0.04	0.1658	8.3	7.9	-4.9
0.102	5	6.4	100.56	0.712	0.702	-1.4	1.5	0.08	0.1944	7.9	7.5	-5.3
0.102	5	6.4	100.61	1.122	1.082	-3.6	2.5	0.18	0.2703	6.8	6.7	-1.9
0.102	5	6.4	100.68	1.492	1.452	-2.7	3.4	0.27	0.3304	6.1	6.1	0.0
0.102	6	6.35	119.72	0.692	0.702	1.4	1.15	0.04	0.1946	11.3	10.9	-3.4
0.102	6	6.35	119.72	0.762	0.782	2.6	1.3	0.05	0.212	10.9	10.3	-5.5
0.102	6	6.4	120.67	0.862	0.862	0	1.5	0.07	0.2276	10.7	10.1	-5.3
0.102	6	6.35	119.76	1.172	1.172	0	2.1	0.13	0.2874	9.4	9.1	-3.7
0.102	7	6.4	140.78	1.022	1.012	-1	1.5	0.07	0.2583	13.7	13.7	-0.2
0.102	7	6.4	140.86	1.632	1.572	-3.7	2.5	0.17	0.348	11.6	11.3	-2.4
0.102	7	6.4	140.95	2.182	2.132	-2.3	3.4	0.26	0.4178	10.1	10.1	-0.3
0.102	10	6.4	201.1	1.162	1.162	0	1.15	0.03	0.2843	26.6	25.4	-4.6
0.102	10	6.35	199.55	1.482	1.462	-1.3	1.5	0.06	0.3334	24.1	23.4	-2.8
0.102	10	6.35	199.65	2.402	2.362	-1.7	2.5	0.16	0.444	19.5	19.5	0.2
0.102	10	12.04	378.27	1.162	1.182	1.7	1.15	0.03	0.1885	61.7	60	-2.8
0.102	11	6.4	221.23	1.632	1.592	-2.5	1.5	0.06	0.3498	28.4	27.9	-1.9
0.128	10	6.38	200.49	1.448	1.428	-1.4	1.15	0.03	0.3235	24.5	23.3	-4.8
0.128	10	6.38	200.64	2.718	2.728	0.4	2.25	0.17	0.4763	18.2	17.7	-3.0
0.128	10	8.75	274.93	1.448	1.428	-1.4	1.15	0.03	0.2651	37.9	36	-4.9
0.128	10	8.75	275.04	2.718	2.728	0.4	2.25	0.17	0.4031	29.1	28	-3.9
0.128	10	12.05	378.59	1.448	1.428	-1.4	1.15	0.03	0.2142	58.2	56	-3.8
0.128	10	12.05	378.67	2.718	2.728	0.4	2.25	0.17	0.3349	46.0	45	-2.2
0.0808	5	8.75	137.5	0.6108	0.6058	-0.8	1.65	0.07	0.1414	12.4	12	-3.4
0.0808	5	12	188.5	0.6108	0.6058	-0.8	1.65	0.07	0.1119	18.5	17.9	-3.5
0.0808	10	6.4	201.11	1.2808	1.2808	0	1.65	0.06	0.3073	25.7	25.3	-1.4
0.0808	10	6.4	201.13	2.0808	2.0808	0	2.75	0.15	0.4145	20.9	20.6	-1.4
0.0808	10	6.4	201.17	2.6308	2.6408	0.4	3.5	0.21	0.4719	18.6	19.06	2.3
0.0808	10	8.75	274.9	1.2808	1.2808	0	1.65	0.06	0.2516	39.3	38.7	-1.6
0.0808	10	8.75	274.9	2.0808	2.0808	0	2.75	0.15	0.3467	32.7	32.2	-1.6
0.0808	10	8.75	275	2.6308	2.6408	0.4	3.5	0.21	0.3997	29.6	29.8	0.8
0.0808	15	8.75	412.38	1.9508	1.8808	-3.6	1.65	0.06	0.3254	76.7	75	-2.2
0.0808	15	12	566	1.9508	1.8808	-3.6	1.65	0.06	0.2667	118.5	119	0.4
0.0808	16	8.75	440	2.0808	2.0808	0	1.65	0.06	0.3467	83.8	83.2	-0.7
0.0808	10	8.75	275	2.0808	2.0808	0	2.75	0.15	0.3467	32.7	32.1	-1.9
0.0808	9	8.75	247	2.0208	2.0808	3	3	0.17	0.3467	26.5	26.4	-0.4
0.0808	8	8.75	220	2.1208	2.0808	-1.9	3.6	0.22	0.3467	21.0	20.8	-0.7
0.102	18	8.75	495	2.092	2.102	0.5	1.15	0.02	0.3467	105.6	102.6	-2.9
0.102	14	8.75	385	2.092	2.102	0.5	1.5	0.06	0.3467	63.9	61.7	-3.4
0.102	9	8.75	248	2.142	2.102	-1.9	2.5	0.17	0.3467	26.4	25.9	-1.9
0.102	7	8.75	193	2.182	2.102	-3.7	3.4	0.26	0.3467	16.0	15.9	-0.5
0.128	15	8.75	412	2.188	2.128	-2.7	1.15	0.03	0.3467	73.0	70.1	-3.9

0.128	9	8.75	248	2.178	2.128	-2.3	2	0.14	0.3467	26.3	25.6	-2.6
0.128	8	8.75	220	2.148	2.128	-0.9	2.25	0.18	0.3467	20.8	20.1	-3.2
0.102	11	8.75	302	1.632	1.602	-1.8	1.5	0.06	0.2906	43.9	42.1	-4.1
0.0808	12	8.75	330	1.5508	1.5808	1.9	1.65	0.06	0.2906	52.5	51.1	-2.7
0.0808	1	9	28.3	0.0808	0.0808	0	1.65	0	0.032	0.8042	0.813	1.1
0.0808	1	8.75	27.4	0.0808	0.0808	0	1.65	0	0.032	0.778	0.764	-1.8
0.0808	2	9	56.6	0.2108	0.2108	0	1.65	0.13	0.032	2.6663	2.468	-7.4
0.102	1	8.95	28.1	0.102	0.102	0	1.15	0	0.0389	0.765	0.764	-0.1
0.102	2	8.95	56.2	0.222	0.222	0	1.15	0.12	0.0389	2.6187	2.231	-14.8

## A.2 Spiral Coils: Coil Geometries and Inductance

Coil Geometry										Inductance		
diam.		Coil	Theory	Theory	Measured	Error	Measured	Gap	Theory	Measured	Error	
Wire	Turns	Diameter	WireLength	Coil Length	Coil Length	in Length	c/a	Distance	L	L	L	
(inc)		(inch)	(inch)	(inch)	(inch)	(%)		(inch)	( $\mu$ H)	( $\mu$ H)	(%)	
0.128	10	6.40	155.0	1.38	1.40	1.3	1.20	0.03	16.6	15.3	-8.1	
0.128	10	8.75	233.0	1.27	1.25	-1.4	1.10	0.01	30.4	27.9	-8.3	
0.102	5	6.50	92.0	0.55	0.55	-0.1	1.35	0.04	7.0	7.1	2.2	
0.102	5	6.75	89.0	0.94	0.94	-0.4	2.30	0.13	5.7	5.6	-1.4	
0.102	6	6.25	99.0	0.89	0.86	-3.6	1.75	0.08	7.6	8.2	7.9	
0.102	6	6.25	92.0	1.25	1.20	-4.0	2.45	0.15	5.9	6.8	14.4	
0.102	10	6.50	163.0	1.24	1.20	-3.2	1.35	0.04	18.8	20.8	10.9	
0.0808	5	8.75	128.0	0.53	0.53	-1.6	1.65	0.05	10.4	10.6	2.0	
0.0808	5	12.00	179.0	0.53	0.53	-1.6	1.65	0.05	15.3	16.5	7.5	
0.0808	10	6.40	161.0	1.20	1.20	0.0	1.65	0.05	18.7	17.7	-5.4	
0.0808	10	6.40	129.0	2.18	2.20	0.8	3.00	0.16	9.7	10.6	8.7	
0.0808	10	8.75	235.0	1.20	1.20	0.0	1.65	0.05	31.4	30.5	-2.8	
0.0808	10	8.75	203.0	2.18	2.20	0.8	3.00	0.16	19.8	20.9	5.5	
0.0808	10	8.75	188.0	2.62	2.60	-0.7	3.60	0.21	16.0	16.6	3.6	
0.0808	10	12.00	339.0	1.20	1.20	0.0	1.65	0.05	50.3	49.8	-1.0	
0.0808	10	12.00	306.0	2.18	2.20	0.8	3.00	0.16	36.2	36.5	0.9	
0.0808	10	12.00	292.0	2.62	2.60	-0.7	3.60	0.21	31.2	31.1	-0.3	
0.0808	15	8.75	321.0	1.87	1.80	-3.6	1.65	0.05	53.1	52.4	-1.2	
0.0808	15	12.00	474.0	1.87	1.80	-3.6	1.65	0.05	91.6	88.5	-3.3	
0.125	14	12.00	379.0	3.25	3.25	0.0	2.00	0.13	49.9	46.5	-6.9	

## Appendix B: Resistance of Constructed Coils

### B.1 Cylindrical Coils: Coil Geometry and Resistance values

Coil Geometry								Resistance							
diam.		Coil	Theory	Measured	Measured	Gap		Theory	Measured	Error	Theory Ro	Theory Rtotal	Measured	Error	
Wire	Turns	Diameter	WireLength	Coil Length	c/a	Distance	Nagaoka	Rdc	Rdc	Rdc	@ 100kHz	@100kHz	Rtotal	Rtotal	
(inc)		(inch)	(inch)	(inch)		(inch)	Factor	(mohm)	(mohm)	(%)	(mohm)	(mohm)	(mohm)	(%)	
0.102	3	6.4	60.34	0.402	1.5	0.1	0.1169	4.9	3.6	-26.5	16.7	22.4	23	2.7	
0.102	4	6.4	80.45	0.552	1.5	0.09	0.1574	6.5	7.2	-10.8	22.2	32.7	33	0.9	
0.102	5	6.35	99.76	0.582	1.15	0.04	0.1658	8.1	10.6	-30.9	27.5	59.0	55	-6.8	
0.102	5	6.4	100.56	0.702	1.5	0.08	0.1944	8.1	7.2	-11.1	27.8	43.7	43	-1.6	
0.102	5	6.4	100.61	1.082	2.5	0.18	0.2703	8.1	8.2	-1.2	27.8	32.9	33	0.3	
0.102	5	6.4	100.68	1.452	3.4	0.27	0.3304	8.1	7.7	-4.9	27.8	30.3	32	5.6	
0.102	6	6.35	119.72	0.702	1.15	0.04	0.1946	9.7	11.6	-19.6	33.1	79.3	78	-1.6	
0.102	6	6.35	119.72	0.782	1.3	0.05	0.212	9.7	8.1	-16.5	33.1	64.7	59	-8.8	
0.102	6	6.4	120.67	0.862	1.5	0.07	0.2276	9.8	9.2	-6.1	33.3	55.2	54	-2.2	
0.102	6	6.35	119.76	1.172	2.1	0.13	0.2874	9.7	7.5	-22.7	33.1	42.8	44	2.8	
0.102	7	6.4	140.78	1.012	1.5	0.07	0.2583	11.4	12.1	-6.1	38.9	67.3	67	-0.4	
0.102	7	6.4	140.86	1.572	2.5	0.17	0.348	11.4	11.3	-0.9	38.9	47.4	52	9.7	
0.102	7	6.4	140.95	2.132	3.4	0.26	0.4178	11.4	10.4	-8.8	38.9	43.0	48	11.6	
0.102	10	6.4	201.1	1.162	1.15	0.03	0.2843	16.3	16.6	-1.8	55.5	182.6	206	12.8	
0.102	10	6.35	199.55	1.462	1.5	0.06	0.3334	16.2	18	-11.1	55.1	104.9	100	-4.7	
0.102	10	6.35	199.65	2.362	2.5	0.16	0.444	16.2	16.9	-4.3	55.1	68.6	76	10.8	
0.102	10	12.04	378.27	1.182	1.15	0.03	0.1885	30.6	30.2	-1.3	104.5	343.5	275	-19.9	
0.102	11	6.4	221.23	1.592	1.5	0.06	0.3498	17.9	20.6	-15.1	61.1	118.8	111	-6.6	
0.128	10	6.38	200.49	1.428	1.15	0.03	0.3235	10.3	7.8	-24.3	43.4	142.6	123	-13.7	
0.128	10	6.38	200.64	2.728	2.25	0.17	0.4763	10.3	8.3	-19.4	43.4	57.0	64	12.3	
0.128	10	8.75	274.93	1.428	1.15	0.03	0.2651	14.1	10.1	-28.4	59.5	195.5	172	-12.0	
0.128	10	8.75	275.04	2.728	2.25	0.17	0.4031	14.1	8.7	-38.3	59.5	78.1	80	2.4	
0.128	10	12.05	378.59	1.428	1.15	0.03	0.2142	19.5	17.9	-8.2	81.9	269.3	245	-9.0	
0.128	10	12.05	378.67	2.728	2.25	0.17	0.3349	19.5	14.5	-25.6	81.9	107.6	108	0.4	
0.0808	5	8.75	137.5	0.6058	1.65	0.07	0.1414	17.7	17.4	-1.7	49.0	71.6	69	-3.6	
0.0808	5	12	188.5	0.6058	1.65	0.07	0.1119	24.3	26.5	-9.1	67.2	98.3	103	4.8	
0.0808	10	6.4	201.11	1.2808	1.65	0.06	0.3073	25.9	26.6	-2.7	71.7	121.4	122	0.5	
0.0808	10	6.4	201.13	2.0808	2.75	0.15	0.4145	26.0	32	-23.1	71.8	85.7	95	10.9	
0.0808	10	6.4	201.17	2.6408	3.5	0.21	0.4719	26.0	28.5	-9.6	71.8	80.0	88	10.0	
0.0808	10	8.75	274.9	1.2808	1.65	0.06	0.2516	35.5	38.5	-8.5	98.1	165.9	162	-2.4	
0.0808	10	8.75	274.9	2.0808	2.75	0.15	0.3467	35.5	38	-7.0	98.1	117.2	123	4.9	
0.0808	10	8.75	275	2.6408	3.5	0.21	0.3997	35.5	39.4	-11.0	98.1	109.3	117	7.0	
0.0808	15	8.75	412.38	1.8808	1.65	0.06	0.3254	53.2	56.5	-6.2	147.1	267.2	244	-8.7	
0.0808	15	12	566	1.8808	1.65	0.06	0.2667	72.9	77.7	-6.6	201.7	366.4	360	-1.7	
0.0808	16	8.75	440	2.0808	1.65	0.06	0.3467	56.7	59.1	-4.2	156.9	287.9	279.4	-3.0	
0.0808	10	8.75	275	2.0808	2.75	0.15	0.3467	35.5	35.4	-0.3	98.1	117.2	117.4	0.2	
0.0808	9	8.75	247	2.0808	3	0.17	0.3467	31.9	32.6	-2.2	88.3	102.0	103.5	1.5	
0.0808	8	8.75	220	2.0808	3.6	0.22	0.3467	28.4	28.3	-0.4	78.5	86.3	87.4	1.3	
0.102	18	8.75	495	2.102	1.15	0.02	0.3467	40.1	40.7	-1.5	136.6	626.1	433	-30.8	
0.102	14	8.75	385	2.102	1.5	0.06	0.3467	31.2	34.6	-10.9	106.3	218.5	196	-10.3	
0.102	9	8.75	248	2.102	2.5	0.17	0.3467	20.0	21.9	-9.5	68.3	84.7	88.9	5.0	

0.102	7	8.75	193	2.102	3.4	0.26	0.3467	15.6	16.3	4.5	53.2	58.7	62.8	7.0
0.128	15	8.75	412	2.128	1.15	0.03	0.3467	21.2	21	-0.9	89.2	370.4	295	-20.4
0.128	9	8.75	248	2.128	2	0.14	0.3467	12.7	13.4	5.5	53.5	75.0	77.7	3.6
0.128	8	8.75	220	2.128	2.25	0.18	0.3467	11.3	10.8	-4.4	47.6	61.3	61.2	-0.2
0.102	11	8.75	302	1.602	1.5	0.06	0.2906	24.5	28	14.3	83.5	162.4	149	-8.3
0.0808	12	8.75	330	1.5808	1.65	0.06	0.2906	42.6	50	17.4	117.7	206.0	192	-6.8

## B.2 Spiral Coils: Coil Geometries and Resistance values

Coil Geometry							Resistance								
diam.		Coil	Theory	Measured	Measured	Gap	Theory	Measured	Error	Theory	Rtotal	Theory	Rtotal	Measured	Error
Wire	Turns	Diameter	WireLength	Coil Length	c/a	Distance	Rdc	Rdc	Rdc	@100kHz	@100kHz	Rtotal	Rtotal	Rtotal	Rtotal
(inc)		(inch)	(inch)	(inch)		(inch)	(mohm)	(mohm)	(%)	(mohm)	(mohm)	(mohm)	(mohm)	(%)	
0.128	10	6.40	155.0	1.40	1.20	0.03	8.0	7	-12.5	33.6	97.1	117	20.4		
0.128	10	8.75	233.0	1.25	1.10	0.01	12.0	9.8	-18.3	50.4	198.9	197	-1.0		
0.102	5	6.50	92.0	0.55	1.35	0.04	7.5	4.6	-38.7	25.5	44.3	46	3.8		
0.102	5	6.75	89.0	0.94	2.30	0.13	7.2	15.37	113.5	24.7	30.2	30	-0.6		
0.102	6	6.25	99.0	0.86	1.75	0.08	8.0	11.7	46.2	27.4	39.8	43	8.0		
0.102	6	6.25	92.0	1.20	2.45	0.15	7.4	7.5	1.4	25.4	30.7	35	14.2		
0.102	10	6.50	163.0	1.20	1.35	0.04	13.2	13	-1.5	45.0	100.9	141	39.7		
0.0808	5	8.75	128.0	0.53	1.65	0.05	16.5	16.9	2.4	45.7	66.8	65	-2.7		
0.0808	5	12.00	179.0	0.53	1.65	0.05	23.1	22.4	-3.0	63.9	93.4	88	-5.8		
0.0808	10	6.40	161.0	1.20	1.65	0.05	20.8	21.1	1.4	57.5	97.3	101	3.8		
0.0808	10	6.40	129.0	2.20	3.00	0.16	16.6	15.2	-8.4	45.9	53.2	68	27.7		
0.0808	10	8.75	235.0	1.20	1.65	0.05	30.3	31.6	4.3	83.9	141.9	152	7.1		
0.0808	10	8.75	203.0	2.20	3.00	0.16	26.1	31.1	19.2	72.2	83.8	108	29.0		
0.0808	10	8.75	188.0	2.60	3.60	0.21	24.3	26.8	10.3	67.1	74.3	94	26.5		
0.0808	10	12.00	339.0	1.20	1.65	0.05	43.7	44.4	1.6	120.8	204.4	196	-4.1		
0.0808	10	12.00	306.0	2.20	3.00	0.16	39.5	43.2	9.4	109.2	126.7	141	11.3		
0.0808	10	12.00	292.0	2.60	3.60	0.21	37.6	39.8	5.9	104.1	115.2	124	7.6		
0.0808	15	8.75	321.0	1.80	1.65	0.05	41.4	42.8	3.4	114.6	208.2	226	8.6		
0.0808	15	12.00	474.0	1.80	1.65	0.05	61.2	65.3	6.7	169.2	307.3	293	-4.7		
0.125	14	12.00	379.0	3.25	2.00	0.13	34.4	32.8	-4.8	84.1	123.6	160	29.5		

## Appendix C: $Q$ of Constructed Coils

### C.1 Cylindrical Coils: Coil Geometries and $Q$

Coil Geometry										Quality Factor		
diam.		Coil	Theory	Theory	Measured	Error	Measured	Gap		Theory	Measured	Error
Wire	Turns	Diameter	WireLength	Coil Length	Coil Length	in Length	c/a	Distance	Nagaoka	Q	Q	Q
(inc)		(inch)	(inch)	(inch)	(inch)	(%)		(inch)	Factor	@100kHz	@100kHz	(%)
0.102	3	6.4	60.34	0.412	0.402	-2.4	1.5	0.1	0.1169	94	86	-9
0.102	4	6.4	80.45	0.562	0.552	-1.8	1.5	0.09	0.1574	105	100	-5
0.102	5	6.35	99.76	0.572	0.582	1.7	1.15	0.04	0.1658	89	89	1
0.102	5	6.4	100.56	0.712	0.702	-1.4	1.5	0.08	0.1944	114	111	-3
0.102	5	6.4	100.61	1.122	1.082	-3.6	2.5	0.18	0.2703	130	127	-3
0.102	5	6.4	100.68	1.492	1.452	-2.7	3.4	0.27	0.3304	127	121	-4
0.102	6	6.35	119.72	0.692	0.702	1.4	1.15	0.04	0.1946	89	87	-3
0.102	6	6.35	119.72	0.762	0.782	2.6	1.3	0.05	0.212	106	109	3
0.102	6	6.4	120.67	0.862	0.862	0	1.5	0.07	0.2276	121	119	-2
0.102	6	6.35	119.76	1.172	1.172	0	2.1	0.13	0.2874	139	129	-7
0.102	7	6.4	140.78	1.022	1.012	-1	1.5	0.07	0.2583	128	123	-4
0.102	7	6.4	140.86	1.632	1.572	-3.7	2.5	0.17	0.348	153	136	-11
0.102	7	6.4	140.95	2.182	2.132	-2.3	3.4	0.26	0.4178	148	131	-12
0.102	10	6.4	201.1	1.162	1.162	0	1.15	0.03	0.2843	92	104	14
0.102	10	6.35	199.55	1.482	1.462	-1.3	1.5	0.06	0.3334	144	147	2
0.102	10	6.35	199.65	2.402	2.362	-1.7	2.5	0.16	0.444	178	160	-10
0.102	10	12.04	378.27	1.162	1.182	1.7	1.15	0.03	0.1885	113	137	21
0.102	11	6.4	221.23	1.632	1.592	-2.5	1.5	0.06	0.3498	150	153	2
0.128	10	6.38	200.49	1.448	1.428	-1.4	1.15	0.03	0.3235	108	119	10
0.128	10	6.38	200.64	2.718	2.728	0.4	2.25	0.17	0.4763	201	175	-13
0.128	10	8.75	274.93	1.448	1.428	-1.4	1.15	0.03	0.2651	122	131	8
0.128	10	8.75	275.04	2.718	2.728	0.4	2.25	0.17	0.4031	234	220	-6
0.128	10	12.05	378.59	1.448	1.428	-1.4	1.15	0.03	0.2142	136	145	7
0.128	10	12.05	378.67	2.718	2.728	0.4	2.25	0.17	0.3349	269	260	-3
0.0808	5	8.75	137.5	0.6108	0.6058	-0.8	1.65	0.07	0.1414	109	109	0
0.0808	5	12	188.5	0.6108	0.6058	-0.8	1.65	0.07	0.1119	119	109	-8
0.0808	10	6.4	201.11	1.2808	1.2808	0	1.65	0.06	0.3073	133	130	-2
0.0808	10	6.4	201.13	2.0808	2.0808	0	2.75	0.15	0.4145	153	137	-11
0.0808	10	6.4	201.17	2.6308	2.6408	0.4	3.5	0.21	0.4719	146	135	-8
0.0808	10	8.75	274.9	1.2808	1.2808	0	1.65	0.06	0.2516	149	150	1
0.0808	10	8.75	274.9	2.0808	2.0808	0	2.75	0.15	0.3467	175	164	-7
0.0808	10	8.75	275	2.6308	2.6408	0.4	3.5	0.21	0.3997	170	158	-7
0.0808	15	8.75	412.38	1.9508	1.8808	-3.6	1.65	0.06	0.3254	180	193	7
0.0808	15	12	566	1.9508	1.8808	-3.6	1.65	0.06	0.2667	203	210	3
0.0808	16	8.75	440	2.0808	2.0808	0	1.65	0.06	0.3467	183	187	2
0.0808	10	8.75	275	2.0808	2.0808	0	2.75	0.15	0.3467	175	171	-3
0.0808	9	8.75	247	2.0208	2.0808	3	3	0.17	0.3467	163	160	-2
0.0808	8	8.75	220	2.1208	2.0808	-1.9	3.6	0.22	0.3467	153	149	-2
0.102	18	8.75	495	2.092	2.102	0.5	1.15	0.02	0.3467	106	149	41
0.102	14	8.75	385	2.092	2.102	0.5	1.5	0.06	0.3467	184	198	8
0.102	9	8.75	248	2.142	2.102	-1.9	2.5	0.17	0.3467	196	183	-7
0.102	7	8.75	193	2.182	2.102	-3.7	3.4	0.26	0.3467	171	159	-7
0.128	15	8.75	412	2.188	2.128	-2.7	1.15	0.03	0.3467	124	149	20

0.128	9	8.75	248	2.178	2.128	-2.3	2	0.14	0.3467	220	206	-6
0.128	8	8.75	220	2.148	2.128	-0.9	2.25	0.18	0.3467	213	205	-4
0.102	11	8.75	302	1.632	1.602	-1.8	1.5	0.06	0.2906	170	178	5
0.0808	12	8.75	330	1.5508	1.5808	1.9	1.65	0.06	0.2906	160	167	4

## C.2 Spiral Coils: Coil Geometries and $Q$

Coil Geometry									Quality Factor		
diam.		Coil	Theory	Theory	Measured	Error	Measured	Gap	Theory	Measured	Error
Wire	Turns	Diameter	WireLength	Coil Length	Coil Length	in Length	c/a	Distance	Q	Q	Q
(inc)		(inch)	(inch)	(inch)	(inch)	(%)		(inch)	@100kHz	@100kHz	(%)
0.128	10	6.40	155.0	1.38	1.40	1.3	1.20	0.03	107.68	81.00	-24.80
0.128	10	8.75	233.0	1.27	1.25	-1.4	1.10	0.01	96.12	85.00	-11.60
0.102	5	6.50	92.0	0.55	0.55	-0.1	1.35	0.04	98.56	97.00	-1.60
0.102	5	6.75	89.0	0.94	0.94	-0.4	2.30	0.13	118.29	117.00	-1.10
0.102	6	6.25	99.0	0.89	0.86	-3.6	1.75	0.08	120.03	121.00	0.80
0.102	6	6.25	92.0	1.25	1.20	-4.0	2.45	0.15	121.80	121.00	-0.70
0.102	10	6.50	163.0	1.24	1.20	-3.2	1.35	0.04	116.82	93.00	-20.40
0.102	10	6.60	140.0	2.02	2.00	-1.0	2.20	0.12	142.69	95.00	-33.40
0.102	20	6.40	227.0	2.71	2.60	-4.2	1.40	0.04	112.54	79.00	-29.80
0.0808	5	8.75	128.0	0.53	0.53	-1.6	1.65	0.05	97.81	103.00	5.30
0.0808	5	12.00	179.0	0.53	0.53	-1.6	1.65	0.05	103.25	117.00	13.30
0.0808	10	6.40	161.0	1.20	1.20	0.0	1.65	0.05	120.89	110.00	-9.00
0.0808	10	6.40	129.0	2.18	2.20	0.8	3.00	0.16	115.03	99.00	-13.90
0.0808	10	8.75	235.0	1.20	1.20	0.0	1.65	0.05	138.96	127.00	-8.60
0.0808	10	8.75	203.0	2.18	2.20	0.8	3.00	0.16	148.63	121.00	-18.60
0.0808	10	8.75	188.0	2.62	2.60	-0.7	3.60	0.21	135.47	111.00	-18.10
0.0808	10	12.00	339.0	1.20	1.20	0.0	1.65	0.05	154.63	160.00	3.50
0.0808	10	12.00	306.0	2.18	2.20	0.8	3.00	0.16	179.45	162.00	-9.70
0.0808	10	12.00	292.0	2.62	2.60	-0.7	3.60	0.21	170.00	157.00	-7.60
0.0808	15	8.75	321.0	1.87	1.80	-3.6	1.65	0.05	160.15	146.00	-8.80
0.0808	15	12.00	474.0	1.87	1.80	-3.6	1.65	0.05	187.17	189.00	1.00
0.125	14	12.00	379.0	3.25	3.25	0.0	2.00	0.13	253.90	182.00	-28.30

## Appendix D: $S_{21}$ Correction

The Bode100 is an excellent tool for measuring the transmission and reflection coefficients of 4-port circuit devices. However, there are a couple assumptions and constraints the device imposes on itself in order to make its high-fidelity measurement. These assumptions lead to erroneous outputs when the source and load impedances are not matched. This section will review the manner in which the Bode100 calibrates its output measurement, how calibrated measurements can incur an error, and adjustments for rectifying the problem.

Beginning with the calibration approach, Fig. 1.2 displays the inner workings and high-level schematic of the Bode100 during normal impedance-matched  $S_{21}$  thru calibration. Fig. 1.2 is an equivalent circuit produced by LTSpice.  $R_{\text{source}}$  and  $R_{\text{load}}$ , representing the Bode100's internal source,  $R_{S,\text{int}}$ , and internal load impedance,  $R_{L,\text{int}}$ , are each  $50 \Omega$  and  $\text{RDUT}$ , representing the device under test impedance, is 0. The  $S_{21}$  parameter formula is composed of a constant, a resistive factor, voltage factor as such:

$$S_{21} = 2 \sqrt{\frac{R_{\text{source}}}{R_{\text{load}}} \frac{V_{\text{load}}}{V_{\text{source}}}} \quad (\text{Eq. D.1})$$

$$\sqrt{\frac{R_{\text{source}}}{R_{\text{load}}}} = \text{resistive factor}$$

$$\frac{V_{\text{load}}}{V_{\text{source}}} = \text{voltage factor}$$

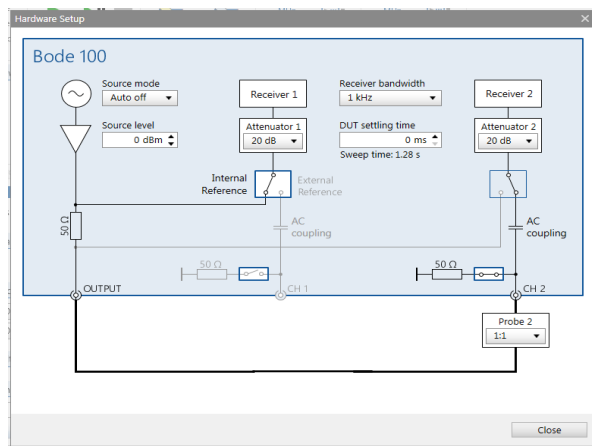


Fig. D.1: Internal hardware setup of Bode100 during calibration

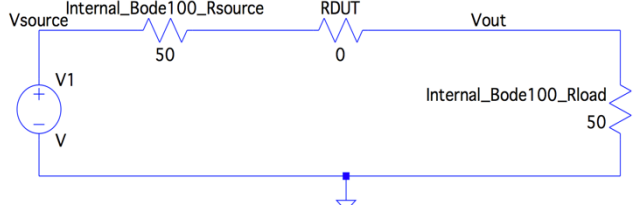


Fig. D.2: Equivalent circuit of the Bode100 calibration setup

During calibration, the Bode100 strives to make  $S_{21}$  equal to unity. In the scenario where the input and output impedances are the Bode100's  $50 \Omega$  internal impedances, the resistance factor is unity and the voltage factor is  $1/2$ . However, this isn't the case for every matched impedance system. Consider externally attaching  $50 \Omega$  in parallel to the Bode100's source resistance and another external  $50 \Omega$  to the load. The equivalent circuit is modeled in Fig. 1.3. In this scenario, the equivalent source and load resistances are equal to each other,  $25 \Omega$ , resulting in a unity resistive factor. However, the voltage divider ratio is not  $1/2$ , it's  $5/4$ . In this situation, the Bode100 will attempt to force the  $S_{21}$  to unity via a self-correcting multiplicative factor, ' $\alpha$ ', Eq.1.2. The formulation is as such, where  $R_{S,eqv}$  is the "Internal Bode100 Rsource" in parallel with the added "External Source" in Fig. 1.3 and  $R_{L,eqv}$  is the "External Load" in parallel with "Internal Bode100 Rload":

$$S_{21}^{BODE} = 2 \sqrt{\frac{R_{\text{source}}}{R_{\text{load}}} \frac{V_{\text{load}}}{V_{\text{source}}}} \alpha \quad (\text{Eq. D.2})$$

During Calibration:  $S_{21}^{BODE} \equiv 1$  and  $\sqrt{\frac{R_{\text{source}}}{R_{\text{load}}}} \equiv 1$ , thus  $2 \frac{V_{\text{load}}}{V_{\text{source}}} \alpha = 1$  (Eq. D.3)

$$R_{L,eqv} = R_{L,int} // R_{L,ext} \text{ and } R_{S,eqv} = R_{S,int} // R_{S,ext}$$

$$\left. \frac{V_{\text{load}}}{V_{\text{source}}} \right|_{RDUT=0} = \frac{R_{L,eqv} // R_{S,int}}{R_{L,eqv} // R_{S,int} + R_{S,int}}, \alpha = \frac{1}{2} \frac{V_{\text{source}}}{V_{\text{load}}} = \frac{R_{L,eqv} // R_{S,int} + R_{S,int}}{2(R_{L,eqv} // R_{S,int})} \quad (\text{Eq. D.4})$$

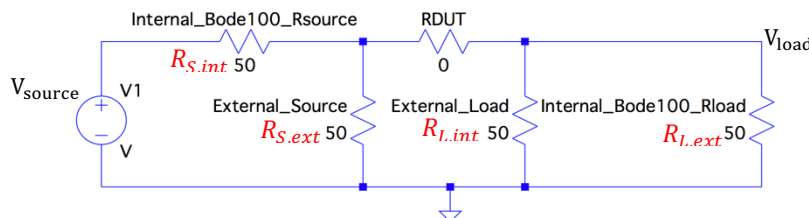


Fig. D.3: Matched equivalent input and output Impedances

The multiplicative factor, ‘ $\alpha$ ’, essentially changes the initially measured voltage factor to  $1/2$ , which works well for matched systems. Thus, for matched systems with additional external resistances, the Bode100 produces a correct output for  $S_{21}$  by determining an adjustment factor during calibration. Fig. 1.4 displays the internals of the  $S_{21}$  measurement using LTSpice. The mechanism by which the Bode100 produces correct  $S_{21}$  outputs for a matched  $50 \Omega$  scenario and matched  $25 \Omega$  scenario, with the ‘ $\alpha$ ’ correction factor, can be observed.

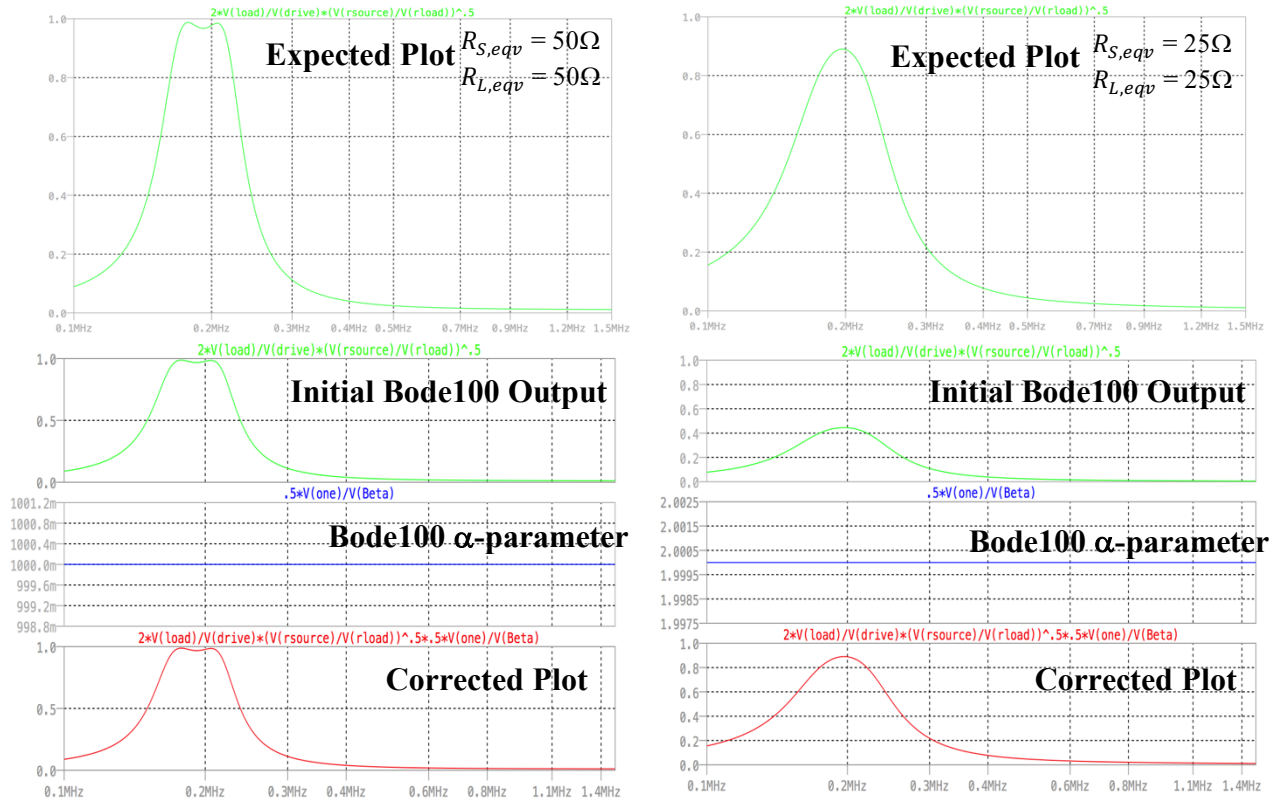


Fig. D.4: Matched  $R_{source} = R_{load} = 50 \Omega$  (left) and matched  $R_{source} = R_{load} = 25 \Omega$  (right). The first image (starting from the top) is the correct  $S_{21}$  Plot. The second is what the Bode100 will initially measure. The third plot (blue) is the voltage correction factor ‘alpha’. Note for the  $50/50$  case, the value of alpha is 1 as expected. Finally, the last plot is the corrected Bode100 plot which is derived from the second and third waveform.

Now, consider the case where the equivalent input and output impedances aren’t equal. Fig. 1.5 displays such a scenario. To create this scenario experimentally, one introduces a  $50 \Omega$  resistance in parallel to the Bode100’s source resistance but doesn’t introduce an accompanying one on the load side. Observing the above  $S_{21}$  formula, in this case, the resistive factor isn’t unity and the voltage factor isn’t  $1/2$ , however, the Bode100 isn’t aware of this imbalance. It continues

to assume a matched system and attempts to force the voltage ratio to  $1/2$  via ‘ $\alpha$ ’. The formulation follows the same from Eq. 1.2-1.4, however there is crucial information for  $S_{21}$  that the Bode100 isn’t accounting for: the resistive factor isn’t unity and the voltage factor isn’t  $1/2$ .

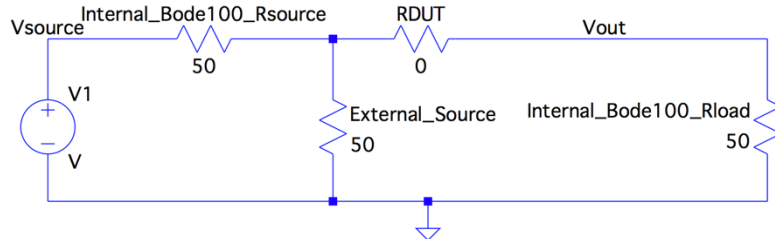


Fig. D.5: Unmatched equivalent input and output

The Bode100 assumes that the resistances are matched and doesn’t offer a method for the user to dictate otherwise. Therefore, the  $S_{21}$  measurements of the Bode100 for unmatched resistances are incorrect and need proper adjustment. This must be done by exporting the data from the Bode100 to another program and re-plotting. MATLAB is utilized in this investigation. To accomplish this, first adjust the voltage factor by multiplication ‘ $\beta$ ’.  $\beta$  is used because the Bode100 assumes the ratio of the output voltage over the input voltage is  $1/2$  and will use  $\alpha$  to make it such. However, in unmatched cases such as in Fig. 1.5, the voltage ratio is not  $1/2$ , it’s  $1/3$ . Therefore,  $\beta$  is used to transform the effects  $\alpha$  into the correct voltage factor. Equations 1.5-1.6 clarify the math for computing  $\beta$ . The ‘Bode Calculated’ voltage factor is what the Bode100 originally calculated and forces to  $1/2$  via  $\alpha$ . The ‘Intended’ voltage factor is the desired voltage ratio of the system and corresponds the actual voltage divider value.

$$\left. \frac{V_{load}}{V_{source}} \right|_{\substack{\text{Bode} \\ \text{Calculated}}} \alpha \beta = \left. \frac{V_{load}}{V_{source}} \right|_{\substack{\text{Intended}}} \quad (\text{Eq. D.5})$$

$$\left. \frac{V_{load}}{V_{source}} \right|_{\substack{\text{Bode} \\ \text{Calculated}}} \alpha = \frac{1}{2}$$

$$\beta = 2 \left. \frac{V_{load}}{V_{source}} \right|_{\substack{\text{Intended}}} = 2 \frac{R_{s,ext}/R_{L,eqv}}{R_{s,int} + R_{s,ext}/R_{L,eqv}} \quad (\text{Eq. D.6})$$

Now that  $\beta$  adjusts the incorrect voltage factor computed by the Bode100, the resistive factor still needs to be adjusted. Eq. 1.3 points out that the Bode100 assumes the resistor ratio to be unity, which isn't the case when the resistors are unmatched. Therefore, one needs to multiply by the correct resistor ratio, Eq. 1.7. Eq. 1.8 describes the two adjustments needed to correct the Bode100 for unmatched load and source impedances.

$$\sqrt{\frac{R_{S,eqv}}{R_{L,eqv}}} \quad (\text{Eq. D.7})$$

$$S_{21}^{Bode} * \beta * \sqrt{\frac{R_{S,eqv}}{R_{L,eqv}}} = S_{21}^{Corrected} \quad (\text{Eq. D.8})$$

It is desirable to visually observe the plots and adjustments of the Bode100 for an unmatched case so an LTspice model simulation was developed to replicate the operation. Fig. 1.6 displays LTspice simulation waveforms for unmatched impedance scenarios. Finally, Fig. 1.8 displays outputs taken by the Bode100 and their MATLAB corrected versions which agree with simulation results!

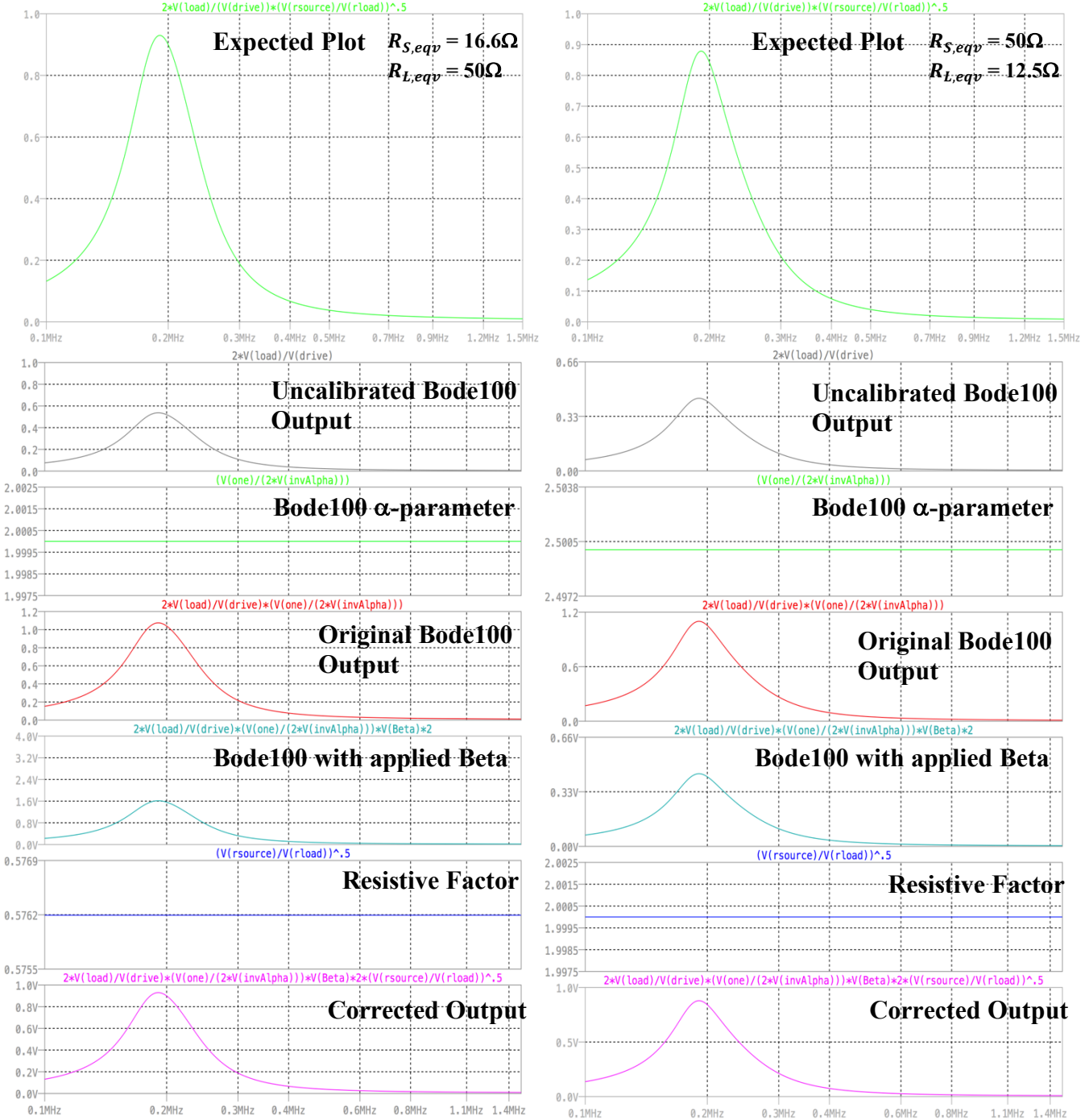


Fig. D.6: Unmatched  $R_{source} = 16$ ,  $R_{load} = 50$  (left). Unmatched  $R_{source} = 50$ ,  $R_{load} = 12.5$  (right). The first (top) plot is the correct  $S_{21}$  plot. The second (gray) represents the base Bode100 measurement. The third (green) plot is the Bode100 ‘alpha’ correction factor and the fourth (red) is Bode100 output (which includes its correction factor). Since the resistors are unmatched, an external ‘beta’ correction factor and resistive factor is needed. The light blue curve is the original bode100 plot with the beta factor and the dark blue is the resistive factor.

Finally, the sixth (pink) is the final ‘corrected’ plot and matches the first (top).

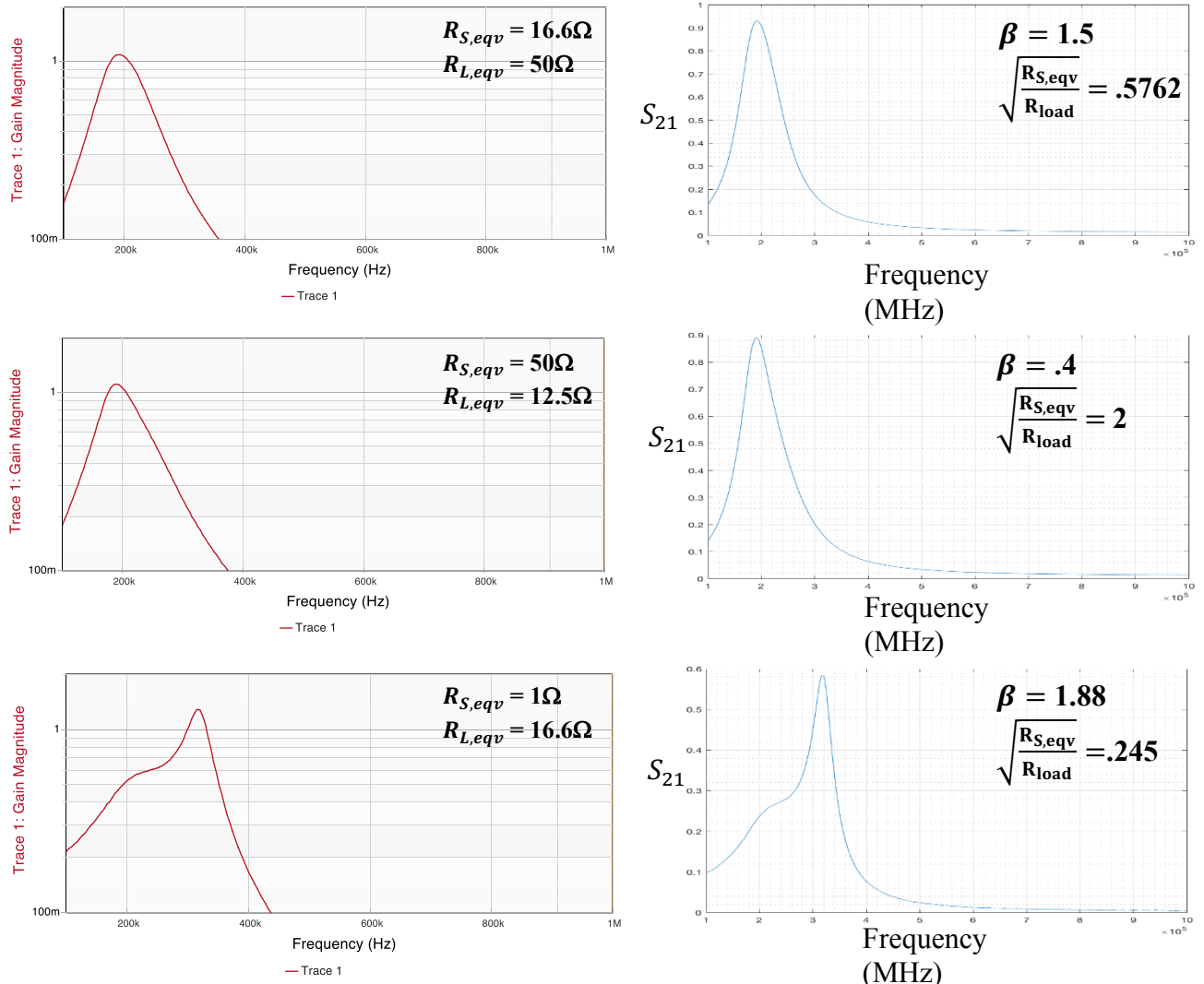


Fig. D.7: Unmatched Bode100 outputs and their adjusted plots. The adjusted plots agree with simulation results. The first (top) plot is the correct  $S_{21}$  plot. The first columns display each row's source and load resistance and the Bode100 output. The second column displays the adjusted graphs and the corresponding beta and resistor factor used to obtain it.

## Appendix E: H-Bridge Schematic

The power amplifier (H-bridge and associated circuitry) resides on a separate PCB from the other circuits.

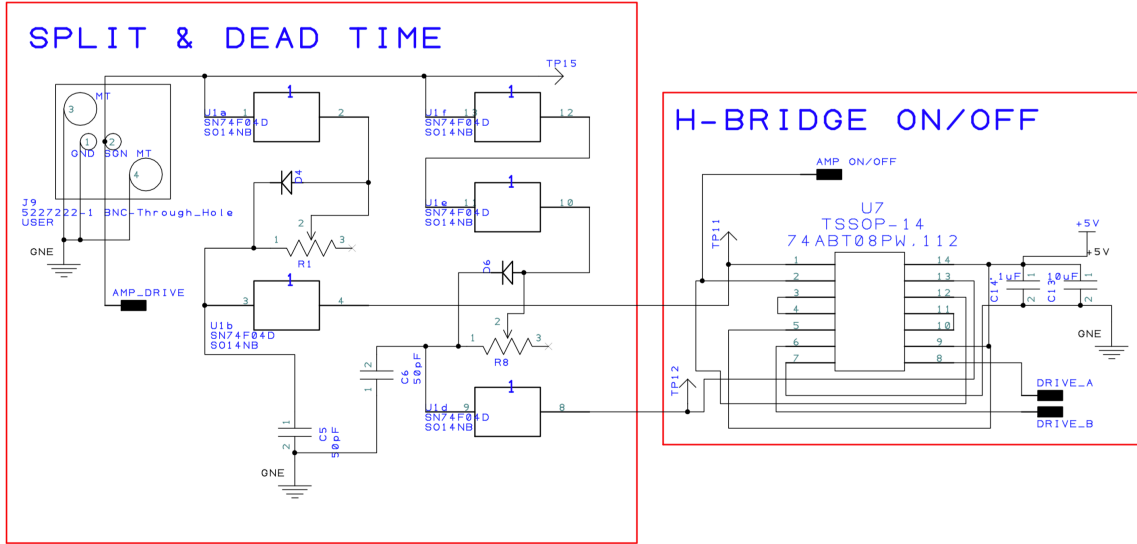


Fig. E.1: Schematic of power amplifier circuit that splits the input drive signal, creates dead-time and allows on/off capability [23]

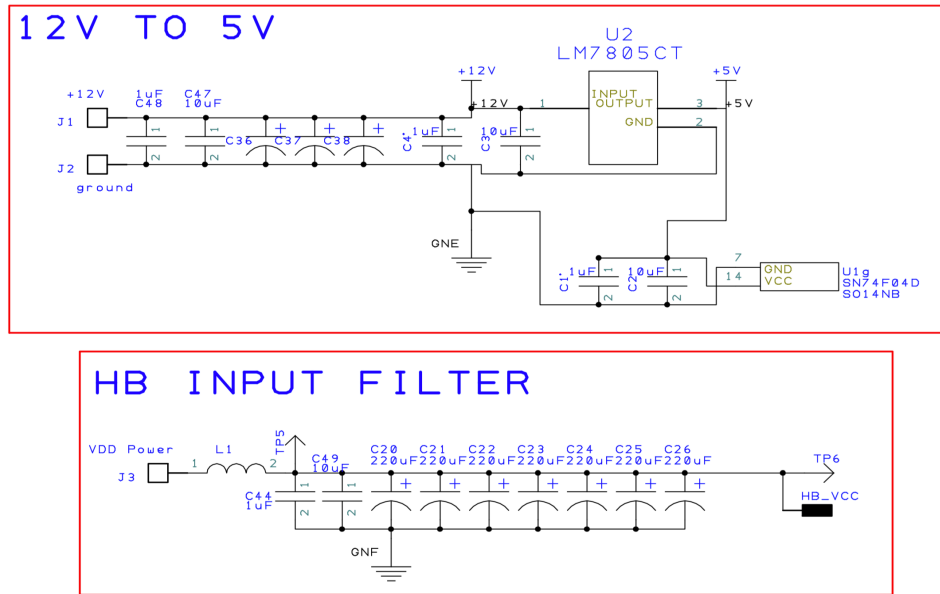


Fig. E.2: Schematic of 12V to 5V converter and H-bridge input filter [23]

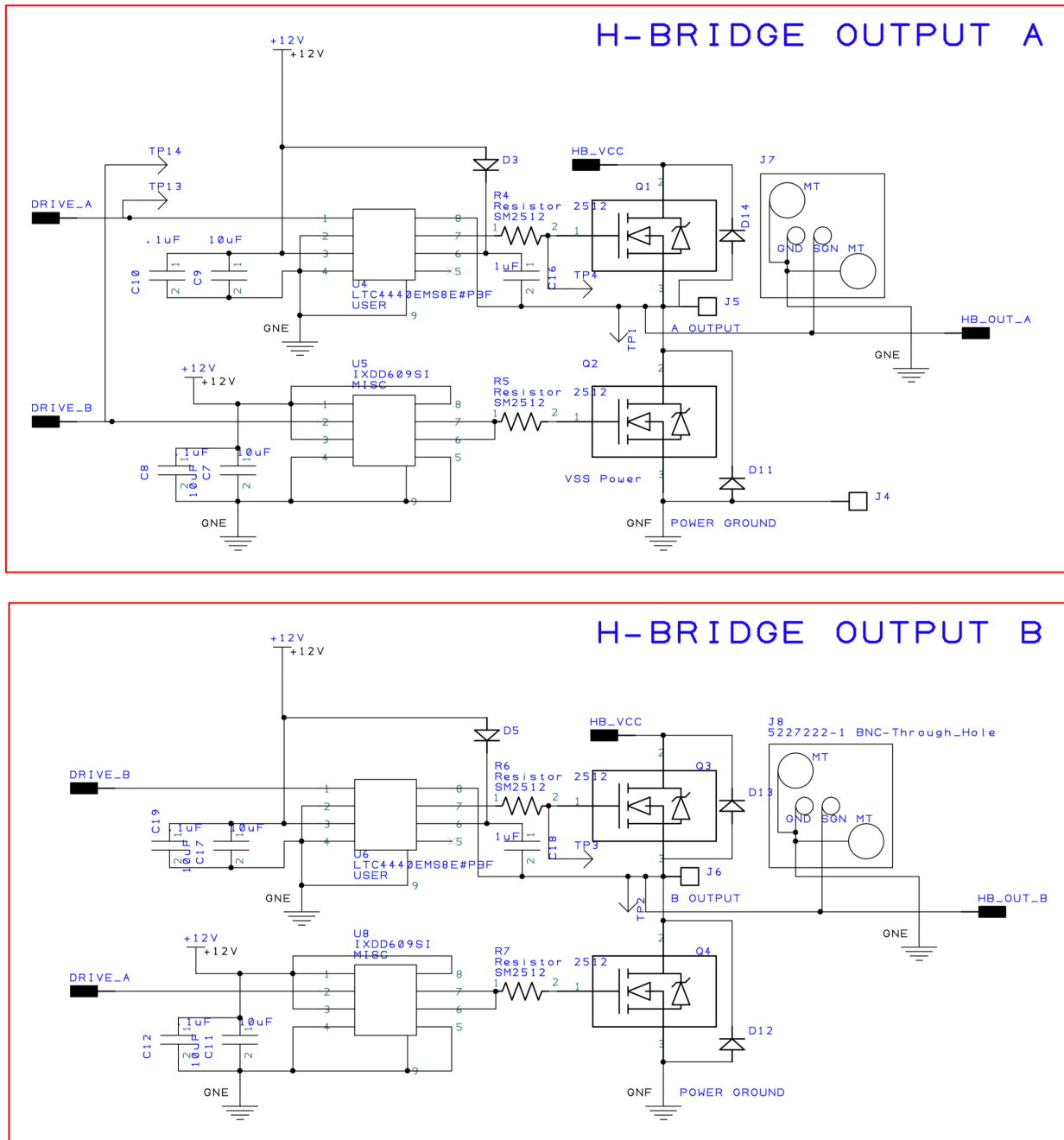


Fig. E.3: Schematic of H-bridge outputs A and B [23]

## Appendix F: MATLAB Code

### F.1 Design Algorithms for Lumped Equivalent Circuit Models

The following calculates the inductance of cylindrical and spiral coils as described in Chapter 4:

#### Cylindrical Inductance.m

```
function L = Cylindrical_Inductance(Diameter_o,len, N)
% NAGAOKA: Inductance of Short length coils, D/L < 1, all inputs INCHES

r = 0.0254 * Diameter_o / 2;
l = 0.0254* len;
ri = r - l;

A = ((4*r^2)/(4*r^2 + l^2))^.5;
k = 1/ (1 + (1/(2*r))^2)^.5;
B = (1 - A^2)^.5;
[K,E] = ellipke(A^2);
Kl = (4/(3*pi*B)) *((B^2/A^2)*(K - E) + E - A);

u = 4*pi*10^-7;

L = Kl*( (4*pi^2 * N^2 * r^2)/ (l) )*10^-7;
end
```

#### Spiral Inductance.m

```
function L = Spiral_Inductance(Do,N,d_wire,ca)
% WHEELER: Inductance of Spiral Coils via Wheelers Formula (INCHES)
% Do is the Design Outer Diameter
% num_turns is the number of turns
% d_wire is diameter of the wire
% absolute space between wires

w = d_wire;
s = (ca -1)*d_wire;
ro = Do/2;
if ((N)*(w+s) > ro)
    disp('Error: Length of Coil exceeds the Specied Outer Radius')
    L = 0;
    return
end

ri = (Do/2 - N*(w+s));
Di = ri *2;

A = (Di + N*(w + s))/2;

L = 1e-6*(N^2*A^2) / (30*A - 11*Di);
end
```

The following calculates the resistance of cylindrical and spiral coils as described in Chapter 4:

#### Proximity Script.m

```
%Script for generating the Prox Table!
%Using Chat's data output the Rp/Ro factor for a set of N parallel conducting
%wires with a c/a dictated by ca

ca_orig = [1.05:.05:1.3, 1.4:1:2, 2.2 2.4, 2.5, 2.6 2.8 3, 3.5, 4];
Table = [1.231 2.267 3.332 4.358 7.060;
0.996 1.689 2.340 2.947 3.501;
0.868 1.400 1.872 2.289 2.661;
0.777 1.210 1.577 1.891 2.163;
```

```

0.704 1.068 1.365 1.613 1.824;
0.644 0.956 1.203 1.405 1.574;
0.546 0.784 0.965 1.108 1.224;
0.470 0.658 0.796 0.903 0.988;
0.408 0.561 0.670 0.753 0.818;
0.358 0.485 0.573 0.638 0.690;
0.316 0.423 0.495 0.549 0.590;
0.281 0.372 0.433 0.477 0.511;
0.252 0.330 0.382 0.419 0.448;
0.205 0.265 0.304 0.331 0.352;
0.170 0.217 0.247 0.269 0.284;
0.156 0.198 0.225 0.244 0.258;
0.144 0.182 0.206 0.222 0.235;
0.123 0.154 0.174 0.187 0.198;
0.106 0.133 0.150 0.160 0.169;
0.077 0.095 0.106 0.114 0.119;
0.058 0.072 0.080 0.085 0.089;];

ca_final = 1.05:.05:4;
ca_int = [1.05, 1.1, 1.125, 1.15, 1.25, 1.5, 2 3 4];
Prox(:,4) = interp1(ca_orig, Table(:,1)', ca_final, 'pchip');
Prox(:,6) = interp1(ca_orig, Table(:,2)', ca_final, 'pchip');
Prox(:,8) = interp1(ca_orig, Table(:,3)', ca_final, 'pchip');
Prox(:,10) = interp1(ca_orig, Table(:,4)', ca_final, 'pchip');
Prox(:,12) = interp1(ca_orig, Table(:,5)', ca_final, 'pchip');
Prox(:,2) = interp1(ca_int,[.316 .299 .291 .283 .254 .192 .116 .054 .031],ca_final, 'pchip');
Prox(:,3) = interp1(ca_int,[.747 .643 .609 .580 .491 .345 .195 .085 .048],ca_final, 'pchip');
Prox(:,5) = interp1(ca_int,[1.742 1.347 1.223 1.142 .896 .572 .295 .121 .066],ca_final, 'pchip');
Prox(:,7) = interp1(ca_int,[2.799 2.021 1.807 1.643 1.224 .732 .358 .142 .076],ca_final, 'pchip');
Prox(:,9) = interp1(ca_int,[3.861 2.648 2.328 2.087 1.495 .853 .402 .155 .083],ca_final, 'pchip');
Prox(:,15) = interp1(ca_orig([2:15,17:end]),[4.282 3.153 2.495 2.087 1.783 1.365 1.089 .894 .749 .638
.550 .480 .375 .302 .249 .209 .178 .125 .093],ca_final, 'pchip');
Prox(:,20) = interp1(ca_orig([3:9,11,13:end]),[3.871 3.047 2.447 2.054 1.537 1.212 .986 .694 .518 .402
.322 .291 .264 .221 .188 .132 .098],ca_final, 'pchip');

%filling in the gaps
Prox2 = interp2( ca_final',[2:10, 12, 15
,20],[Prox(:,(2:10)),Prox(:,12),Prox(:,15),Prox(:,20)]',ca_final',[1:20], 'linear');
Prox2 = Prox2';

%The rest of the table
Prox3 = interp2(ca_final', [1:20], Prox2',ca_final',[1:60] , 'spline');
Prox3 = Prox3';
Prox = Prox3;

%surf(Prox(3:end, 1:30)); zlabel('Rp/Ro'); xlabel('Turns'); ylabel('c/a');


```

## Cylindrical Resistance.m

```

function R = Cylindrical_Resistance(freq,Do,N,dw,ca,Proximity)
% Finding Q of a Cylindrical coil
run('ProximityScript');
warning('off','last')
r = dw*.0254/2;

p = 1.68e-8;
A = pi*(dw*.0254/2)^2;
l = pi*Do*N*.0254;

u = pi*4e-7;
d = (p/(pi*freq*u))^5;
B = pi*r^2 - pi*(r - d)^2;

if r>=d
    A = B;
end

Rskin = p*l/(A);

if (Proximity == 1)
    ca_final = 1.05:.05:4;
    o = find(abs(ca_final - ca) < 1e-5);
    PF = Prox(o, N);
else
    PF = 0
end
R = (1 + PF)*Rskin;

```

## Spiral Resistance.m

```
function R = Spiral_Resistance(freq,Do,N,dw,ca,Proximity)
run('ProximityScript');
warning('off','last')

s = (ca - 1)*dw*.0254;
dw = .0254*dw;
r = dw/2;
ro = Do*.0254/2;
ri = ro - N*(dw+s);

%Length Calculation
tend = 2*pi*N;
b = (dw+s)/(2*pi);
fun = @(theta) ((ri + (b)*theta).^2 + (b)^2).^.5;
l = integral(fun,0,tend);
length = l/.0254;

%Resistance calculation
p = 1.68e-8;
A = pi*r^2;

u = pi*4e-7;
d = (p/(pi*freq*u)).^.5;
B = pi*r^2 - pi*(r - d)^2;

if r>=d
    A = B;
end

Rskin = p*l/(A);

if (Proximity == 1)
    ca_final = 1.05:.05:4;
    o = find(abs(ca_final - ca) < 1e-5);
    PF = Prox(o, N);
else
    PF = 0
end
R = (1 + PF)*Rskin;
```

The following calculates the coupling coefficient between cylindrical coils and spiral coils as described in Chapter 5:

## Cylindrical Coupling.m

```
function K = Cylindrical_Coupling(distance,r1,r2,L1,L2,N1,N2,Dw1,Dw2,CA1,CA2)

% KCyl: Coupling Coefficients of Cylindrical Coils
% All inputs are in inches/uH
% Subscript '1' indicates our primary coil and whose "left-most" point
% is treated as the origin. Subscript '2' is the secondary coil whose
% distance from the origin is inputed as the 'distance'

% 'distance' is the distance from the origin to the closest turn of the
% secondary coil to the origin
% 'r' is Coil Radius
% 'L' is Inductance
% 'N' is Number of Turns
% 'Dw1' is Diameter of Wire
% 'CA' is C/A
%Conversion to meters
distance = distance * .0254;
r1 = r1 * .0254;
r2 = r2 * .0254;
Dw1 = Dw1 * .0254;
Dw2 = Dw2 * .0254;
G1 = (CA1-1)*Dw1;
G2 = (CA2-1)*Dw2;

%Calculation of M
```

```

u = 4e-7 *pi;
M = 0;

for n = 1:N1
    for i = 1:N2
        %d = abs(distance - (n-1)*(Dw1+S1)+ (i-1)*(Dw2 + S2));
        d = abs(distance - (N1 - 1)*(Dw1+G1) + (N1-n)*(Dw1 + G1) + (i-1)*(Dw2+G2));
        dist(n,i) = d/.0254;
        m = ((4*r1*r2)/((r1 + r2)^2 + d^2))^.5;
        [Km,Em] = ellipke(m^2);
        M_temp = 2*(u/m)*(r1*r2)^.5 * ((1 - (m^2)/2)*Km - Em);
        M = M_temp + M;
    end
end
%Calculation of K
K = M/(L1*L2)^.5;
if K>=1
    error('Unrealizable Geometry: Overlapping Coils Detected')
end

end

```

## Spiral Coupling.m

```

function K = Spiral_Coupling(distance,ro1,ro2,L1,L2,N1,N2,Dw1,Dw2,CA1,CA2)
% K_of_Spiral: Inductance of Coaxial Spiral Coils, all inputs in inches/uH
% ro1 is outer radii of first coil
% ro2 is outer radii of second coil
% distance is distance between coils
% L1 is the inductance of the first coil
% L2 is the inductance of the second coil
% Dw is the wire diameter
% S is coil spacing (absolute inches)

%Conversion to meters
d = distance * .0254;
ro1 = ro1 * .0254;
ro2 = ro2 * .0254;
S1 = (CA1-1)* Dw1*.0254;
S2 = (CA2-1)* Dw2*.0254;
Dw1 = Dw1 * .0254;
Dw2 = Dw2 * .0254;

%Calculation of M
u = 4e-7 *pi;
M = 0;
for N1i = 1:N1
    r1 = ro1 - (N1i-1)*(Dw1 + S1);
    for N2i = 1:N2
        r2 = ro2 - (N2i-1)*(Dw2 + S2);
        m = ((4*r1*r2)/((r1 + r2)^2 + d^2))^.5;
        [Km,Em] = ellipke(m^2);
        M_temp = 2*(u/m)*(r1*r2)^.5 * ((1 - (m^2)/2)*Km - Em);
        M = M_temp + M;
    end
end

%Calculation of K
K = M/(L1*L2)^.5;
if K>=1
    error('Impossible Geometry: Overlapping Coils Detected')
end

end

```

## F.2 Possible Coils

The following calculates power loss for a range of user specified arrangements.

### Possible Coils.m

```
%Possible Coil Script
%Implemented to aid the selection of coils by analyzing their L,R,Q, and Ploss

%USER INPUT SETTINGS
current = 2.5; %Current expected in coils
freq = 100e3; %Frequency of operation
ca = 1.7:1:2.2; %c/a of interest
Do = 8.75; %Outer Diameter of coils
N = [2:30]; %Number of turns on the coils
dw = .125; %Wire diameter of the coils
Llow = 50e-6;%Lower Bound for Inductance (uH)
Lhigh = 80e-6;%Higher Bound for Inductance (uH)

%THE REST OF THE PROGRAM IS NOT USER CONFIGURABLE
clear Output; n = 1; %Variable initialization
for Ni = 1: length(N) %Iterate through all turns

    for cai = 1:length(ca) %Iterate through all c/a

        L = Cylindrical_Inductance(Do,(N(Ni) - 1)*dw*ca(cai)+dw,N(Ni)); %Calculate Inductance
        Rtotal = Cylindrical_Resistance(freq,Do,N(Ni),dw,ca(cai),1); %Calculate Total Resistance
        Q = 2*pi*freq*L/Rtotal; %Calculate Q Factor

        P = current^2 * Rtotal; %Calculate Power loss

        if (L>Llow && L<Lhigh) %If inductances are within the desired range, promote coil to output
matrix
            Output(n,[1:5]) = [N(Ni), ca(cai), Q, L/1e-6,P];
            n = n +1;
        end
    end
end

%Plot Q,c/a,Ploss,N
subplot(1,2,1)
scatter(Output(:,1),Output(:,3), 'filled')
grid on; grid minor
title({strcat('Q Factor (c/a,Ploss): with Freq: ', num2str(freq)),strcat('dw = ', num2str(dw), ',Do = ', num2str(Do), ',Current = ', num2str(current))}, 'FontSize',20)
xlabel('Turns', 'FontSize',20)
ylabel('Quality Factor', 'FontSize',20)
a = strcat('(',num2str((Output(:,2))), ',',num2str(round(Output(:,5),1)), ')');
b = cellstr(a);
text(Output(:,1),Output(:,3), b, 'FontSize',16)
xt = get(gca, 'XTick');
set(gca, 'FontSize', 16)
xt = get(gca, 'YTick');
set(gca, 'FontSize', 16)

%Plot Inductance
subplot(1,2,2)
scatter(Output(:,1),Output(:,4),'r','filled')
grid on; grid minor
title({strcat(num2str(Lhigh/1e-6), 'uH>Inductance>',num2str(Llow/1e-6), 'uH (c/a,Ploss): with Freq: ', num2str(freq)), strcat('dw = ', num2str(dw), ',Do = ', num2str(Do), ',Current = ', num2str(current))}, 'FontSize',20)
xlabel('Turns', 'FontSize',20)
ylabel('Inductance', 'FontSize',20)
text(Output(:,1),Output(:,4), b, 'FontSize',16)
xt = get(gca, 'XTick');
set(gca, 'FontSize', 16)
xt = get(gca, 'YTick');
set(gca, 'FontSize', 16)
```

### F.3 Simulation Program

The simulation code that performs the calculation of the coreless transformer response from first principles has three main modules. The first module calculates the lumped-parameter equivalent circuit elements based upon the coils materials and user input physical arrangement (such as number of turns, spacings,etc.). These lumped parameter values are transferred to a separate LTspice circuit analysis simulation program, which is the second module. The third module takes the results of the circuit analysis performed by LTspice and then analyzes the data for the desired performance factors such as power transfer efficiency coefficient  $S_{21}$ .

#### F.3.1 First Module

This module is separated into two parts: the collection of user input values concerning the physical structure of the transformer, and the calculation of the resultant lumped parameter circuit values. It is all performed within the *Cylindrical\_Coil\_Simulator.m* script.

#### Cylindrical Coil Simulator.m

```
%Cylindrical_Coil_Simulator

dw = .125; %Wire diameter of ALL COILS (inches)
Do2 = 8.75; %Coil Diameter of Coil2/3 (inches)
ca = 2; %Ratio Pitch over the wire diameter for ALL COILS (greater than 1)
N1 = 1; %Turns on Coil1 (integer)
N4 = 6; %Turns on Coil4 (integer)

f1 = .75; %Fractional length of the primary resonant coil in which the drive coil will be centered upon
(matrix/scalar)
f2 = .75; %Fractional length of the primary resonant coil in which the drive coil will be centered upon
(matrix/scalar)

Nmain = 18; %Number of Turns on Resonant Coils (matrix)
D23close = .75; %Distance between the closest turns of Coil2 and Coil3 (inches)
Rsource = .5; %Resistance of the source impedance (ohms)
Rload = 16.6; %Resistance of the load impedance (ohms)
C1 = 10e-9; %Capacitance attached to Coil2 (farads)
C2 = 10e-9; %Capacitance attached to Coil3 (farads)
RadialDist = .5; %Difference in diameter between Coil1/4 and Coils2/3 (inches)

B1 = 1; %Resistance Multiplier for Coil1
B2 = 1; %Resistance Multiplier for Coil2
B3 = 1; %Resistance Multiplier for Coil3
B4 = 1; %Resistance Multiplier for Coil4
Proximity = 1; %Binary value enabling Proximity-effect-influenced resistance
PlotOption = 2;%Option 1 or 2
```

**Declare input  
Physical  
Parameters of Coil  
Arrangement**

```
%Rest of the Program, do not alter from this point onward
Do3 = Do2; %Coil Diameter of Coil3
Do1 = Do2 + RadialDist; %Coil Diameter of Coil1
Do4 = Do1; %Coil Diameter of Coil4

%Calculating Coil1
l1 = dw*ca*(N1-1); %Length of Coil1
L1 = Cylindrical_Inductance(Do1,l1+dw,N1); %Inductance of Coil1

%Calculating Coil4
l4 = dw*ca*(N4-1); %Length of Coil4
L4 = Cylindrical_Inductance(Do4,l4+dw,N4); %Inductance of Coil4
```

**Calculation of Lumped  
Equivalent Models Using  
Design Algorithms**

```

clear ALLS21; %Collects all plots (N,f1,f2) of length(S21)
for Ni = 1:length(Nmain) %Iterate through all resonant coil turns

    %Calculating Coil2
    N2 = Nmain(Ni); %Designate number of turns on Coil2
    l2 = dw*ca*(N2-1); %Length of Coil2
    L2 = Cylindrical_Inductance(Do2,l2+dw,N2); %Inductance of Coil2

    %Calculating Coil3
    N3 = Nmain(Ni); %Designate number of turns on Coil3
    l3 = dw*ca*(N3-1); %Length of Coil3
    L3 = Cylindrical_Inductance(Do3,l3+dw,N3); %Inductance of Coil3

    clear f1f2Output;
    for fli = 1:length(f1) %Iterate through all f1 values

        clear S21peaks;
        for f2i = 1:length(f2) %Iterate through all f2 values

            %Evaluate Ks
            K12 = Cylindrical_Coupling(l1/2 -(1-
f1(fli))*l2, Do1/2,Do2/2, L1,L2, N1,N2,dw,dw,ca,ca); %Coupling between Coils 1 and 2
            K23 =
Cylindrical_Coupling(l2+D23close, Do2/2,Do3/2, L2,L3, N2,N3,dw,dw,ca,ca); %Coupling between Coils 2 and 3
            K34 = Cylindrical_Coupling(l3*f2(f2i) -
l4/2, Do3/2,Do4/2, L3,L4, N3,N4,dw,dw,ca,ca); %Coupling between Coils 3 and 4
            K13 =
Cylindrical_Coupling(l1/2+l2*f1(fli)+D23close, Do1/2,Do3/2, L1,L3, N1,N3,dw,dw,ca,ca); %Coupling between Coils 1 and 3
            K24 = Cylindrical_Coupling(l2+D23close+l3*f2(f2i)-
l4/2, Do2/2,Do4/2, L2,L4, N2,N4,dw,dw,ca,ca); %Coupling between Coils 2 and 4
            K14 = Cylindrical_Coupling(l1/2+l2*f1(fli)+D23close+l3*f2(f2i)-
l4/2,Do1/2,Do4/2, L1,L4, N1,N4,dw,dw,ca,ca); %Coupling between Coils 1 and 4
            K = [K12 K23 K34 K13 K24 K14];
            %Simulation Extra Parameters; Renaming
            Ldrive = l1;
            Lmag1 = l2;
            Lmag2 = l3;
            Lload = l4;

            %Calculate Resistance of Coils at Resonance Frequency
            Rtot1 = Cylindrical_Resistance(1/(L2*C1)^.5,Do1,N1,dw,ca,1);
            Rtot2 = Cylindrical_Resistance(1/(L2*C1)^.5,Do2,N2,dw,ca,1);
            Rtot3 = Cylindrical_Resistance(1/(L3*C2)^.5,Do3,N3,dw,ca,1);
            Rtot4 = Cylindrical_Resistance(1/(L3*C2)^.5,Do4,N4,dw,ca,1);

            %Run Simulation to Locate frequency peak
            run('Master.m'); %Finds the frequency of S21 peak and calls it Freq

```

### F.3.2 Second Module

This module is separated into four parts. First, it clears the data storage files of prior remnant information. Second, it creates the netlists employed by LTspice that define the circuits with the lumped parameter values determined in the first module. Third, it runs the LTspice simulations using an estimated value for the effective resistances to get an improved estimate of the resonant frequency for the calculation of the coil resistance. Fourth it reruns the coil lumped parameter calculations for resistance at the corrected frequency. Finally, it runs the LTspice simulations with the corrected lumped parameters and collects the results. It starts at Master.m, then calls SpiceModels.m to generate the LTspice model, and returns to Master.m, where it then reruns the lumped calculations, and returns to Master.m for the last time.

## Master.m

## Data Clean Up

```
%Master Script Nested Inside Simulator

%Deleting all LTspice related files from previous runs
delete ./SpiceModels/*.cir;
delete ./SpiceModels/*.raw;
delete ./SpiceModels/*.log;
disp('Cleaning Complete')

disp(horzcat('Circuit Undergoing Simulation'))

%Generate SpiceModel Netlist
SpiceModel(Ldrive, Lmag1, C1, Lmag2, C2, Lload, K12, K23, K34, K13, K24, K14);
```

## Netlist Generation

## SpiceModel.m

```
function SpiceModel(Ldrive, Lmag1, C1, Lmag2, C2, Lload, K12, K23, K34, K13, K24, K14)

%Creat name for the file, a composition of component parameters
name = strcat(num2str(Ldrive,3), '_', num2str(Lmag1,3), '_', num2str(Lmag2,3), '_', num2str(Lload,3),
              '_', num2str(K12,3), '_', num2str(K23,3), '_', num2str(K34,3), '_', num2str(K13,3), '_',
              num2str(K24,3), '_', num2str(K14,3), '_SpiceModel.cir');
fid = fopen(strcat('SpiceModels/', name), 'wt');
fprintf(fid, '%s\n', strcat('* C:\Users\ChatAngel\Documents\MATLAB\MatlabSpice\SpiceModels\',
                           name)));
```

%Extract Resistance value from scope pf external script

```
Rtot1=evalin('base','Rtot1');
Rtot2=evalin('base','Rtot2');
Rtot3=evalin('base','Rtot3');
Rtot4=evalin('base','Rtot4');
Rsource=evalin('base','Rsource');
Rload=evalin('base','Rload');
```

%Text that acts as an LTspice Netlist

```
text = [horzcat('Rdcl N001 Primary ',num2str(Rtot2),'\n') ...
horzcat('Rdc2 Secondary N002 ',num2str(Rtot3),'\n') ...
horzcat('Lmag1 N003 N001 {Lmag1var}\n') ...
horzcat('Lmag2 N004 N002 {Lmag2var}\n') ...
'V1 Drive 0 AC 1\n' ...
'C3 secondary Primary 5p\n' ...
horzcat('C4 Primary N003 {C1var}\n') ...
horzcat('C5 Secondary N004 {C2var}\n') ...
'R1 N001 N003 30k\n' ...
horzcat('Ldrive 0 N005 {Ldrivevar}\n') ...
horzcat('Lload 0 N006 {Lloadvar}\n') ...
horzcat('RdcDrive N005 Ch1 ',num2str(Rtot1),'\n')...
horzcat('RdcLoad Load N006 ',num2str(Rtot4),'\n')...
'C6 Ch1 0 1p\n'...
'C7 Load 0 1p\n'...
'C8 secondary Load 1p\n'...
'C9 Primary Ch1 1p\n'...
horzcat('R4 Ch1 Drive ',num2str(Rsource),'\n') ...
horzcat('R5 Load 0 ',num2str(Rload),'\n') ...
'K23 Lmag1 Lmag2 {K23var}\n' ...
'.ac oct 500 1e3 1000e3\n' ...
'K12 Ldrive Lmag1 {K12var}\n' ...
'K34 Lmag2 Lload {K34var}\n' ...
'K13 Ldrive Lmag2 {K13var}\n' ...
'K24 Lmag1 Lload {K24var}\n' ...
'K14 Lload Ldrive {K14var}\n' ...
horzcat('V2 Rsource 0 AC ',num2str(Rsource),'\n') ...
horzcat('V3 Rload 0 AC ',num2str(Rload),'\n') ...
horzcat('.param Ldrivevar=',num2str(Ldrive),' Lmag1var=',num2str(Lmag1), ' C1var=', num2str(C1), ' Lloadvar=',
       num2str(Lload), ' Lmag2var=', num2str(Lmag2), ' C2var=', num2str(C2), ' K12var=',
       num2str(K12), ' K23var=', num2str(K23), ' K34var=', num2str(K34), ' K13var=', num2str(K13), ' K24var=',
       num2str(K24), ' K14var=', num2str(K14), '\n') ...
'.save V(Load)\n' ...
'.save V(Ch1)\n'...
'.save I(R5)\n'...
'.save I(R4)\n'...
'.save V(drive)\n'...
'.save V(rsouce)\n' ...
```

## ← Netlist Model

```

'.save V(rload)\n' ...
'.backanno\n' ...
'.end\n' ];

%Print the text to a file
fprintf(fid , text);

fclose(fid);
end

```

### Master.m (cont)

```

%Compose name of file created by SpiceModel
name = strcat(num2str(Ldrive,3), '_', num2str(Lmag1,3), '_', num2str(Lmag2,3), '_', num2str(Lload,3),
        '_', num2str(K12,3), '_', num2str(K23,3), '_', num2str(K34,3), '_', num2str(K13,3), '_',
        num2str(K24,3), '_', num2str(K14,3), '_SpiceModel.cir');

%Use a system call to run LTspice on the netlist file
Here the user uses Matlab's "systemcall" function to use enable LTspice to simulate the generated netlist

Return to Master.m to Initiate LTspice Simulation

```

```

disp(horzcat('Netlist Generation/Simulation Complete'))

%Call Evaluation Function to Extract S21 features
[Freq,S21plot] = Evaluation; %A is S21 peak value and freq

```

```

%Re-calculate the Total (Skin and Proximity) of Coils at
%the right frequency, 'Freq', and apply Beta factors
Rtot1 = Cylindrical_Resistance(Freq,Do1,N1,dw,ca,1)*B1;
Rtot2 = Cylindrical_Resistance(Freq,Do2,N2,dw,ca,1)*B2;
Rtot3 = Cylindrical_Resistance(Freq,Do3,N3,dw,ca,1)*B3;
Rtot4 = Cylindrical_Resistance(Freq,Do4,N4,dw,ca,1)*B4;

```

```

%Run resistance-accurate Simulation to find S21 values.
run('Master.m'); %Dumps S21 peak in A(1) and peak freq at A(2)

```

**2<sup>nd</sup> Set of Simulations**

**Re-adjustment of Resistance values in *Cylindrical\_Coil\_Simulator.m***

#### F.3.3 Third Module

This module is separated into two parts. First, it collects LTspice output data and performs the specified analysis to create the selected set of output waveforms with the *Evaluation.m* script. Second, the *Cylindrical\_Coil\_Simulator.m* script is used to plot the generated waveforms.

### Evaluation.m

```

function [Freq,S21] = Evaluation
files = dir(fullfile('./SpiceModels/', '*.raw'));
L = length(files);

for i = 1:L
    file = files(i).name; %Extract name as cell array
    file = fullfile(file); %Extract name as char array

    %Use LTSpice2Matlab to extract data

```

**Here the user must run the “LTSpice2Matlab” command on the .raw file created by LTSPICE. Name the output of the function, ‘raw\_data’.**

```

    %Create the S21 parameter plot from the LTspice Waveforms
    S21 =
    (2*raw_data.variable_mat(3,:)/raw_data.variable_mat(1,:))*(raw_data.variable_mat(4,:)/raw_data.variable_mat(5,:))^5;

    %Find the Peak Frequency
    [maximum, freq] = max(abs(S21));
    Freq = raw_data.freq_vect(freq);

end

```

**MATLAB Analysis and Evaluation**

```

fclose('all');

disp('Evaluation Complete')

```

```

    ALLS21(Ni,f1i,f2i,:) = S21plot; %Collecting ALL the S21 WaveForm Plots
end

end

%Plotting Options

if (PlotOption == 1)
    clear S21peaksN;
    for Ni = 1:length(Nmain)
        clear f1f2Peaks;
        figure;
        for fli = 1:length(f1)
            subplot(1,length(f1),fli)
            for f2i = 1:length(f2)

                s21length = length(ALLS21);
                waveform = ALLS21(Ni,fli,f2i,:);
                plot(logspace(3,6,s21length),abs(waveform(:)), 'LineWidth',2)
                title({strcat('S21, f1=',num2str(f1(fli))), ...
                    strcat('N2=N3=', num2str(Nmain(Ni)), ', L2=L3=',num2str(L2)), ...
                    strcat('N1 =',num2str(N1,3), ', L1 =', num2str(L1,3), ', N4 =',num2str(N4,3), ', L4 ...
                    =', num2str(L1,3)), 'FontSize',20)
                xlabel('Frequency', 'FontSize',20);
                ylabel('S21 Output', 'FontSize',20);
                hold on
                ylim([0 1]);
                f1f2Peaks(fli,f2i) = abs(max(waveform(:)));
            end
            grid on; grid minor;
            legend(cellstr(strcat(num2str(f2), 'f2=%g'), ' with S21max: ', num2str(f1f2Peaks(fli,:)),3 ...
            )), 'FontSize',20)
            xt = get(gca, 'XTick');
            set(gca, 'FontSize', 16)
            xt = get(gca, 'YTick');
            set(gca, 'FontSize', 16)
        end
        [M,I] = max(f1f2Peaks(:));
        [f1val, f2val] = indsub(size(f1f2Peaks), I);
        S21peaksN(Ni,1) = f1(f1val);
        S21peaksN(Ni,2) = f2(f2val);
        S21peaksN(Ni,3) = M;
    end
    figure;
    plot(Nmain, S21peaksN(:,3), 'LineWidth',2)
    a = num2str(S21peaksN(:,[1 2]), 'f1=%g, f2=%g'); %f positions of coils
    b = cellstr(a);
    text(Nmain,S21peaksN(:,3)', b, 'FontSize',11)
    title({'S21 while varying turns on CYLINDRICAL resonant coils',...
        strcat('N1 =',num2str(N1,3), ', L1 =', num2str(L1,3), ', N4 =',num2str(N4,3), ', L4 =', ...
        num2str(L1,3)), 'FontSize',20)
    xlabel('Number of Turns on Resonant Coil', 'FontSize',20);
    ylabel('Highest S21 for f1/f2 explored', 'FontSize',20);
    grid on; grid minor;
    hold on
    xt = get(gca, 'XTick');
    set(gca, 'FontSize', 16)
    xt = get(gca, 'YTick');
    set(gca, 'FontSize', 16)
end

if (PlotOption == 2)
    figure;
    for Ni = 1:length(Nmain)
        s21length = length(ALLS21);
        waveform = ALLS21(Ni,f1i,f2i,:);
        plot(logspace(3,6,s21length),abs(waveform(:)), 'LineWidth',2)
        title({strcat('S21', ...
            strcat('f1=', num2str(f1(1)), ', f2=',num2str(f2(1))), ...

```

## Plotting Options

```

        strcat('N1 =',num2str(N1,3),', L1 =', num2str(L1,3), ', N4 =',num2str(N4,3), ', L4 =',
num2str(L4,3))), 'FontSize',20)
        xlabel('Frequency (MHz)', 'FontSize',20);
        ylabel('S21 Output', 'FontSize',20);
        hold on
    end
    grid on; grid minor;
    legend(cellstr(strcat(num2str(Nmain,'Turns=%g') )), 'FontSize',16)
    ylim([0 1])
    xt = get(gca, 'XTick');
    set(gca, 'FontSize', 16)
    xt = get(gca, 'YTick');
    set(gca, 'FontSize', 16)
end

```